UPPSALA
UNIVERSITET

Digital Comprehensive Summaries of Uppsala Dissertations from the Faculty of Science and Technology 1467

Atomistic spin dynamics and relativistic effects in chiral nanomagnets

KONSTANTINOS KOUMPOURAS

ACTA
UNIVERSITATIS
UPSALIENSIS
UPPSALA
2017

ISSN 1651-6214
ISBN 978-91-554-9791-0
urn:nbn:se:uu:diva-312462

Dissertation presented at Uppsala University to be publicly examined in Polhemsalen, Ångströmlaboratoriet, Lägerhyddsvägen 1, Uppsala, Monday, 27 February 2017 at 09:00 for the degree of Doctor of Philosophy. The examination will be conducted in English. Faculty examiner: Professor Elena Vedmenenko (Institute of applied Physics, University of Hamburg (Germany)).

Abstract

Koumpouras, K. 2017. Atomistic spin dynamics and relativistic effects in chiral nanomagnets. *Digital Comprehensive Summaries of Uppsala Dissertations from the Faculty of Science and Technology* 1467. 97 pp. Uppsala: Acta Universitatis Upsaliensis. ISBN 978-91-554-9791-0.

In this thesis, studies based on magnetization dynamics on atomic length scales are presented for a number of magnetic systems, where Dzyaloshinskii-Moriya (DM) interaction is present. First-principle methods, based on density functional theory (DFT), have been used to study the pairwise magnetic interactions, such as Heisenberg exchange and DM interaction, which are the crucial parameters for the helimagnetic systems. The first part of this thesis concerns the theoretical background: basics of DFT, atomistic spin dynamics and magnetic skyrmions. The second part concerns the ground state and dynamical properties of helimagnets.

Magnetic interaction parameters have been calculated for heterostructures, such as Co/Ni/Co on heavy metal non-magnetic substrates. These parameters are strongly dependent on the material of the substrate. Furthermore, the magnetization dynamics of domain wall and skyrmion are studied and our results show that motion is influenced by the spin-Hall effect (SHE) which arises from the non-magnetic substrate. Similar studies of magnetic interaction parameters have been made for several half-Heusler compounds MnZSn (Z=Tc, Ru, Rh, Os, Ir and Pt) and the phase diagram of the $MnPt_{0.99}Ir_{0.01}Sn$ alloy proves the existence of skyrmions in a wide range of temperature and external magnetic field.

The manipulation of low-dimensional magnetic structures (skyrmions and solitons) with spin transfer torques have been investigated. The nucleation and annihilation processes of skyrmion, by the use of spin polarised current, are essential and the impact of different edges (antiferromagnetic, magnetically softer and stiffer) on both processes is studied. When the edge is magnetically softer, less current is required for skyrmion nucleation and annihilation. Furthermore, one-dimensional magnetic solitons are used to explore concepts of logical operations in a prototype majority gate device, since they are stable and can be easily created and manipulated by spin currents.

Lastly, edge dislocations in FeGe helimagnet have been studied. These dislocations described in terms of thermally driven dynamics by the use of atomistic spin dynamics approach and possibly explain some unusual jumps of the spiral wavelength observed by time-dependent experiments.

Konstantinos Koumpouras, Department of Physics and Astronomy, Materials Theory, Box 516, Uppsala University, SE-751 20 Uppsala, Sweden.

ISSN 1651-6214
ISBN 978-91-554-9791-0
urn:nbn:se:uu:diva-312462 (http://urn.kb.se/resolve?urn=urn:nbn:se:uu:diva-312462)

Dedicated to my family

List of papers

This thesis is based on the following papers, which are referred to in the text by their Roman numerals.

I **A spin dynamics approach to solitonics**
K. Koumpouras, A. Bergman, O. Eriksson, and D. Yudin
Scientific Reports 6, 2016

II **Local dynamics of topological magnetic defects in the itinerant helimagnet FeGe**
A. Dussaux, P. Schoenherr, K. Koumpouras, J. Chico, K. Chang, L. Lorenzelli, N. Kanazawa, Y. Tokura, M. Garst, A. Bergman, C. L. Degen, and D. Meier
Nature Communications 7, 12430 (2016)

III **A majority gate with chiral magnetic solitons**
K. Koumpouras, D. Yudin, C. Adelmann, A. Bergman, O. Eriksson, and M. Pereiro
Preprint

IV **Relativistic interactions in low-dimensional Co heterostructures**
J. Chico, K. Koumpouras, L. Bergqvist, and A. Bergman
Preprint

V **Search for high–temperature skyrmionic phase in Mn–based half–Heusler alloys from simulations**
K. Koumpouras, J. Chico, L. Bergqvist, and A. Bergman
Preprint

VI **Relativistic effects in domain wall and skyrmion dynamics in magnetic heterostructures**
J. Chico, K. Koumpouras, L. Bergqvist, and A. Bergman
Preprint

VII **The effect of edge interactions on current driven creation and annihilation of skyrmion**
K. Koumpouras, and A. Bergman
Preprint

Contents

1. Introduction

Magnetic storage is a field which has been around for a long time and not only these last decades as many people may think. It started in 1888 by the American engineer Oberlin Smith [1] and even nowadays the main idea remains the same, read and write heads are used to store and retrieve the data. In the last 30-35 years there has been a huge growth of this kind of magnetic storage devices, the capacity has increased from kilobytes to terabytes and the data transfer rate has grown from bytes per second to 100+ megabytes per second.

The big successes on writing and reading data came with the change from mechanical devices to electronic devices. The driving force behind this change was the discovery of new electronic devices with smaller size and they perform faster logical operations by using electronic currents. The bottleneck of such devices based on electron transport is the further decrease of their size because of the Joule heating.

An alternative direction for the solution of the previous problem and in general for better performance of such devices can be the change from the conventional electronic devices to devices which exploit the spin of the electron (spintronics) or the excitations of the magnetic structures such as spin waves (magnonics). In spintronics, the interesting phenomena are taking place at the nanoscale level which means that, ideally, the size of future devices can be reduced, faster transfer speeds and higher bit density, can be achieved. The research on spintronics have started with the discovery of the Giant Magneto-Resistance (GMR) effect [2, 3] by Peter Grünberg and Albert Fert who was awarded the 2007 Physics Nobel Prize for their work on magnetic manipulation of electronic currents.

A very important role in the investigation of spintronics plays the growth of new synthesizing techniques, like Molecular Beam Epitaxy (MBE) and Pulsed Laser Deposition (PLD). Those two techniques give the opportunity of building up new nano-structures and thin films. Another important aspect for the spintronics is also the growth of high definition microscopes (e.g SEM, TEM).

On the other hand, in magnonics a whole new concept is introduced where the information carrier is not coming from the motion of electrons but from excitations of the magnetic structure which are called spin waves or magnons. The main advantage of this idea is the reduction of information losses and the increase of its transmission speed as well as the absence of Joule heating. Magnonic diodes and transistors have already been introduced by several research groups [4, 5, 6].

In what can be seen as an inverse of the GMR effect, John Slonczewski and Luc Berger proposed that the magnetization of a material can be influenced by

a spin polarised current. This effect is called spin transfer torque (STT) [7, 8]. Based on this idea, Stuart Parkin proposed a racetrack memory device where the spin transfer torque effect is used to move ferromagnetic domain walls by using a spin polarised electronic current [9]. The high-speed performance is the characteristic which makes domain walls attractive for constructing logic devices, such as Magnetic Random Access Memories (MRAMs). However, in order to achieve these extraordinary speeds, very high current densities are needed which are of the order of $j \sim 10^{12}$ A/m^2.

In 2009, a non-trivial magnetic structure was discovered [10] which attracted the research interest in condensed matter systems. This structure is called skyrmion lattice. Magnetic skyrmions are topologically stable chiral spin structures with a whirling configuration where the magnetic structure has a very smooth variation. This last property makes them couple successfully with the spin polarised electronic current and the result of this coupling is an extremely low depinning current density which is about $j \sim 10^6$ A/m^2. In other words, 5-6 orders of magnitude less current density is needed to put them in motion compare to domain walls. Additional to their small depinning current, skyrmions are promising candidates for future data storage devices because of the weak influence of defects and their flexibility to avoid pinning centres [11] due to their topological protection.

Since the new studied devices are based on the spin of the electron, it can be argued that the most interesting phenomena takes place on the nanometer length scale. In other words, a detailed characterization of magnetic ground state properties, as well as the magnetisation dynamics, in atomistic scale is required for a full understanding if these phenomena. It is well-known that the origin of magnetism in solids is the spin and angular momentum of the electrons and for this reason, it can only be explained and understood in the concept of quantum mechanics. Thus, the electronic structure is very important for the material's magnetic properties and ab-initio methods can be a very useful tool for extracting the important information of the magnetic ground state properties with very good accuracy.

Simple models are often used for the description of magnetism in materials. A very popular and common model is the Heisenberg's model [12] which predicts the exchange coupling between two atomic magnetic moments. The Hamiltonian arising from Heisenberg's model, which is called Heisenberg Hamiltonian, can be extended in such a way that in addition to the exchange constant J, it also includes the magnetocrystalline energy and a third magnetic contribution which is called Dzyaloshinskii-Moriya interaction (DMI). This last contribution is an antisymmetric exchange interaction between two atomistic magnetic moments. All the previous constants can in fact be calculated by using density functional theory (DFT) methods. To study the magnetization dynamics of atomic magnetic moments the Landau-Lifshitz (LL) or the Landau-Lifshitz-Gilbert (LLG) equation [13, 14] can be used. This method

is powerful and has been successful for investigating the time evolution of magnetism in small length scales and in more complex magnetic structures.

In the present thesis, magnetization dynamics is investigated by using a two-step approach. As already mentioned above, the magnetism in solids can be understood from quantum mechanics and the magnetic properties are explained by the electronic structure. Thus, in order to model the behaviour of solids, the first step is the materials specific calculations from first principles. The methods to calculate the electronic structure, used in the thesis, are the Korringa-Kohn-Rostoker (KKR) approach [15, 16] and the exchange interactions are calculated by the Liechtenstein, Katsnelsson, Antropov and Gubanov (LKAG) formula [17, 18], which both are described in Chapter 3. After extracting the necessary information from the first step, the parameters are mapped into the Hamiltonian which is used in the LLG equation of motion for atomistic magnetization dynamics studies. This is the second step of our approach. In Chapter 4 is discussed the derivation of LLG equations of motion for the atomic spins as well as the current driven magnetisation dynamics predicted from Berger [8, 19, 20] and Slonczewski [7].

Chapter 5 discusses the formation and the stability of magnetic skyrmions as well as their experimental observation in B20 non-centrosymmetric chiral ferromagnets. Furthermore, is presented the dynamics of such structures and how they are influenced by the presence of magnetic and non-magnetic defects. Magnetic skyrmions exist in the FeGe which exhibits a helical spin-spiral ground state and magnetic defects in the ground state is of great interest since they promote the formation of magnetic skyrmions. The dynamics of this kind of defects are studied from theoretical point of view by using the LLG equation of motion in Chapter 6, where the magnetic properties of the material were first calculated by using the KKR approach. As previously mentioned, magnetic skyrmions are promising candidates for future data storage devices in which the writing and deleting bits of information are very crucial. This means that the nucleation and annihilation processes of magnetic skyrmions at the edges of the system are very important and they are studied in Chapter 9 by investigating energy barriers of different kind of edges in terms of atomistic spin dynamics calculations.

Beside the magnetic skyrmions, lower dimensional structures like quasi-one-dimensional magnetic solitons are of great interest nowadays which are also very good candidates for future data storage devices. By the use of toy models, in Chapter 7 is studied the behaviour and the dynamics of such structures by means of atomistic spin dynamics calculations. Moreover, the use of magnetic solitons in a functional and dynamic three-input majority gate is investigated, where the input and the output signals are encoded in the chirality of the solitons, allowing to perform logical operations.

The Dzyaloshinskii-Moriya interaction has gathered much attention because it is very important for the stabilisation of non-collinear magnetic configurations like magnetic skyrmions and solitons. DMI is present in the B20

structures (MnSi, FeGe and MnGe) with broken inversion symmetry, but it has been proposed that at the surface of magnetic thin films on top of heavy metal a symmetry breaking takes place which leads to a strong DMI. In Chaper 8, Co monolayers, Co trilayers and heterostructures of Co/Ni/Co deposited on different types of heavy metals are studied by performing ab-initio calculations for the electronic and magnetic properties. Another class of materials which exhibit strong DMI is the half-Heuslers compounds MnZSn, where Z is a transition metal (Tc, Ru, Rh, Os, Ir, Pt). All these half-Heusler compounds and the $MnPt_{1-x}Ir_xSn$ alloy are studied in Chapter 10 by performing first principles calculations. Furthermore, the phase diagram of $MnPt_{0.99}Ir_{0.01}Sn$ is investigated in terms of atomistic spin dynamics calculations.

2. Magnetism

Magnetism was discovered since the ancient years and it has a long history until nowadays. Ancient Chinese and Greeks mention permanent magnets from the fourth century B.C. and according to the texts Chinese were using magnetic compasses for navigation (first for orientation on land and then at the sea). From then, very important discoveries on the properties of magnetism have been made through all these years and today the research on magnetism is to a large extent driven by the technological innovations in information technology and has a particular focus on data storage and memory applications.

2.1 Magnetic moment

A magnetic dipole can be modelled by two opposite magnetic charges (positive and negative) with equal magnitude where d is the distance between them, as represented in Fig. 2.1, and it can be expressed as $\mathbf{m} = q_m \mathbf{d}$. Where q_m is the strength of the pole.

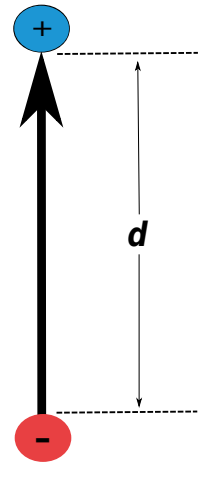

Figure 2.1. Representation of magnetic dipole moment **m**.

Before the discovery of spin from quantum mechanics, it was believed that the origin of the magnetic moments of atoms, and as a consequence, the magnetisation of solids, is the motion of electrons (current) in a close circular

loop. The magnitude of magnetic dipole moment arising by a rotating electric charge is given by

$$|\mathbf{m}| = \mu_0 IS, \tag{2.1}$$

where μ_0 is the magnetic permeability of the vacuum, I is the current of the loop and S the area of the loop.

The classical relation of the magnetic dipole moment can be written as:

$$\mathbf{m} = -\frac{e\mu_0}{2m_e}\mathbf{L}. \tag{2.2}$$

where e is the charge of the electron, μ_0 is the magnetic permeability of the vacuum, m_e is the electron mass and $\mathbf{L}$ is the classical angular momentum which depends on the distance $\mathbf{r}$ and the momentum $\mathbf{p}$.

When Neils Bohr announced his famous atomic model, which took his name and is called Bohr's model, he gave three very important rules. In our case, we will focus on the last rule which is saying: "Electrons can only gain and lose energy by jumping from one allowed orbit to another, absorbing or emitting electromagnetic radiation with a frequency f determined by the energy difference of the levels according to the Planck relation: $\Delta E = E_2 - E_1 = hf$, where h is the Planck's constant". By using this rule he discovered that the angular momentum $\mathbf{L}$ is quantised and is constrained to discrete values by the by the quantum number n. So, the quantum angular momentum is given by:

$$L = mur = \frac{hr}{\lambda} = \frac{hr}{\left[\frac{2\pi r}{n}\right]} = \frac{nh}{2\pi} = n\hbar. \tag{2.3}$$

By adding the quantum angular momentum to the expression for magnetic dipole moment (Eq. 2.2) we get the expression for quantum magnetic moment which is:

$$\mathbf{m} = -\frac{e\mu_0}{2m_e}n\hbar. \tag{2.4}$$

Only the component of quantum angular momentum can be observed along a quantisation axis (let's assume z) on which the field is aligned. Thus, the expectation value of the quantum magnetic moment is:

$$\langle \mathbf{m}_z \rangle = -\frac{e\mu_0}{2m_e}\hbar L_z. \tag{2.5}$$

The above relation is used to define the *Bohr magneton* which is $\mu_B = e\hbar/2m_e$. The value of the *Bohr magneton* is $\mu_B = 0.927 \times 10^{-23}$ Am^2=1.17×10^{-29} V m s, and is very common to use μ_B as the unit for the magnetic moment instead of V m s.

2.1.1 Classical dipole and external magnetic field

The magnetic dipole moment interacts with an external magnetic field and this interaction can be observed by the simple experiment of a magnetic needle, as can be found in a common compass, which is aligned with the earth's magnetic field. From this example of the magnetic needle we come to a conclusion that the magnetic dipole moments are aligned with a uniform external magnetic field when they under its influence. As we can see in Fig. 2.2 when an external magnetic field is applied perpendicular to the dipole, two forces are acting at the edges where the positive (head) and the negative (tail) charges are located and it starts rotating to the direction of the external field **H**. Since the initial position of the magnetic dipole moment is perpendicular to the external magnetic field and the final is parallel to it, the energy of the system is $E = \int \mathbf{F} \cdot d\mathbf{l}$, where **F** is the force and **l** the distance (see Fig. 2.2). As mentioned in the previous section the magnetic dipole moment is $\mathbf{m} = q\mathbf{d}$ and the force is $\mathbf{F} = q\mathbf{H}$. The energy of the system now is given by:

$$E = \int \mathbf{F} \cdot d\mathbf{l} = 2q \int \mathbf{H} \cdot d\mathbf{l} = qdH \int_{\pi/2}^{0} cos\phi d\phi = -\mathbf{m} \cdot \mathbf{H}. \qquad (2.6)$$

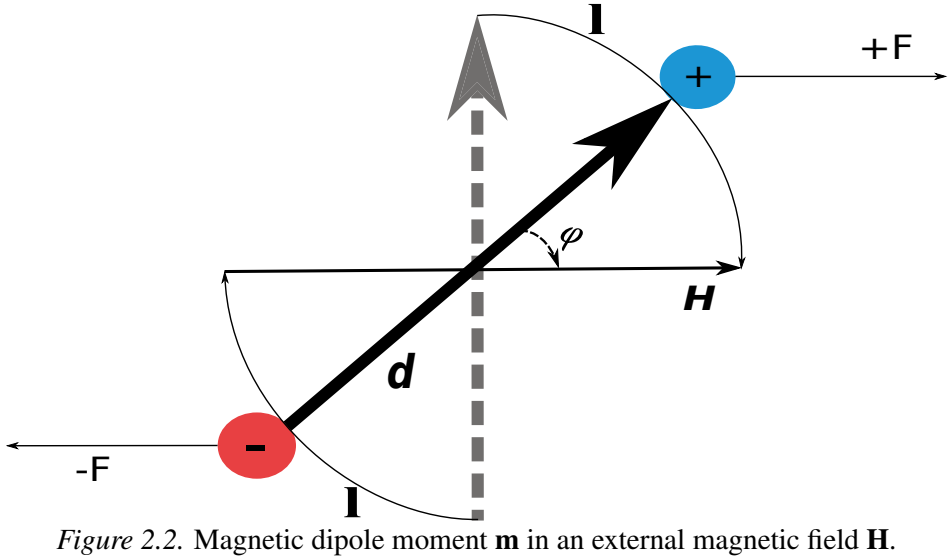

Figure 2.2. Magnetic dipole moment **m** in an external magnetic field **H**.

2.2 Simple magnetic models

Investigating the properties of magnetism by using magnetic models is very important not only for the magnetism itself but for other branches of science as well. More specific, in the area of magnetic storage applications, magnetic models play a crucial role for the improvement of existing materials and the

investigation for new candidates. By the time of Maxwell's equations, which show the connection between different electromagnetic fields, a lot of questions arisen and by now more and more questions are looking for an answer since research takes place in nanometer scale and more complex phenomena are involved. Here is the point where magnetic models have the opportunity to give very important answers in a simple and effective way.

2.2.1 Ising model

The Ising model is perhaps the simplest of all magnetic models. Here one takes into only two possible states for each atom: spin-up (↑) and spin-down (↓) which are treated as classical entities. In fact, many areas of science and technology are using extensions of this very simple model, not only in physics but also in chemistry and biology. In the past, it had been observed that in the absence of external magnetic fields or electric currents, some systems and by extension some materials exhibit a spontaneous magnetisation. This is a result of strong interactions between the atoms known as exchange interactions which were first introduced by Heisenberg and Bloch. The details of these interactions will be discussed in the following chapters.

Ising model was the first attempt to express the interaction between atoms in the simplest way and the Hamiltonian of the system is defined as:

$$\mathscr{H} = -\frac{1}{2}\sum_{i\neq j} J_{ij} s_i s_j, \tag{2.7}$$

where s_i and s_j are the spins on sites i and j respectively, and J_{ij} is the exchange interaction between spins i and j. It should also be pointed out here that the exchange interaction J is taking place between the nearest neighbours of the system. As mentioned before, in the Ising model there are only two states allowed, thus $s_i = \pm 1$. In Fig. 2.3 it is shown the configuration of two neighbouring spin when $J > 0$ (ferromagnetic state) and $J < 0$ (antiferromagnetic state).

2.2.2 Heisenberg model

The Heisenberg model looks very similar to the previous simple magnetic model, Ising model. The difference between these two models is that the spins are here three-dimensional unit vectors ($|\vec{S}| = 1$) which means that they are allowed to rotate in any direction compared to the Ising model in which only two states are allowed. The Heisenberg model is defined in terms of the Heisenberg Hamiltonian which is:

$$\mathscr{H} = -\frac{1}{2}\sum_{i\neq j} J_{ij} \vec{S}_i \cdot \vec{S}_j, \tag{2.8}$$

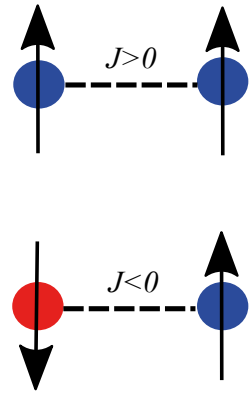

Figure 2.3. Configuration of spins under ferromagnetic ($J > 0$) and antiferromagnetic exchange ($J < 0$).

where $\vec{S}_i$ is the spin unit vector on site i and J_{ij} is the interaction between the i-th and j-th site. Usually the interaction between nearest neighbours is enough to describe most of the systems. This choice is valid because this interaction is related to the overlap of wavefunctions and as the distance is increased the value of J is decreasing rapidly and it can be neglected for second and third nearest neighbours. On the other hand, in some cases more long ranged interactions are needed to describe the material properly, where the second and the third neighbour interaction is important.

The interaction is between nearest neighbours only due to the fact that is related to the overlap of wavefunctions and as the distance is increased the value of J is decreasing rapidly and it can be neglected for second and third nearest neighbours.

2.2.3 Extended Heisenberg model

The simple Heisenberg Hamiltonian can be used in various cases to describe the magnetic properties of systems and materials, but sometimes only the Heisenberg exchange interaction is not enough to describe the system. For instance, in a system with a strong spin-orbit coupling, the magnetization is influenced and it cannot be described by only the Heisenberg exchange. The spin-orbit coupling results in the magnetocrystalline anisotropy and the anti-symmetric Dzyaloshinskii-Moriya interaction [21, 22] which gives a chiral magnetic configuration as a ground state.

According to the previous examples, is necessary to add more terms in the Heisenberg Hamiltonian to describe more complex systems. This Hamiltonian is called the extended Heisenberg Hamiltonian and is given by:

$$\mathscr{H} = -\frac{1}{2}\sum_{i\neq j} J_{ij}\vec{S}_i \cdot \vec{S}_j - \frac{1}{2}\sum_{i\neq j} \mathbf{D}_{ij}\vec{S}_i \times \vec{S}_j + K\sum_i (\vec{S}_i \cdot \hat{\mathbf{e}})^2 - \sum_i \mathbf{B}\cdot\vec{S}_i, \qquad (2.9)$$

where $\mathbf{D}_{ij}$ is the antisymmetric exchange interaction, the so-called Dzyaloshinskii-Moriya interaction [21, 22], K is the constant of uniaxial anisotropy where the magnetic easy axis is oriented along $\hat{\mathbf{e}}$ and $\mathbf{B}$ is the external magnetic field.

2.3 Magnetic ordering

All materials can be classified into two main categories depending on their magnetic properties: those which exhibit spontaneous magnetisation and those which do not. The materials which carry permanent magnetic moments, can be further categorised to the ones which result in a long-ranged order of the magnetic moments and the ones which do not have any order. A final classification of the magnetic materials is coming from the preferable configuration of their magnetic moments and this is called magnetic ordering of the material.

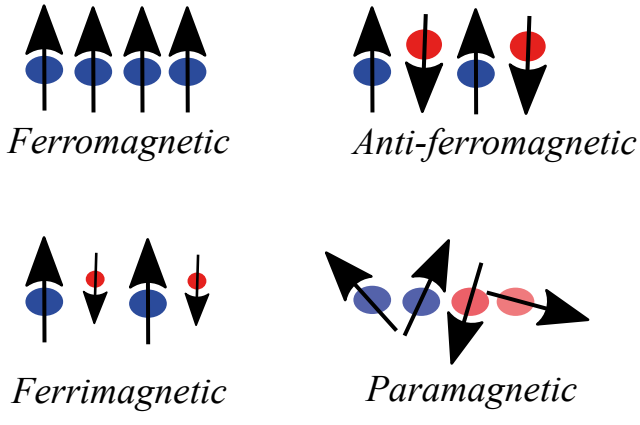

Figure 2.4. The main classification of the materials with spontaneous magnetisation. There are four cases according to their configuration: *ferromagnetic* (upper left panel), *anti-ferromagnetic* (upper right panel), *ferrimagnetic* (lower left panel) and *paramagnetic* (lower right panel).

There are four main types of magnetic ordering as illustrated in Fig. 2.4 which can be easily described by the simple Heisenberg model. The main

types of magnetic ordering are: the ferromagnetic, anti-ferromagnetic, ferrimagnetic and paramagnetic. The paramagnetic materials, despite the fact that they have magnetic moments, do not result in any long-range order without the presence of an external magnetic field. The exchange interaction J of those materials is very weak with respect to thermal energy. The moments are oriented in a random direction and as a consequence, there is no net magnetic moment. On the other hand, the strength of exchange interaction J in ferromagnetic materials is big enough and their magnetic moments are aligned parallel below a critical temperature. Some materials exhibit a long-range order but the total net magnetisation is zero and they called anti-ferromagnets. In anti-ferromagnets, there is a strong exchange interaction like in ferromagnets, and the only difference is the sign of J which in this case is negative. The negative J forces the magnetic moments to be aligned antiparallel and the system is considered to consist of two opposite sublattices which explains the zero net magnetisation. A similar case to anti-ferromagnets is the ferrimagnetics, where again the exchange interaction is negative but the two opposite sublattices have different net magnetic moments which results in performing a small net magnetisation and not zero as in the previous case.

The magnetic ordering of the ferrimagnets, anti-ferromagnets and ferromagnets as presented in Fig. 2.4, is valid up to a critical temperature T_c which is known as Curie temperature for the ferrimagnets and ferromagnets and Neel temperature for anti-ferromagnets. For example, a ferromagnet at $T = 0$ the total magnetisation along the aligned axis is maximum and as the temperature is increased in the system, the value of the magnetisation in decreasing. As the critical temperature is approached by keep increasing the temperature the magnetisation drops to zero and the system behaves like a normal paramagnet.

2.4 Non-collinear magnetism

As mentioned in the previous section, in collinear magnets (ferromagnets, anti-ferromagnets and ferrimagnets) the magnetic moments are pointing along a common magnetisation axis which usually is the $z-$axis for convenience. For ferromagnets the magnetic moments of the whole lattice are oriented on $+z-$axis, for anti-ferromagnets are oriented alternatively on $\pm z-$axis and the same for ferrimagnets with the difference that in $-z$ direction the length of the magnetic moment is smaller. However, there are plenty magnetic structures which do not belong in the category of collinear magnets and they are called non-collinear magnetic structures. In these structures, the direction of the magnetic moments is not along the same axis (e.g. $z-$axis) but it changes from site to site in the lattice. Even though that they have not been used much in applications, non-collinear magnets have been known for more than half a century [23, 24].

Non-collinear magnetism can be found in a variety of materials and usually in systems with frustrated anti-ferromagnetic interaction (e.g. triangular lattices), in systems with different exchange interactions between neighbours (e.g. fcc Fe) and in systems where different types of exchange interactions are competing each other (e.g. domain walls, skyrmions).

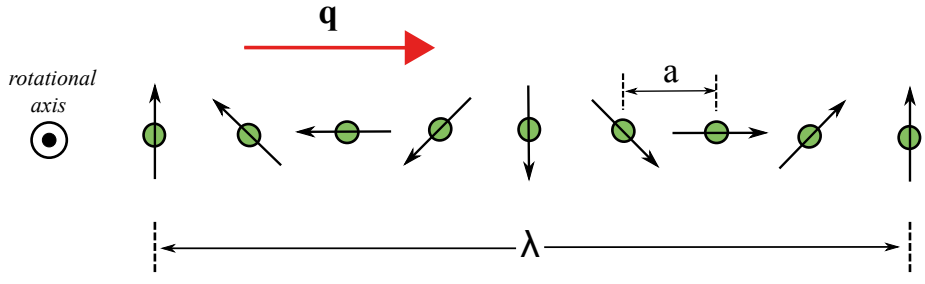

Figure 2.5. Schematic representation of one-dimensional spin-spiral configuration with a wavelength period λ, nearest neighbours distance a and out of plane rotational axis.

Chiral magnets (or spin spirals) belong to the general class of non-collinear magnets and their non-collinearity occurs from the broken inversion symmetry in the unit cell which in turn gives rise to the Dzyaloshinskii-Moriya interaction. A spin spiral is a periodic structure as can be seen from Fig. 2.5 where λ is the period. The magnetic moments are rotating around an axis who is fixed and is called rotation axis. In the case of Fig. 2.5 is out of plane. The spin spiral vector $\mathbf{q}$ is showing the direction of the spiral propagation and its length depends on the wavelength period λ. The units of the propagation vector $\mathbf{q}$ are given in $2\pi/a$, where a is the distance between the neighbouring magnetic moments (see Fig. 2.5). A spin spiral is given in cartesian coordinates [25],

$$\mathbf{m}(\mathbf{r}) = m(\mathbf{r})[cos\phi sin\theta, sin\phi sin\theta, cos\theta]. \tag{2.10}$$

The angle ϕ is defined as $\phi = \mathbf{q} \cdot \mathbf{R}$, where $\mathbf{q}$ is the propagation vector of the spin spiral and $\mathbf{R}$ is the lattice vector. θ is the azimuthal angle between $\mathbf{m}$ and the rotational axis. In our example of the one-dimensional spin spiral, the angle θ is equal to $\pi/2$ which means that the rotational plane of the magnetic moments is perpendicular to the rotational axis.

2.5 Landau-Lifshitz-Gilbert equation

The ground state properties of a magnetic system can be calculated by the extended Heisenberg Hamiltonian, but what happens when someone is interested to investigate the dynamics of a system? Then an equation of motion needs to be obtained in order to observe the dynamical behaviour of a magnetic system.

We will start from the simplest case where the magnetisation **M** is under the influence of an external magnetic field **B**. We have to mention here that the total field which is acting on the magnetisation is not exclusively coming from the external field but also from different interactions taking place in the material. If we want to be more precise, in the equation of motion an effective field $\mathbf{B}_{eff}$ should be included rather than just the external field **B**. The effective field is described by $\mathbf{B}_{eff} = -\partial\mathscr{H}/\partial\mathbf{M}$. $\mathscr{H}$ is the Hamiltonian of the system. The effective field now, exerts a torque and forces the magnetic moment to precess around the direction of the field (see left panel of Fig. 2.6):

$$\frac{d\mathbf{M}}{dt} = -\gamma\mathbf{M}\times\mathbf{B}_{eff}, \tag{2.11}$$

where γ is the gyromagnetic ratio.

From the equation (2.6) is given that the energy of the system is minimized if the magnetic moments are aligned with the effective field. According to the equation (4.8), the energy will not change since the motion of the moment is perpendicular to the field. Due to energy dissipation from the system an extra term is needed in order to damp the motion of **M** and eventually be aligned with the field (see right panel of Fig. 2.6). After adding this damping term, equation (4.8) becomes:

$$\frac{d\mathbf{M}}{dt} = -\gamma\mathbf{M}\times\mathbf{B}_{eff} - \gamma\frac{\lambda}{M_s}\mathbf{M}\times(\mathbf{M}\times\mathbf{B}_{eff}), \tag{2.12}$$

where M_s is the saturation magnetisation of the investigated system and λ is the damping term which is expressing the dissipative energy. The equation (2.12) is the famous Landau-Lifshitz (LL) equation [13], which describes the damped motion of magnetic moment under the influence of a field.

Later, Gilbert modified the Landau-Lifshitz equation of motion and introduced another form of the same equation where the time derivative of magnetisation is inserted in the right hand side of equation (2.12) and this new equation of motion is called Landau-Lifshitz-Gilbert (LLG) equation of motion [14]:

$$\frac{d\mathbf{M}}{dt} = -\frac{\gamma}{1+\alpha^2}\mathbf{M}\times\mathbf{B}_{eff} + \frac{\alpha}{M_s}\mathbf{M}\times\frac{d\mathbf{M}}{dt}, \tag{2.13}$$

where α is the Gilbert damping. Both LL and LLG equations are giving the same results in the case of very small damping ($\alpha \ll 1$), nevertheless larger values of damping are described more realistic by the LLG equation and this is one reason that it is used more often.

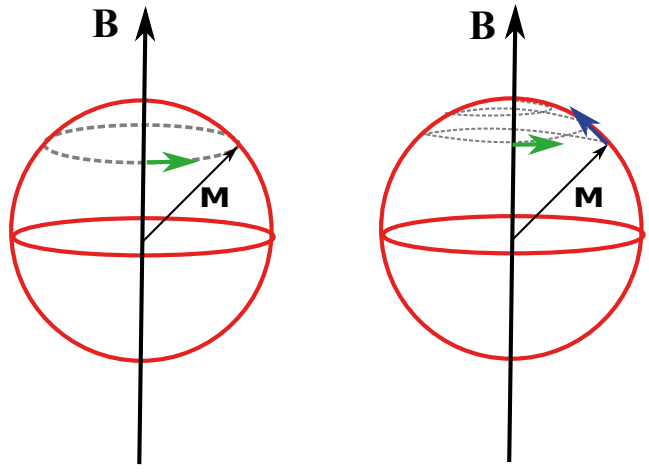

Figure 2.6. Schematic representation of magnetic moment under the influence of magnetic field only with the precession (left panel) and both precession and damping (right panel). The green arrow indicates the precession and blue the damping.

3. Density functional theory (DFT)

For the improvement of technology, the discovery of new materials is needed which is not an easy task and a deeper understanding of several phenomena is necessary. As we are scaling down in size the use of quantum mechanics for the study of these materials becomes unidirectional. Electronic properties of solids are crucial for the prediction of their behaviour but the calculation of these properties is rather complicated since the atomic nuclei and the electrons compose a very difficult many-body problem which is impossible to be solved analytically for many-electron systems. A very good method for solving this problem is the density functional theory (DFT) which is a first-principle method and reduces the many-body problem into finding the electron density $n(\mathbf{r})$, which is the key variable. To accomplish that, the DFT starts by adopting the Born-Oppenheimer approximation [26], which neglects the motion of the nuclei and they considered to be frozen. The interaction between the nuclei and the electrons is replaced by an effective potential. DFT is a very powerful tool since it is very accurate and the properties of the solids can be calculated by the knowledge of atomic number and the structure of the elements.

3.1 The many body problem

The main problem for the description of material properties is the treatment of interactions taking place between many particles, like many-electron atoms, molecules and bulk materials. Actually is impossible to solve analytically the quantum equations and various approximations are needed.

All the solid state systems consist of nuclei and electrons which all interact via the Coulomb force. The many-body Hamiltonian describing all the interactions of such systems is given by:

$$\mathscr{H} = \hat{T}_n + \hat{T}_e + \hat{V}_{nn} + \hat{V}_{ee} + \hat{V}_{ne}, \tag{3.1}$$

where $\hat{T}_n$ and $\hat{T}_e$ are the kinetic energies of the nuclei and the electrons respectively, while $\hat{V}_{nn}$, $\hat{V}_{ee}$ and $\hat{V}_{ne}$ are the Coulomb interactions between the electrons, the nuclei and the electrons with the nuclei repsectively. By substituting these terms in the Hamiltonian it can be written as:

$$\mathscr{H} = -\frac{\hbar^2}{2M_i}\sum_i \nabla_i^2 - \frac{\hbar^2}{2m}\sum_k \nabla_k^2 + \frac{1}{2}\sum_{i\neq j}\frac{Z_i Z_j e^2}{|R_i R_j|} + \frac{1}{2}\sum_{l\neq k}\frac{e^2}{|r_k - r_l|} - \sum_{k,i}\frac{Z_i e^2}{|r_k - R_i|} \tag{3.2}$$

where M is the nuclei mass, m is the electron mass, R the coordinates of the nucleus, r coordinates of electrons and Z the atomic number. As previously mentioned, with the Bohr-Oppenheimer approximation, the nuclei of the system are treated as being stationary because of their big mass compare to the electrons mass ($M \ll m$). Considering this approximation the first and the third term of the Hamiltonian can be neglected and the Coulomb interaction between the nuclei and the electrons is represented by an external potential $\hat{V}_{ext}$ which is interacting with the electrons of the system. After this approximation, the Hamiltonian reads:

$$\mathscr{H} = -\frac{\hbar^2}{2m}\sum_k \nabla_k^2 + \frac{1}{2}\sum_{l\neq k}\frac{e^2}{|r_k - r_l|} + \hat{V}_{ext}. \tag{3.3}$$

3.2 Density Functional Theory

The basic idea under the DFT is to use the electron density instead of the electron wavefunction and the first theoretical step for the DFT was given by Hohenberg and Kohn [27]. In the work of Hohenberg and Kohn two theorems are proven which state:

Theorem I: *For any system of interacting particles in an external potential $V_{ext}(\mathbf{r})$, the density is uniquely determined.*

Theorem II: *A universal functional for the energy $E[n]$ can be defined in terms of the density. The exact ground state is the global minimum value of this functional.*

According to the above theorems the energy functional can be written as:

$$E[n(\mathbf{r})] = F[n(\mathbf{r})] + \int V_{ext}(\mathbf{r})n(\mathbf{r})d^3r, \tag{3.4}$$

where the functional $F[n(\mathbf{r})]$ is independent from $V_{ext}(\mathbf{r})$ and includes the kinetic energy and the interaction between electrons.

3.3 Kohn-Sham equations

Kohn and Sham have been shown an ansatz [28] in which they simplify the many-body problem to an effective non-interacting single particle problem by using the same ground state electron density $n_0(\mathbf{r})$. The Schrödinger equation —from here is called Kohn-Sham equation— with this approach becomes:

$$\left(-\frac{\hbar^2}{2m}\nabla^2 + V_{eff}(\mathbf{r})\right)\psi_i(\mathbf{r}) = \varepsilon_i\psi_i(\mathbf{r}) \tag{3.5}$$

where ε_i are the Khon-Sham eigenvalues, ψ_i are the Kohn-Sham orbitals and $V_{eff}(\mathbf{r})$ is the effective potential:

$$V_{eff}(\mathbf{r}) = V_{ext}(\mathbf{r}) + \int d^3r' \frac{2n(\mathbf{r})}{|\mathbf{r}-\mathbf{r}'|} + V_{xc}(\mathbf{r}). \tag{3.6}$$

$V_{ext}(\mathbf{r})$ is the potential generated by the nuclei, the second term is the electron-electron interaction and $V_{xc}(\mathbf{r})$ is the exchange-correlation potential which includes all the many-body effects. The relation between the ground state electron density and the wavefunctions which are solutions of equation (3.5) is

$$n(\mathbf{r}) = \sum_{i=1}^{N} |\psi_i(\mathbf{r})|^2, \tag{3.7}$$

N is the number of the eigenstates. To complete the simplification of many-body problem a last challenge remains, to approximate the $V_{xc}(\mathbf{r})$ in order to make DFT accurate. In the following section we will briefly mention the two main approximations for the exchange-correlation potential.

3.4 Local and non-local density approximations

In order to use the Kohn-Sham approach to find the ground properties of the system we investigate, an approximation for finding the exchange-correlation potential $V_{xc}(\mathbf{r})$ is needed. The most common is the so-called local density approximation (LDA) [29, 30] which assumes that the exchange-correlation potential is the one of a homogeneous electron gas and it depends on the charge density at each point in space. LDA is very successful in systems where a smooth variation of $n(\mathbf{r})$ is present but surprisingly it works very well also for systems with inhomogeneous electron density.

Despite the fact that LDA is very successful, an improved approach was necessary to describe systems where the LDA is failing. The improved approach is called Generalised Gradient Approximation (GGA) [31] which is taking into account not only the homogeneous electron density but also its local gradient (∇n). By using the GGA, the ionization and binding energies are improved. Both of the previous approaches fail to describe the ground state properties of strongly correlated systems and some other corrections are required such as LDA+U [32, 33] and dynamical mean field theory (DMFT) [33, 34] which improve the band gaps in insulators [35].

3.5 Spin polarised systems

The Kohn-Sham equations as introduced above are not able to describe magnetic systems since they are not taking into consideration the spin degree of

freedom. However, an extension of LDA introduced by von Barth and Hedin [36] gives the opportunity to handle spin polarised densities within DFT. This approach is known as local spin density approximation (LSDA).

In order to introduce the spin into the Kohn-Sham equations, a spin dependent exchange-correlation potential is needed. To achieve that, the electron density $n(\mathbf{r})$ has to be replaced by the generalised density matrix $p(\mathbf{r})$:

$$p(\mathbf{r}) = \frac{n(\mathbf{r})}{2}\mathbf{l} + \frac{\mathbf{m}(\mathbf{r})}{2}\sigma, \tag{3.8}$$

where $\mathbf{l}$ is the 2×2 unit matrix, $\mathbf{m}(\mathbf{r})$ is the magnetisation density and $\sigma = (\sigma_x, \sigma_y, \sigma_z)$ are the Pauli matrices. The wavefunctions now are in the form of spinors

$$\psi_i(\mathbf{r}) = \begin{pmatrix} \alpha_i(\mathbf{r}) \\ \beta_i(\mathbf{r}) \end{pmatrix}. \tag{3.9}$$

The spin projections are represented by $\alpha_i(\mathbf{r})$ and $\beta_i(\mathbf{r})$ and the density matrix becomes

$$p(\mathbf{r}) = \sum_{i=1}^{N} \begin{pmatrix} |\alpha_i(\mathbf{r})|^2 & \alpha_i(\mathbf{r})\beta_i(\mathbf{r})^* \\ \alpha_i(\mathbf{r})^*\beta_i(\mathbf{r}) & |\beta_i(\mathbf{r})|^2 \end{pmatrix}. \tag{3.10}$$

By the use of density matrix, one can describe the electron and magnetisation density:

$$n(\mathbf{r}) = Tr[p(\mathbf{r})] = \sum_{i=1}^{N} |\psi_i(\mathbf{r})|^2 \tag{3.11}$$

$$\mathbf{m}(\mathbf{r}) = \sum_{i=1}^{N} \psi_i(\mathbf{r})^{\dagger} \sigma(\mathbf{r}) \psi_i(\mathbf{r}). \tag{3.12}$$

N is the number of states in the system. Similar to the electronic density expansion to 2×2 matrix, the Hamiltonian has to be expanded as well to a matrix in order to express the spin dependent part. This means that kinetic energy and effective potential are written in form of spinors by generalising first the Kohn-Sham equation:

$$\sum_{\beta=1}^{2} \left[-\delta_{\alpha\beta}\nabla^2 + V_{eff}^{\alpha\beta}(\mathbf{r}) \right] \psi_{i\beta}(\mathbf{r}) = \varepsilon_i \delta_{\alpha\beta} \psi_{i\beta}(\mathbf{r}). \tag{3.13}$$

The Hamiltonian of the system can be separated to a magnetic and non-magnetic, which is written as follows:

$$\mathscr{H} = \sum_{\beta=1}^{2} \left[-\nabla^2 \delta_{\alpha\beta} + V_0^{\alpha\beta}(\mathbf{r}) + (\mathbf{B}_{eff}(\mathbf{r}) \cdot \sigma) \right], \tag{3.14}$$

where $V_0^{\alpha\beta}(\mathbf{r})$ is the non-magnetic potential and $\mathbf{B}_{eff}(\mathbf{r}) \cdot \sigma$ is the magnetic one.

3.6 Relativistic electrons

Spin and orbital angular momentum of electrons are the origins of magnetism in solids. In the non-relativistic Schrödinger equation only the spin angular momentum is taken into account and then, Dirac proposed an equation in which beside the magnetic part (spin angular momentum) is taking into account relativistic effects [37] as well. In the relativistic density functional theory (RDFT), the ground state energy of the system (E') is a functional of the four component current, $j^{\mu}(\mathbf{r})$ and it can be written:

$$E'[j^{\mu}] = T_s[j^{\mu}] + E_{ext}[j^{\mu}] + E_H[j^{\mu}] + E_{xc}[j^{\mu}], \tag{3.15}$$

where $T_s[j^{\mu}]$ is the kinetic energy of the system, $E_{ext}[j^{\mu}]$ is the external potential energy, $E_H[j^{\mu}]$ is the Hartree energy and $E_{xc}[j^{\mu}]$ is the exchange-correlation energy.

The Dirac equation is expressed as:

$$E'\Psi = \mathscr{H}_D\Psi \tag{3.16}$$

and the Hamiltonian is given by:

$$\mathscr{H}_D = -eV(\mathbf{r}) + \beta mc^2 + \alpha \cdot (c\mathbf{p} + e\mathbf{A}(\mathbf{r})). \tag{3.17}$$

In the above Hamiltonian, c is the speed of light in the vacuum, $\mathbf{p}$ is the momentum operator, m is the mass of the electron, V is the external scalar potential and $\mathbf{A}(\mathbf{r})$ is a vector potential. α is a 4×4 matrix and is equal to:

$$\alpha_i = \begin{pmatrix} 0 & \sigma_i \\ \sigma_i & 0 \end{pmatrix} \tag{3.18}$$

where σ_i are the Pauli matrices. β is also a 4×4 matrix:

$$\beta = \begin{pmatrix} \mathbf{1} & 0 \\ 0 & -\mathbf{1} \end{pmatrix} \tag{3.19}$$

and the unit entries of β are 2×2 matrices.

The wavefunction Ψ, is a four component wave function and it can be written as a two-vector, large and small components ψ and χ. For these two components we end up in the equations:

$$\left(E' - mc^2 + eV(\mathbf{r})\right)\psi = \sigma \cdot (c\mathbf{p} + e\mathbf{A}(\mathbf{r}))\,\chi \tag{3.20}$$

$$\left(E' + mc^2 + eV(\mathbf{r})\right)\chi = \sigma \cdot (c\mathbf{p} + e\mathbf{A}(\mathbf{r}))\,\psi \tag{3.21}$$

where E' is the energy of eq. (3.16). By making an approximation for χ and then insert it in (3.20) it gives the following:

$$\begin{aligned}[E+eV(\mathbf{r})-\frac{1}{2m}\left(\mathbf{p}(\mathbf{r})+\frac{e}{c}\mathbf{A}(\mathbf{r})\right)^2+\frac{1}{2mc^2}\left(E+eV(\mathbf{r})\right)^2 \\ +i\frac{e\hbar}{(2mc)^2}\mathbf{E}(\mathbf{r})\cdot\mathbf{p}-\frac{e\hbar}{(2mc)^2}\sigma\cdot(\mathbf{E}(\mathbf{r})\times\mathbf{p})-\frac{e\hbar}{2mc}\sigma\cdot\mathbf{B}(\mathbf{r})]\psi=0.\end{aligned} \tag{3.22}$$

Here, the electric field $\mathbf{E}$ is the gradient of the potential V, the magnetic field $\mathbf{B}$ is the curl of $\mathbf{A}$ and $E = E' - mc^2$. The first three terms represent the non-relativistic Hamiltonian, the fourth is the correction to the kinetic energy and the fifth is the Darwin term. The two later terms do not include spin matrices and they are called scalar relativistic terms. The two last terms of eq. (3.22) describe the interaction of spins with the magnetic field and more specific the last one is the Zeeman term.

The sixth term of the above equation is the spin-orbit interaction and if we consider a spherically symetric potential, $V(r)$, this term can be rewritten as:

$$\sigma\cdot(\mathbf{E}(\mathbf{r})\times\mathbf{p})=\sigma\cdot(\nabla V(r)\times\mathbf{p})=\frac{1}{r}\frac{dV(r)}{dr}\sigma\cdot(\mathbf{r}\times\mathbf{p})=\frac{1}{r}\frac{dV(r)}{dr}(\sigma\cdot\mathscr{L})=\xi\sigma\cdot\mathscr{L}, \tag{3.23}$$

where where ξ is the spin-orbit coupling constant and $\mathscr{L}$ is the orbital angular momentum. In transition metal compounds, since the spin-orbit coupling constant is much smaller than the band energy, the spin-orbit coupling term is introduced as a perturbation. The relativistic description of the DFT gives the opportunity to describe phenomena which cannot be done by the non-relativistic DFT such as Dzyaloshinskii-Moriya interaction and magneto-crystalline anisotropy.

3.7 Korringa-Kohn-Rostoker approach

The Korringa-Kohn-Rostoker method (KKR) is a multiple-scattering method for the calculation of material's electronic structure. It was introduced by Korringa in 1947 [15] and by Kohn and Rostoker in 1954 [16]. Within this method, the solutions of Kohn-Sham equations (3.5) are based on green's function $G(E,\mathbf{r},\mathbf{r}')$. The first step in this approach is to obtain the scattering properties of each atom and afterwards the multiple-scattering of all atoms is determined. In order to fullfill the second step, the sum of the outgoing waves from each atom is equal to the incident wave. The potential around the atoms is considered spherical within the Wigner-Seitz cell, in other words the atomic sphere approximation (ASA) is used.

The Green's function is defined as:

$$(E-\mathscr{H})G(E,\mathbf{r},\mathbf{r}')=\delta(\mathbf{r}-\mathbf{r}'), \tag{3.24}$$

where $\mathscr{H}$ is the Hamiltonian and E is the energy. The relation between the unperturbed Green's function $G_0(E)$, which is used for the free electron, and the perturbed Green's function $G(E)$ is given by the use of Dyson equation. If the solution of eq. (3.24) is G_0 for the unperturbed $\mathscr{H}_0$, the Green's function G for the perturbed system $\mathscr{H}=\mathscr{H}_0+\Delta V$ is written as:

$$\begin{aligned} G(E) &= G_0(E)+G_0(E)\Delta V G(E) \\ &= G_0(E)+G_0(E)TG_0(E), \end{aligned} \tag{3.25}$$

where T is the $T-$operator and is related to the perturbation ΔV by $TG_0(E)=\Delta V G(E)$. The $T-$operator, is taking into account all the scattering properties of the entire system:

$$T(E)=\sum_{ij}\tau_{ij}(E), \tag{3.26}$$

where

$$\tau_{ij}(E)=t_i(E)\delta_{ij}+t_i(E)\sum_{k\neq i}G_0^{ik}(E)\tau_{kj}(E). \tag{3.27}$$

The scattering path operator τ_{ij} transfers a wave at site i to a wave at site j and takes into account all the possible paths. The τ-matrix can be rewritten as:

$$\tau=\left(t^{-1}-G_0\right)^{-1}, \tag{3.28}$$

which is the fundamental equation of multiple scattering theory.

3.8 Calculation of exchange interactions

From ab-initio calculations it is possible to estimate the exchange interaction J_{ij} between two magnetic atoms and use it in our Hamiltonian. There are two methods of calculating the exchange interaction, one is the frozen magnon approximation [38, 39] and the other one is the real space method by using the Liechtenstein-Katsnelson-Antropov-Gubanov (LKAG) formula [17, 18] based on the multiple scattering theory (MST). The later is the approach which is used in the KKR method [40] and extract the parameters we need. In the later approach, the J_{ij} parameter is obtained from a small angle perturbations from the reference state which usually is ferromagnetic and the differences in energy are calculated by using the local force theorem:

$$
\begin{aligned}
J_{ij} &= -\frac{1}{\pi}\Im\int_{-\infty}^{\varepsilon_F} Tr_L\left\{(t_{i\uparrow}^{-1}-t_{i\downarrow}^{-1})\tau_{ij}(t_{j\uparrow}^{-1}-t_{j\downarrow}^{-1})\tau_{ji}\right\}d\varepsilon \\
&= \frac{1}{\pi}\Im\int_{-\infty}^{\varepsilon_F} Tr\left\{\left[\hat{n}_i\cdot\hat{\sigma},t_i^{-1}\right]\tau_{ij}\left[\hat{n}_j\cdot\hat{\sigma},t_j^{-1}\right]\tau_{ji}\right\}d\varepsilon.
\end{aligned}
\tag{3.29}
$$

In the above equation, ε_F is the Fermi energy, τ_{ij} is the scattering path operator, t is the perturbed single-site scattering matrix. Since Eq. (3.29) is obtained for a small angle deviation around the rotational axis $\hat{n}_i$ from the reference state, it means that is more accurate for small values of temperature than temperatures close to Curie temperature where the angles are larger and make LKAG formula less accurate. We have to note here that in the non-relativistic ferromagnetic case the rotational axis $\hat{n}_i$ is the $\hat{y}$. It is worth mentioning here that the approach discussed before, about calculating the exchange parameter, does not make any assumptions about the nature of the exchange if it is a direct exchange, RKKY or super-exchange.

Collinear magnetic materials and in some cases non-collinear order (e.g. systems with frustration in exchange interaction J) are understood well within the Heisenberg model but on the other hand materials with non-collinear magnetic ordering due to broken inversion symmetry cannot be defined by the same model. To describe the later magnetic systems a new term has to be added in the magnetic Hamiltonian and this was first introduced by Dzyaloshinskii [21] and Moriya [22] who proposed that this interaction comes from the symmetry of the lattice where some symmetry rules have to be fulfilled. This new term is called Dzyaloshinskii-Moriya interaction and enters in the Hamiltonian as:

$$
\mathscr{H}_{DM} = -\frac{1}{2}\sum_{i,j}\mathbf{D}_{ij}\cdot\hat{m}_i\times\hat{m}_j \tag{3.30}
$$

where $\mathbf{D}_{ij}$ is the DM vector and $\hat{m}$ is the unit vector of the magnetic moment.

In order to calculate DM interaction from ab-initio calculations, a generalisation of the LKAG formula is necessary. As mentioned before the LKAG formula is non-relativistic and the origin of DM interaction is the spin-orbit coupling which has to be introduced in LKAG formalism and end up with a relativistic expression. A technique developed by Udvardi *et al* [41] made possible to map the generalised exchange interaction in the Hamiltonian and Ebert and Mankovsky [42] developed an alternative method for the general expression of exchange coupling. In the last case the general form of the exchange coupling is:

$$
\mathscr{H}_{ex} = -\frac{1}{2}\sum_{i,j}\hat{m}_i\underline{\underline{J}}_{ij}\hat{m}_j, \tag{3.31}
$$

where $\underline{\underline{J}}_{ij} = J_{ij}\mathbf{1} + \mathbf{S}_{ij} + \mathbf{A}_{ij}$ is the exchange coupling tensor. The trace of the tensor is the scalar Heisenberg exchange J_{ij} as introduced before and the antisymmetric part $\mathbf{A}_{ij}$ of this tensor is the DM interaction. The difference between these two interactions is that the first one there is only one axis of rotation and in the case of DM interaction there are two ($\hat{n}^1$ and $\hat{n}^2$). The expression of the exchange coupling is given from:

$$J_{ij}^{a_i a_j} = \frac{1}{\pi}\Im \int_{-\infty}^{\varepsilon_F} Tr\left\{ \left[\hat{n}_i^{a_i}\cdot\mathbf{J}, t_i^{-1}\right] \tau_{ij} \left[\hat{n}_j^{a_j}\cdot\mathbf{J}, t_j^{-1}\right] \tau_{ji} \right\} d\varepsilon. \tag{3.32}$$

$\mathbf{J}$ is the total angular momentum and $a = 1,2$ specifies the rotation axis.

4. Atomistic spin dynamics

Micromagnetism uses the LLG equation (Eq. 2.13) which has been introduced earlier to study the magnetisation dynamics in micrometers scale in order to understand the magnetization dynamics. This approach is very successful but it suffers from some limitations. The main limitation is that the ground state properties from first-principles calculations can be directly mapped into the micromagnetic Hamiltonian. Another limitation of this method is the incapability of capturing rapidly fluctuations of magnetic textures in space. Atomistic spin dynamics approach tries to fill the gap and connect the electronic structure of the material with the dynamical response of the magnetization [43]. Thus, the atomistic spin dynamics approach provides us with the possibility to study the dynamics with different chemical compositions and complex magnetic ordering.

4.1 Atomistic equations of motion

In the previous chapter, the spin polarised Kohn-Sham equations were introduced in order to describe magnetic systems. However, those equations describe time-independent systems and in order to allow for a description of the dynamics of the magnetic systems, time should be included in the equation. By neglecting the spin-orbit coupling the time-dependent Kohn-Sham Hamiltonian becomes [43]:

$$\mathscr{H}^{KS}_{\alpha\beta} = \sum_{\beta=1}^{2} \left[-\nabla^2 \delta_{\alpha\beta} + V_0(\mathbf{r},t)\delta_{\alpha\beta} + (\sigma \cdot \mathbf{B}^{eff}(\mathbf{r},t))_{\alpha\beta} \right]. \tag{4.1}$$

The first term of the Hamiltonian is the kinetic term, the second term is the non-magnetic part of the potential and the third term the magnetic part of the potential.

The time-dependent charge and spin density are defined as $n(\mathbf{r},t) = \psi^{\dagger}(\mathbf{r},t)$ $\psi(\mathbf{r},t)$ and $s(\mathbf{r},t) = \psi^{\dagger}(\mathbf{r},t)\hat{S}\psi(\mathbf{r},t)$ respectively where $\hat{S}$ is the spin operator. Now, the Schrödinger KS equation can be written as:

$$i\frac{\partial \psi(\mathbf{r},t)}{\partial t} = \mathscr{H}^{KS}\psi(\mathbf{r},t) \tag{4.2}$$

and

$$-i\frac{\partial \psi^{\dagger}(\mathbf{r},t)}{\partial t} = \left[\mathscr{H}^{KS}\psi(\mathbf{r},t)\right]^{\dagger}. \tag{4.3}$$

By using the charge density as defined above, we are able to express straightforwardly the time evolution of it:

$$\begin{aligned}
\frac{\partial n(\mathbf{r},t)}{\partial t} &= \frac{\partial}{\partial t}[\psi^{\dagger}(\mathbf{r},t)\psi(\mathbf{r},t)] \\
&= \psi^{\dagger}(\mathbf{r},t)\frac{\partial \psi(\mathbf{r},t)}{\partial t} + \frac{\partial \psi^{\dagger}(\mathbf{r},t)}{\partial t}\psi(\mathbf{r},t) \\
&= \frac{1}{i}[\psi^{\dagger}(\mathbf{r},t)\mathscr{H}^{KS}\psi(\mathbf{r},t) - [\mathscr{H}^{KS}\psi(\mathbf{r},t)]^{\dagger}\psi(\mathbf{r},t)] \\
&= \frac{1}{i}\nabla\cdot\left[[\nabla\psi^{\dagger}(\mathbf{r},t)]\psi(\mathbf{r},t) - \psi^{\dagger}(\mathbf{r},t)\nabla\psi(\mathbf{r},t)\right] \\
&= -\nabla\cdot\mathbf{Q}_n^{KS},
\end{aligned} \tag{4.4}$$

where $\mathbf{Q}_n^{KS}$ is the charge current density and is defined as:

$$\mathbf{Q}_n^{KS} = \frac{1}{i}\left[\psi^{\dagger}(\mathbf{r},t)[\nabla\psi(\mathbf{r},t)] - [\nabla\psi^{\dagger}(\mathbf{r},t)]\psi(\mathbf{r},t)\right]. \tag{4.5}$$

Similar to the time evolution of charge density we can calculate the time evolution of spin density $s(\mathbf{r},t) = \psi^{\dagger}(\mathbf{r},t)\hat{S}\psi(\mathbf{r},t)$ as well.

$$\begin{aligned}
\frac{\partial s(\mathbf{r},t)}{\partial t} &= \frac{\partial}{\partial t}[\psi^{\dagger}(\mathbf{r},t)\hat{S}\psi(\mathbf{r},t)] \\
&= \psi^{\dagger}(\mathbf{r},t)\hat{S}\frac{\partial \psi(\mathbf{r},t)}{\partial t} + \frac{\partial \psi^{\dagger}(\mathbf{r},t)}{\partial t}\hat{S}\psi(\mathbf{r},t) \\
&= \frac{1}{i}[\psi^{\dagger}(\mathbf{r},t)\hat{S}\mathscr{H}^{KS}\psi(\mathbf{r},t) - [\mathscr{H}^{KS}\psi(\mathbf{r},t)]^{\dagger}\hat{S}\psi(\mathbf{r},t)] \\
&= \frac{1}{2i}\left[[\hat{S}\nabla\psi^{\dagger}(\mathbf{r},t)]\psi(\mathbf{r},t) - \psi^{\dagger}(\mathbf{r},t)\hat{S}\nabla\psi(\mathbf{r},t)\right] - \gamma\mathbf{s}\times\mathbf{B}^{eff} \\
&= -\nabla\cdot\mathbf{Q}_s^{KS} - \gamma\mathbf{s}\times\mathbf{B}^{eff},
\end{aligned} \tag{4.6}$$

where $\mathbf{B}^{eff}$ is the magnetic part of the KS equation and $\mathbf{Q}_s^{KS}$ is the spin current density which is defined as:

$$\mathbf{Q}_s^{KS} = \frac{1}{2i}\left[[\hat{S}\nabla\psi^{\dagger}(\mathbf{r},t)]\psi(\mathbf{r},t) - \psi^{\dagger}(\mathbf{r},t)\hat{S}\nabla\psi(\mathbf{r},t)\right], \tag{4.7}$$

and the term $\nabla\cdot\mathbf{Q}_s^{KS}$ defines the spin current process in the magnetic system.

To solve the time dependent KS equation is rather complicated, but by using some approaches the equation can be separated and keep the part of main interest. The first step is to use the adiabatic approximation. As introduced

earlier in Chapter 3, the most famous adiabatic approximation is the Bohr-Oppenheimer approximation where the ions are considered as slow variables because of their big mass and on the other hand the electrons are considered fast variables because of their small mass. Similar to the previous example, the adiabatic approximation allows us to separate the equation of motion atomic spins and the equation of motion of electrons, where the first one is the slower variable and the second one the faster. In our case the separation is not made possible because of the difference in masses, like Bohr-Oppenheimer approximation, but due to their difference in energy. The excitation energies of the direction of magnetisation are of the order of meV and the energies of electronic structure are of the order of eV. This approach allows us to put aside the time evolution of charge density which then is represented as a potential for the effective magnetic field that will perform a torque on the magnetisation. Thus, our interest is focused on the equation (4.6) which contains two terms: the first one is the contribution of spin currents in the equation of motion of spins, and the second one is the precession of spins under the influence of an effective field. However, the contribution of spin current is neglected in atomic moment approximation which postulates very small fluctuations of the atomic moment length [44]. The spin current term attracts the attention when one tries to describe the very important effect of spin transfer torque (STT) [8, 7, 45] which will be described later in this chapter.

After the adiabatic approximation discussed above, a second simplification is introduced, the so-called atomic moment approximation (AMA). By using the atomic moment approximation, space is separated into spheres where each sphere is located on a magnetic atom. If the spin density of magnetic atom on site i is integrated over this sphere, then the total spin is related to the atomic magnetic moment and we can do the replacement $\mathbf{s}(\mathbf{r},t) \rightarrow \mathbf{m}_i(t)$ [44].

By neglecting the spin current and using the atomic moment approximation from equation (4.6) we end up in:

$$\frac{d\mathbf{m}_i}{dt} = -\gamma \mathbf{m}_i \times \mathbf{B}^i_{eff}(\mathbf{r},t). \tag{4.8}$$

The above equation of motion, which comes from the time-dependent Kohn-Sham equation, has the same form of the precessional motion as in the widely used LLG equation of motion.

The equation (4.8) would be valid in an ideal case where the spin system is completely isolated and it doesn't exchange any energy with the lattice or the environment. Of course, this is not true and the atomic magnetic moment can relax by dissipating energy and angular momentum to the surrounding, and on top of that the moments respond to changes in applied external fields. Thus, the mechanism which describes the dissipation of the energy and angular momentum and resulting in a damped motion of atomic magnetic moment can be expressed by an additional term as introduced by Gilbert. By introducing the damping term the equation (4.8) in LL form becomes:

$$\frac{d\mathbf{m}_i}{dt} = -\frac{\gamma}{1+\alpha^2}\mathbf{m}_i \times \mathbf{B}^i_{eff}(\mathbf{r},t) - \frac{\gamma\alpha}{(1+\alpha^2)m}\mathbf{m}_i \times (\mathbf{m}_i \times \mathbf{B}^i_{eff}(\mathbf{r},t)), \quad (4.9)$$

where α is the damping coefficient, $\mathbf{m}_i$ is the atomic magnetic moment on site i and $\mathbf{B}^i_{eff}$ is the effective field acting on the magnetic moment.

4.2 Langevin dynamics

In the previous section, the precession and the damping term of the LLG equation for atomic magnetic moments have been shown (Eq. 4.9). This equation can now be used to combine the description of the magnetization dynamics with results from first principles calculations. The derivation in the previous section was done by considering zero temperature but the behaviour of magnetic systems at finite temperature is of course of great interest. Thus, temperature effects should also be included in the equation of motion. In this work we use Langevin dynamics which is used to simulate the temperature effects as a stochastic field [46] which exerts a stochastic torque on the atomic moment apart from precession and damping torque. By redefining the effective field of the equation of motion we are able to include the stochastic field:

$$\mathbf{B}^i_{eff} = \mathbf{B}^i_{eff} + \mathbf{b}(t), \quad (4.10)$$

where $\mathbf{b}(t)$ is the stochastic field.

The stochastic fields are fluctuating fields with a Gaussian distribution which is modelled as white noise. In principle, with the choice of white noise the stochastic fields are uncorrelated in time and in each of the directions. This is expressed by satisfying the following criteria:

$$\langle \mathbf{b}(t) \rangle = 0 \quad (4.11)$$

$$\langle \mathbf{b}_i(t)\mathbf{b}_j(t') \rangle = 2D\delta_{ij}\delta(t-t') \quad (4.12)$$

$$D = \frac{\alpha}{(1+\alpha^2)}\frac{k_B T}{\mu_B m}. \quad (4.13)$$

The first of the criteria shows that the time average of the stochastic field is zero. In second criterion (Eq. 4.12), the Dirac delta ($\delta(t-t')$) denotes that the stochastic field is uncorrelated in time, while the Kronecker delta (δ_{ij} where $i = \{x,y,z\}$) express that is uncorrelated in space. D is the strength of the stochastic field which is related to the temperature T as we can see from equation (4.13) [47]. The fluctuation strength (D) and the relaxation are correlated to each other and it comes from the main statement of the fluctuation-dissipation theorem [48, 49].

By adding the stochastic field to equation (4.9) we arrive at a stochastic Landau-Lifshitz-Gilbert (SLLG) equation:

$$\frac{d\mathbf{m}_i}{dt} = -\frac{\gamma}{1+\alpha^2}\left[\left(\mathbf{m}_i \times (\mathbf{B}^i_{eff} + \mathbf{b}^i(t))\right) + \frac{\alpha}{m}\mathbf{m}_i \times \left(\mathbf{m}_i \times (\mathbf{B}^i_{eff} + \mathbf{b}^i(t))\right)\right], \tag{4.14}$$

where the stochastic field is both included in the precession term and the damping term.

4.3 Current driven magnetisation dynamics

It has been found that the magnetisation dynamics of a system is influenced by the presence of spin polarised currents. The description of this effect was first predicted from Berger [8, 19, 20] and followed by Slonczewski [7] who showed that is possible to reverse the magnetisation in a magnetic multilayered system by a spin polarised current. This phenomena is called spin transfer torque (STT) and arises from the exchange of angular momentum between the electron of the current and the magnetic moments. This discovery has opened up a new discussion about innovational device applications such as magnetic random access memory (MRAM) or high density recording media [9]. The main advantage over using external fields in switching magnetisation is the reduced power electrical consumption.

If a spin polarised current is flowing in the magnetic material and the spins of the electrons are aligned with the local magnetisation there is no exchange of angular momentum and the electrons travel unperturbed. On the other hand, if there is a smooth variation of the magnetization, the spins of the electron current and the local magnetic moments will try to align and a transfer of angular momentum takes place. Because of the exchange interaction, a rotation of the magnetic moment occurs and the magnetic texture with the spatial variation starts moving. Thus, another condition for rotating the magnetic moment is the number of injected spins in the magnetic system, in other words, if the spin current is low then the magnetic moment stays unperturbed but if it is high then results in the rotation.

In order to map the STT effect in atomistic magnetisation dynamics, additional terms need to be introduced to the SLLG equation of motion (Eq. 4.14). Since the spin transfer torque needs a smooth variation of magnetisation to act, the additional terms should depend on the gradient of the magnetisation and the SLLG equation takes the form [50]:

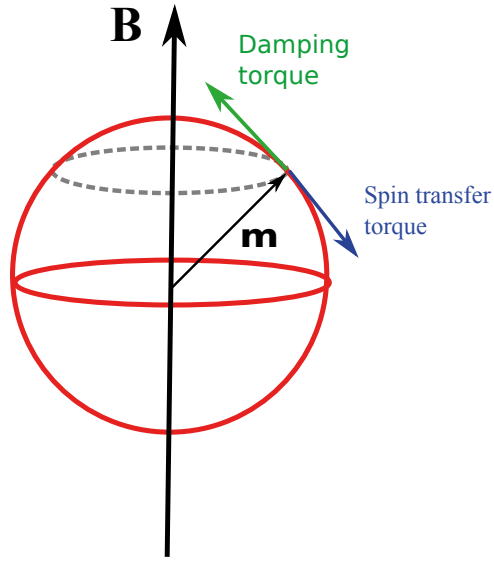

Figure 4.1. Schematic representation of the influence of spin transfer torque on magnetic switching.

$$\frac{d\mathbf{m}_i}{dt} = -\frac{\gamma}{1+\alpha^2}\left[\left(\mathbf{m}_i \times \left(\mathbf{B}^i_{eff} + \mathbf{b}^i(t)\right)\right) + \frac{\alpha}{m}\mathbf{m}_i \times \left(\mathbf{m}_i \times \left(\mathbf{B}^i_{eff} + \mathbf{b}^i(t)\right)\right)\right] + \frac{1+\beta\alpha}{1+\alpha^2}\frac{\mathbf{u}}{m_i^2} \cdot \left(\mathbf{m}_i \times [\mathbf{m}_i \times \nabla \mathbf{m}_i]\right) - \frac{\alpha-\beta}{1+\alpha^2}\frac{\mathbf{u}}{m_i} \cdot [\mathbf{m}_i \times \nabla \mathbf{m}_i]. \tag{4.15}$$

Two new parameters are entering the above equation of motion: the non-adiabatic parameter β [51, 52] which describes the the violation of spin conservation during the spin-transfer process and the velocity term $\mathbf{u}$ which is in units of velocity. The velocity term is expressed as:

$$\mathbf{u} = \frac{\mathbf{j}_e P g \mu_B}{2eM_s}, \tag{4.16}$$

where $\mathbf{j}_e$ is the current density, P the polarisation, M_s the saturation magnetisation of the magnetic system, g the Landé factor, e the electronic charge and μ_B the Bohr magneton.

4.4 Spin-Hall effect

As mentioned above, one way of manipulating spin textures is by means of spin polarised currents which as mentioned earlier can be important for spin-

tronic applications. An alternative way for manipulating the same spin textures has recently arisen, which is based on current induced spin-orbit (SO) torques through the spin Hall effect (SHE) [53]. These phenomena have been shown to be present in a magnetic layer deposited on a non-magnetic conductive layer that exhibits a strong spin-orbit coupling [54]. The influence of SHE on the manipulation of spin textures have been demonstrated by recent experiments [55, 56] of magnetic films on a heavy metal substrate, where the dynamics could not be explained by only the traditional spin transfer torque.

Since an increasing number of materials with large values of spin Hall angle are reported [57, 58, 59], these spin currents which are connected to the SHE are becoming very important and they increase the efficiency of transport phenomena. So as to express this notable effect, an additional torque is required in the above SLLG equation of motion (4.15) and it is given by [60]:

$$\tau_{SHE} = -\gamma \frac{\hbar a_{SHE} |j_e|}{2eM_s t_f} \left[\hat{m} \times \left(\hat{j}_e \times \hat{z}\right) \times \hat{m}\right], \tag{4.17}$$

where γ is the gyromagnetic ratio, a_{SHE} is the spin Hall angle, $|j_e|$ is the value of the current density, M_s the saturation magnetisation and t_f the thickness of the ferromagnetic layer. The direction of the torque is given by $[\hat{m} \times (\hat{j}_e \times \hat{z}) \times \hat{m}]$, where $\hat{m}$, $\hat{j}_e$ and $\hat{z}$ are the unit vector of the local magnetisation, the direction of the polarised current and the out-of-plane direction, respectively. The effect of both STT and SHE are studied in **paper VI** for domain walls as well as for skyrmions in a combination of model systems and material specific calculations.

4.5 The magnetic Hamiltonian

The central term of the atomistic spin dynamics is the effective field $\mathbf{B}^i_{eff}$ and all the important interactions that are present in the system should be included in this field, including the interatomic exchange interaction, Dzyaloshinskii-Moriya (DM) interaction, magnetocrystalline anisotropy and external magnetic field (Zeeman term). The most convenient way to obtain the effective field is to introduce all the interactions in an effective Hamiltonian and then the effective magnetic field can be found from the partial derivative of the Hamiltonian with respect to each local magnetic moment:

$$\mathbf{B}^i_{eff} = -\frac{\partial \mathscr{H}}{\partial \mathbf{m}_i}. \tag{4.18}$$

Details of how the interatomic exchange interaction and DM interaction are evaluated from first-principles theory can be found in the previous Chapter 3. We have to mention here that the effective Hamiltonian used in this work is classical and there are no quantum operators involved. The described magnetic Hamiltonian has four terms:

$$\mathscr{H} = \mathscr{H}_{Heis} + \mathscr{H}_{DM} + \mathscr{H}_{MAE} + \mathscr{H}_{Zeeman}. \tag{4.19}$$

The first term is the Heisenberg exchange interaction, the second is the Dzyaloshinskii - Moriya interaction, the third the magnetocrystalline anisotropic energy and the fourth is the Zeeman energy.

Depending on the system of interest, not all terms in equation (4.19) are necessarily present. However, the dominant term of the above Hamiltonian is normally the Heisenberg exchange interaction, in other words, it has the biggest contribution in energy and is the most important interaction. This term accordingly expresses the exchange interaction between atoms on sites i and j:

$$\mathscr{H}_{Heis} = -\frac{1}{2}\sum_{i\neq j} J_{ij}\mathbf{m}_i \cdot \mathbf{m}_j, \tag{4.20}$$

where $\mathbf{m}$ is the atomic magnetic moment and J_{ij} is the interatomic exchange parameter which describes the change of energy when the atomic magnetic moments on sites i and j are changing their direction from their initial configuration. The minus sign of the equation (4.20) is a convention that ensures that a positive value of J_{ij} corresponds to a ferromagnetic ground state and in a case of negative value the corresponding ground state is antiferromagnetic.

In systems with broken inversion symmetry and spin-orbit coupling, such as non-centrosymmetric B20 structures (MnSi [10]) or many low-dimensional magnets (one layer of Fe on top of Ir(111) [61]), a non-collinear magnetic order has sometimes been observed to be the ground state, an effect which typically cannot be explained by introducing only the Heisenberg exchange, thus additional interactions must be introduced. This interaction is described by the second term of the Hamiltonian (4.19) which was proposed by Dzyaloshinskii [21] and Moriya [22] and is expressed in the Hamiltonian in the following way:

$$\mathscr{H}_{DM} = -\frac{1}{2}\sum_{i,j} \mathbf{D}_{ij} \cdot (\mathbf{m}_i \times \mathbf{m}_j), \tag{4.21}$$

where $\mathbf{D}_{ij}$ is the vector of Dzyaloshinskii-Moriya interaction and is calculated from first principles (see Chapter 3).

In systems with low symmetry the spin-orbit coupling is often enhanced which means that the effect of magnetocrystalline anisotropy is large. On the other hand, in cubic systems the spin-orbit coupling is very weak and the effect of the magnetocrystalline anisotropy is also very weak. For this reason, in our Hamiltonian we keep only the uniaxial anisotropy which is dominant and is written:

$$\mathscr{H}_{uni} = K\sum_i (\mathbf{m}_i \cdot \hat{\mathbf{e}}_K)^2, \tag{4.22}$$

where $\hat{\mathbf{e}}_K$ gives the direction of the easy axis and K is the uniaxial anisotropy constant. Once in the $\mathscr{H}_{uni}$ there is positive sign it means that a negative value of K corresponds to the easy axis anisotropy and otherwise corresponds to the hard axis. If the cubic anissotropy is indeed important it can be added to the Hamiltonian (4.19) as well.

The last term of the Hamiltonian (4.19) is the Zeeman term and expresses the interaction between the atomic magnetic moments and the external magnetic field:

$$\mathscr{H} = -\mathbf{B}_{ext} \cdot \sum_i \mathbf{m}_i, \tag{4.23}$$

$\mathbf{B}_{ext}$ is an applied external field.

4.6 Coarse-graining exchange interactions

Sometimes the description of non-trivial magnetic structures is difficult from the atomistic point of view because of their size. For example, the spin-spiral ground state of a helimagnet can have a long wavelength, depending on the system, which means that an atomistic description of such a system would have a huge computational cost and additionally if the magnetization changes very smoothly then it can be considered as ferromagnet on an atomic level. Furthermore, a direct comparison with experimental results is often more than necessary and desirable. For both reasons, it is very convenient to have an efficient and simple methodology for coarse-graining the exchange interactions.

A straightforward but arguably naive approach is based on resolving the system into a number of ferromagnetic grains so that the system is divided into a number of cubic blocks and the interaction between these blocks is only the sum of those atomic exchange interactions which are reaching the region outside of each block (e.g. the next nearest neighbour interaction of the second last magnetic moment from the block boundaries). This approximation may be an effective way to bridge from atomistic magnetization dynamics to micromagnetism for certain switching scenarios in ferromagnets at low temperatures but on the other hand is difficult to use it in a case of non-uniform magnetisation, like smooth domain walls, spin-spirals or even finite temperature excitations in ferromagnets.

A better and improved solution for a coarse grain approach is to base the description of the system so that at least long-wavelength magnons can be properly described. It is well known [62] that the energy of magnetic excitations, magnons, in the limit of long wavelengths follows a square dispersion relation as given by:

$$E(\mathbf{q}) \approx \mathbb{D}q^2, \tag{4.24}$$

where **q** and is a vector in the corresponding Brillouin zone, q is the magnitude of **q** and $\mathbb{D}$ is the spin stiffness constant. For a cubic system with one atom per unit cell, the spin wave stiffness [62] is described by:

$$\mathbb{D} = \frac{2}{3}\sum_{i,j}\frac{J_{ij}}{\sqrt{m_i m_j}}|r_{ij}|^2. \tag{4.25}$$

The distance between the magnetic moments on sites i and j is r_{ij} and m_i is the magnitude of the magnetic moment. If λ is a wavelength of the spin wave then $q = 2\pi/\lambda$. If we consider that the each coarse-grained volume in our system is built of a cubic block that consists of $N \times N \times N$ atoms, then the wavelength as expressed in terms of the blocks is $\lambda_{block} = \lambda/N$ and $q_{block} = 2\pi/\lambda_{block} = Nq$. Since in both the atomistic and the coarse-grained cases, the spin wave dispersion relation 4.24 should hold we can get the following relation:

$$\begin{aligned} \mathbb{D}q^2 &= \mathbb{D}_{block}q_{block}^2 \\ \Rightarrow \mathbb{D} &= N^2\mathbb{D}_{block}, \end{aligned} \tag{4.26}$$

where the parameters of $\mathbb{D}$ in equation (4.25) can be calculated from ab-initio calculations and from eq (4.26) it is posible to extract the J_{ij}^{block} interaction from:

$$J_{ij}^{block} = \frac{\mathbb{D}}{r_{block}^2}, \tag{4.27}$$

where $r_{block} = Nr_{inter}$ is the size of the block and r_{inter} is the interatomic distance between two neighbouring atomic magnetic moments.

5. Magnetic skyrmions

In this chapter, we will introduce magnetic skyrmions as topological protected magnetic structures. We will continue with describing their formation, stabilisation and the kind of materials they exist. Finally, we will present their dynamics and why their properties put them as potential candidates for information carriers in magnetic storage devices.

5.1 Introduction to topology and skyrmion number

Magnetic structures which exhibit non-trivial configuration like domain walls, solitons and skyrmions are known as "topological defects" and their stability can be explained from a topological point of view. The basic idea behind the concept of topology in magnetism is that two magnetic structures are topological equivalent when the one can continuously be transformed to the other one without overcoming an infinite energy barrier. On the other hand, two magnetic structures are inequivalent in terms of topology when is impossible to continuously transform one into the other [63]. In reality the term of an infinite energy barrier does not apply, for example real systems are finite and a topological protected structure such as skyrmion, can be moved out of the sample as it is shown later in this chapter. Thus, in real systems a deformation of two unequivalent magnetic structures into each other can happen in the case of overcoming a finite energy barrier as presented in **paper VII**.

In order to further elaborate on the concept of topology in magnetic structures we can consider the configurations of Fig. 5.1 which are characterised by the winding number that can be interpreted how many times the magnetization is wrapped around a circle. Since, the winding number w counts wraps, it is an integer number and configurations with different w, e.g. **a** and **c** from Fig. 5.1, are topologically inequivalent and are thus not able to continiously twist into each other. The obtained two dimensional skyrmion structure (Fig. 5.2) is topological protected and is characterised by the skyrmion number (which is the same with the winding number):

$$N_{sk} = \frac{1}{4\pi} \int \int \hat{\mathbf{n}} \cdot \left(\frac{\partial \hat{\mathbf{n}}}{\partial x} \times \frac{\partial \hat{\mathbf{n}}}{\partial y} \right) d^2\mathbf{r}, \tag{5.1}$$

which is the integral of the solid angle and gives the number of times wraps the unit sphere [64, 65]. $\hat{\mathbf{n}}$ is the unit vector pointing in the direction of magnetisation. If the magnetisation at the center of the skyrmion is pointing up, then $N_{sk} = +1$ and if is pointing down $N_{sk} = -1$.

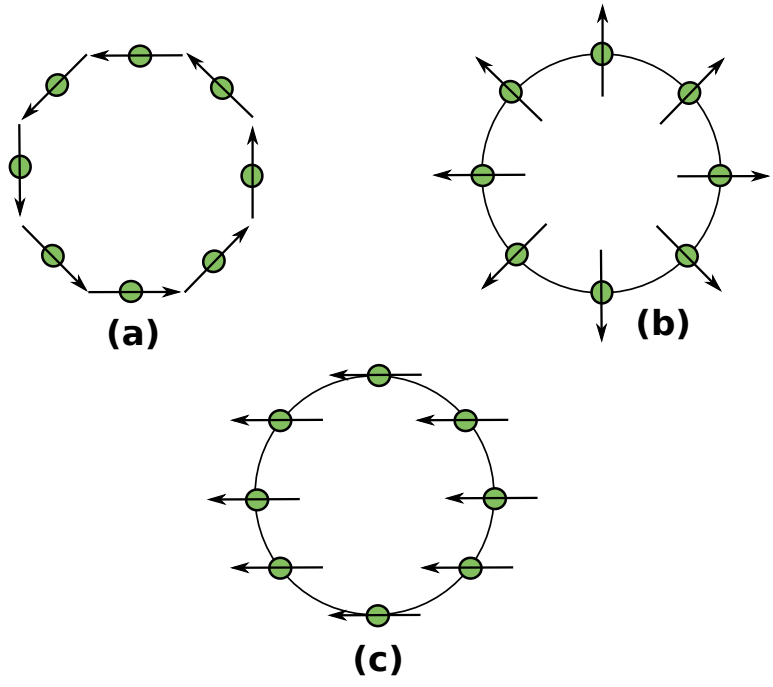

Figure 5.1. Examples of configurations with winding number $w = 1$ (**a** and **b**) which are able to transform into each other by a global rotation in the plane. In the case of (**c**), the winding number is zero ($w = 0$) and the structure cannot transform into the first two due to their difference in w.

5.2 Introducing skyrmions

In the early 60s the nuclear physicist Tony Skyrme suggested a theoretical model in which skyrmions are topological non-trivial quasi-particles in field theory [66]. Since the proposal of Skyrme's model, many different alternative models are being used in several fields of physics, for example in Bose-Einstein condensates [67, 68], liquid crystals [69] etc. However, in recent years there has been very high interest in the area of solid state magnetism for non-trivial spin textures, which are called magnetic skyrmions. The spins of this non-trivial magnetic texture can be described as pointing in all directions wrapping a sphere as we can see in Fig.5.2a and the number of wraps coincides to the topological invariant which makes the structure topologically stable. Since the magnetic skyrmion is stable from the topological point of view means that it cannot be continuous transformed to a trivial topological structure such as ferromagnetic or antiferromagnetic structure. This last important property of skyrmions along with their ability to avoid pinning centers and the small value of depinning current makes them very good candidates for using them as information carriers.

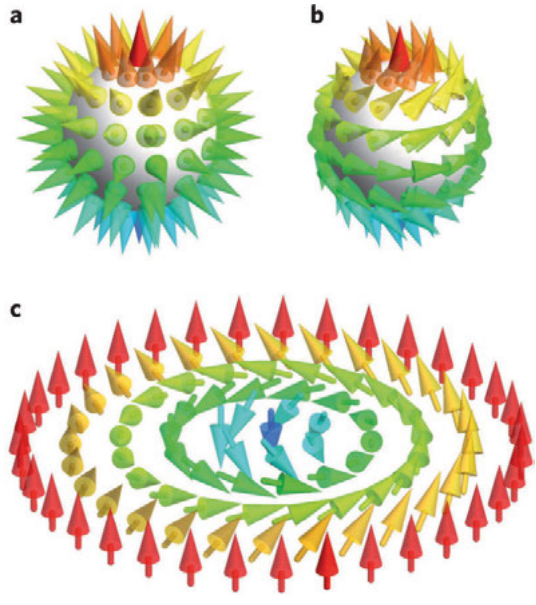

Figure 5.2. Schematic representation of the two-dimensional skyrmion. **(a)** Hedgehog type skyrmion as proposed by Tony Skyrme, **(b)** gradual rotation of spins and **(c)** the two-dimensional projection of the right sphere. This picture is taken from [70].

5.3 Formation and stability of skyrmions

The formation of a magnetic skyrmion can take place in several systems as a result to different mechanisms, which are the following [71]: a) long-ranged dipolar interactions in thin-layer magnetic systems with perpendicular easy axis anisotropy (PMA), b) systems with broken inversion symmetry which gives rise to Dzyaloshinskii-Moriya interaction, and c) exchange interactions in frustrated systems and in systems with four-spin exchange interactions. The size of the skyrmion depends on the mechanism and the strength of the governing interactions, thus with the first mechanism skyrmions have a typical size of 100nm - 1μm, with the second 5nm - 100 nm and with the last two, $<$ 5nm. In this thesis, we will focus on the second mechanism (Dzyaloshinskii-Moriya interaction) and the rest are beyond the scope of the thesis.

For the class of systems studied here, the broken inversion symmetry gives rise to the Dzyaloshinskii-Moriya interaction and its competition with the Heisenberg exchange interaction (J) is responsible for the formation of skyrmions [72, 73, 74]. The ground state of such systems is the helical spin-spiral state. Due to their magnetic order being determined by the chirality-inducing DMI, these materials are also called chiral magnets and some examples of those magnets with B20 structure are: MnSi [10], FeGe [75, 76, 77, 78], $Fe_{1-x}Co_xSi$ [79, 80] and $Mn_{1-x}Fe_xGe$ [81].

The Heisenberg exchange interaction J favours a ferromagnetic orientation of the magnetic moments (Fig. 5.3a) and on the other hand, the DM interac-

tion as it is expressed in atomistic spin dynamics (Eq. 4.21) favours a rotation of $\pi/2$ as illustrated in Fig. 5.3b. When both interactions are present in the system, the ground state helical modulation is stabilised [82, 83] (Fig. 5.3c).

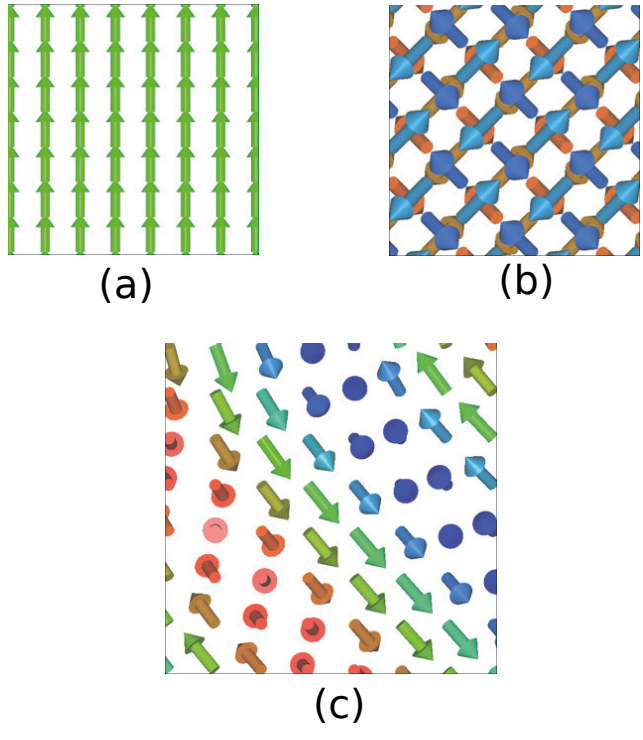

Figure 5.3. **(a)** Orientation of magnetic moments under the influence of only the Heisenberg exchange interaction, **(b)** the $\pi/2$ angle between neighbouring magnetic moments when only the DM interaction is present and **(c)** spin-spiral configuration when both interactions are present in the system.

By applying an external magnetic field of suitable strength (and temperature in the case of bulk systems) into the spin-spiral state, the system enters the skyrmion phase where the magnetic moments of the skyrmion perimeter have direction parallel to the external magnetic field and the ones at the center are antiparallel. The size of the skyrmion depends on the strength of the DM interaction (D) and the Heisenberg exchange interaction (J). In the case of small D/J ratio then the skyrmion favours a slow rotation of its magnetic moments which is translated in a big size skyrmion. On the other hand, if the D/J ratio is big then it favours a faster rotation which makes the skyrmion small in size.

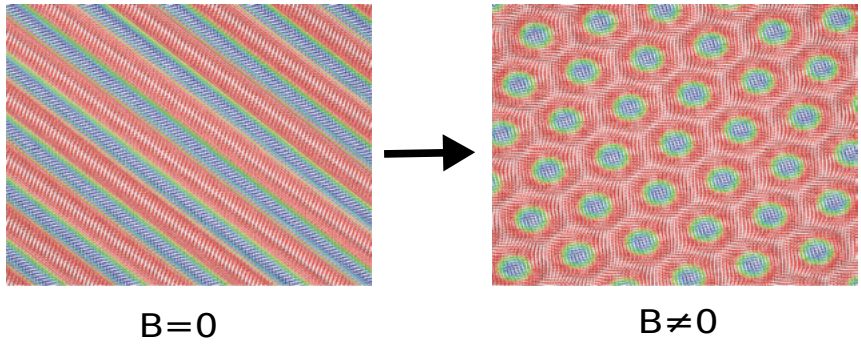

Figure 5.4. Transition from two-dimensional spin-spiral ground state to skyrmion phase by applying parpandicular external magnetic field. The colour scheme of the figure is chosen in a way that the magnetic moments pointing out of plane towards the reader are blue and in the opposite direction are red. The external magnetic field is in direction of the red region.

5.4 Classification of skyrmions

The magnetic structure of skyrmions are stable due to their topological protection which means that small changes in the system, e.g. external magnetic field or temperature, are not able to deform the skyrmion structure.

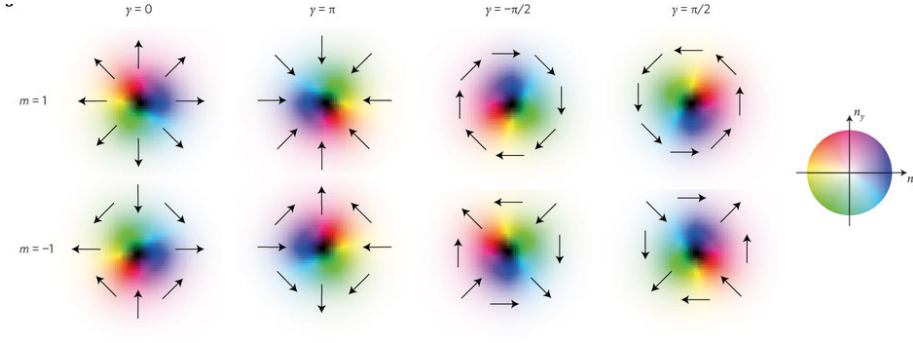

Figure 5.5. Different configurations of magnetic moments according to the skyrmion number and helicity. This picture is taken from [71].

With respect to their topological properties, skyrmions are categorised to different types. The two main categories have been already introduced and depend on the skyrmion number N_{sk}, if it is +1 or -1. Apart from the two main categories, there are more subcategories where the structure depends on the helicity γ. The origin of the helicity is the direction of the DM interaction which is determined by the symmetries of the crystal structure [84, 85]. In Fig. 5.5 are presented the configurations of magnetic moments around the center of the skyrmion for different values of skyrmion number (+1 or -1), of the helicity (γ) and its sign (+ or -).

5.5 Experimental observation in chiral magnets

It was mentioned in the previous section, that one class of materials where the skyrmion structure exists is the non-centrosymmetric ferromagnets which according to the space group they belong to the B20 alloys. MnSi belongs in this class of alloys with B20 space group and its structure is shown in Fig. 5.6c. The strongest and most important interactions between the magnetic atoms are the exchange interaction J and Dzyaloshinskii-Moriya interaction D, in contrast to the magnetic anisotropy which is relatively weak. The phase diagram of external magnetic field (B) with respect to the temperature (T) of bulk MnSi is shown in Fig. 5.6c. Under the influence of zero external magnetic field and under the critical temperature T_c, which is approximately 30 K, the helical spin order is stabilised due to the competition of the two main interactions J and D. The lattice constant of MnSi is $a = 4.56\ \mathring{A}$ and the period of the spin spiral is $\lambda = 190\ \mathring{A}$ which indicates that the exchange interactions between the Mn magnetic atoms are rather weak. By looking the MnSi phase diagram it is easily noticed that there are five different phases instead of the usual two of the ferromagnets (ferromagnetic below T_c and paramagnetic above). Of course, the two typical phases exist in this compound as well, above T_c the paramagnetic phase occurs and in large enough external magnetic field the magnetic moments are fully aligned with the direction of the field which gives a result to the ferromagnetic state. The three phases that remain are non-collinear and as mentioned above in low external field the helical spin state is stabilised, and the magnetic moments precess around a rotational axis which is perpendicular to the field. By increasing the external magnetic field, moments tend to align with the field and there is a transition from the helical state to the conical one.

Just below the critical temperature T_c, a narrow region in the T-B phase diagram can be observed, which is called A-phase and that is the fifth magnetic state of the compound and in this region, several properties such as magnetic susceptibility and magnetoresistance [86] have been experimentally shown to exhibit a strange behaviour. The exact spin texture of the A-phase was not identified for many years until 2009, when skyrmion phase was discovered by small angle neutron scattering (SANS) experiment [10]. In this experiment, magnetic Bragg reflections in reciprocal space appear due to the scattered neutron beam, which makes it possible to investigate the A-phase of the sample. The results of the SANS experiment are presented in Fig. 5.6a where the external magnetic field is perpendicular to the observation plane, the Bragg peaks have a symmetric six-fold pattern and its origin is the superposition of three spin spirals with an angle of 120° between them. This pattern can be considered as a triangular skyrmion lattice and an example of a closed packed lattice from our model simulations is shown on the right panel of Fig. 5.4, where a six-fold symmetry of the neutron scattering peaks can be also seen here. However, only the results of the SANS experiment cannot reproduce the exact structure of the A-phase and it was necessary to be combined with measure-

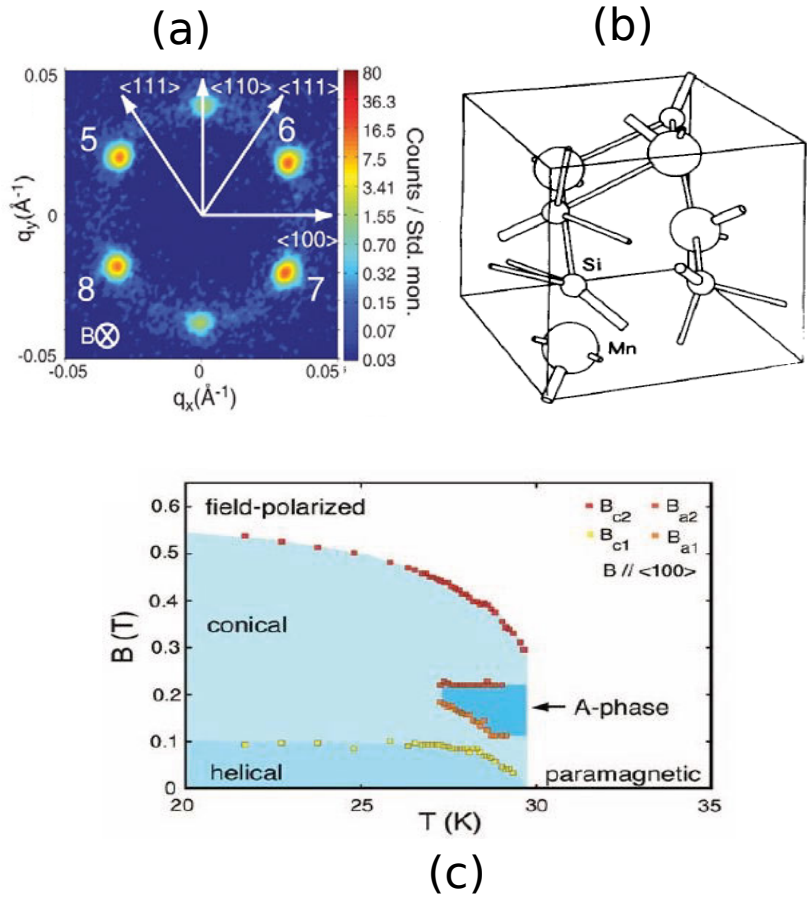

Figure 5.6. **(a)** Experimental measurement of SANS in the case of $T = 27.7$ K and $B = 0.162$ T. **(b)** unit cell structure of the non-centrosymmetric MnSi B20 compound and **(c)** T-B phase diagram of bulk MnSi. Figures (a) and (c) are taken from [10].

ments of the topological Hall effect [87]. Skyrmions during their motion give an extra contribution to the Hall effect because of the change in the magnetic field.

The next step regarding the magnetic structure of the A-phase, was the direct experimental observation obtained by using Lorentz transmission electron microscopy (TEM) for the thin films of the chiral magnet $Fe_{0.5}Co_{0.5}Si$ [88]. The advantage of TEM over the SANS, is the real space representation of the in-plane component of the magnetic moments which gives a clear picture of the A-phase structure as is shown in Fig. 5.7b. Since with TEM only the in-plane components of the magnetic moments are measured, the ones that they have out-of-plane component only (parallel and antiparallel to the ap-

plied external field) are coloured black as it is presented in the Fig. 5.7c where at the center has antiparallel direction and at the perimeter where is parallel. In Fig. 5.7 are shown the real space images for the spin-spiral ground state ($B = 0$) with a wavelength of several nanometers and for the skyrmion lattice under the influence of $B = 50$ mT.

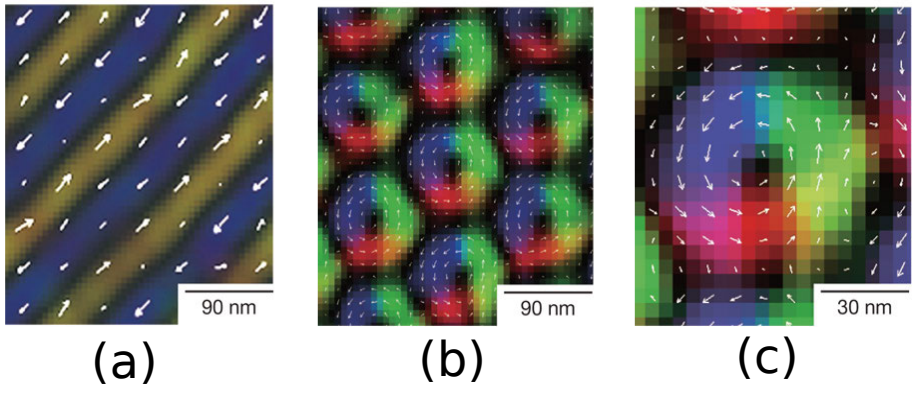

Figure 5.7. Real-space figures from the analysis of Lorentz transmission electron microscopy measurements for the chiral magnet $Fe_{0.5}Co_{0.5}Si$. **(a)** Helical spin-spiral structure of the ground state ($B = 0$). **(b)** The structure of the skyrmion crystal when a perpendicular external field is applied ($B = 50$ mT) and **(c)** zoomed-in picture of one skyrmion. This figure is taken from [88].

A big issue about the skyrmion structures is the temperature in which are stable and still well defined. Most of the B20 structures exhibit a low critical temperature T_c and since the A-phase is present just below this temperature, the skyrmions exist in low temperatures as well. The existence of such structures up to room temperature is a big challenge for the community. One of the few (if not the only one) B20 structures which exhibit high temperature for the skyrmions, is the thin film FeGe where the formation of a skyrmion crystal is taking place up to 275 K [77, 89]. Furthermore, skyrmion formation takes place at and above room temperature in alloys with different chiral space group than B20 and those are the β-Mn-type Co-Zn-Mn alloys in which skyrmions observed both in bulk and thin films [90]. Since DMI is also arising from the symmetry breaking at the interfaces [91, 92, 93, 94], multilayers are investigated for skyrmion formation at room temperature. It was found that Co thin films in-between of two heavy metals (Ir/Co/Pt trilayer) [95], Fe/Ni bilayers on top of Cu/Ni/Cu(001) and ultrathin transition metal ferromagnets (Pt/Co/Ta and Pt/CoFeB/MgO) [96] favor the formation of skyrmions at and above room temperature. In all these multilayers, perpendicular magnetic anisotropy is present which is very important for the skyrmion size and by tuning the anisotropy, the skyrmion size can be changed which

results in a larger bit density. Another case of observing individual skyrmions at room temperature is in heavy metal/ultrathin ferromagnet/insulator trilayers with broken inversion symmetry [92] where skyrmions are created by a sparse magnetic stripe when the stripe is forced by a current to move through a geometrical constriction. In this device, magnetic domains and skyrmion bubbles are both present which indicates that are metastable.

5.6 Dynamics of skyrmion

There is now a large effort focused on the discovery of the next generation magnetic storage devices which will be more efficient and faster than the current technology. Ferromagnetic domain walls were very promising candidates due to the fact that is possible to move them in a race-track memory [9] by using spin polarised current utilizing the STT effect [7, 8] between the electrons in the current and the magnetization texture at the domain wall. The disadvantage of this proposal is that it has been found that large threshold current density is required to move the domain walls ($j_c = 10^{10} - 10^{12}$ A/m^2) which results in an unwanted Joule heating of the proposed device. However, it was also found that the magnetic skyrmions in chiral B20 magnets can be moved by spin polarised currents [97, 89, 98, 99, 100, 101] by using much smaller current density ($j_c = 10^5 - 10^6$ A/m^2) which would then mean a reduction of the Joule heating with several orders of magnitude. Furthermore, the magnetic skyrmions have the ability to avoid pinning centers, which is not happening in the case of domain walls, and these properties make them strong candidates for information carriers.

As mentioned earlier, the size of the skyrmions in most investigated chiral magnets is quite big. Thus, most of the important theoretical research efforts that has been done on skyrmions has been pursued in the micromagnetic regime. In this section, a micromagnetic description will be used for the motion of skyrmions starting from the continuum Hamiltonian [102] which is expressed as:

$$\mathscr{H} = \int d\mathbf{r} \left[A(\nabla \mathbf{M})^2 + D\mathbf{M}(\nabla \times \mathbf{M}) - B\mathbf{M} \right], \tag{5.2}$$

where A is the exchange energy strength, D is the strength of the DM interaction and the third term of the integral is the Zeeman term.

Similar to the expression of Landau-Lifshitz-Gilbert (LLG) (Eq.4.15) equation of motion for discrete magnetic moments which is introduced in the previous chapter, the LLG for the continuum case, including the spin torque effect [11] is:

$$\frac{d\mathbf{M_r}}{dt} = -\gamma \mathbf{M_r} \times \mathbf{B_r^{eff}} + \frac{\alpha_G}{M} \mathbf{M_r} \times \frac{d\mathbf{M_r}}{dt} + \frac{p\alpha^3}{2eM} (\mathbf{j} \cdot \nabla) \mathbf{M_r} - \frac{p\alpha^3 \beta}{2eM^2} [\mathbf{M_r} \times (\mathbf{j} \cdot \nabla) \mathbf{M_r}]. \tag{5.3}$$

Here $\gamma = g\mu_B/\hbar$ is the gyromagnetic ratio, p is the spin polarisation of the current, e is the charge and α and α_G are the lattice constant and the Gilbert damping respectively. The effective magnetic field is:

$$\mathbf{B_r^{eff}} = -\frac{1}{\gamma\hbar} \frac{\partial \mathscr{H}}{\partial \mathbf{M_r}}. \tag{5.4}$$

The first two terms of the right-hand side of equation (5.3) are the precession and damping term respectively and the two last terms (third and fourth) are expressing the coupling between the magnetisation of the system and the spin-polarised electric current $\mathbf{j}$.

The motion of skyrmions can be studied by using the Thiele equation [103] which is obtained by solving the LLG equation of motion and is expressed as [99, 100]:

$$\mathbf{G} \times (\mathbf{v}_s - \mathbf{v}_d) + \mathscr{D}(\beta \mathbf{v}_s - \alpha_G \mathbf{v}_d) + \mathbf{F}_{pin} - \nabla U = 0. \tag{5.5}$$

The first term is the Magnus force in which $\mathbf{v}_s$ is the velocity of the conduction electrons and $\mathbf{v}_d$ is the skyrmion drift velocity. The second term describes the dissipative force, where β is the non-adiabatic term and the third term is the phenomenological pinning force caused by the presence of the defects. The last term is the force due to the potential of the environment.

5.6.1 Motion in infinite system

Iwasaki *et. al.* [11] in their work present the dependence of the skyrmion velocity which is parallel ($v_{||}$) to the direction of the electric current on the value of the current density. They examine the velocity for both cases of helical state (HL) and the skyrmion state (SkX) with impurities(w/) and without (w/o). Finally, in their calculations, they also include different values of the non-adiabatic parameter β.

Within their model the helical spin-spiral ground state is considered as a set of Bloch walls in a ferromagnetic background and in this frame is easier to compare the velocities of these two different configurations by changing only the applied external magnetic field and all the other parameters are remain the same. The impurity concentration chosen by the authors were $x = 0\%$ in the clean case and $x = 0.1\%$ in the dirty case. At this point, it is necessary to mention that the impurities here are considered as sites with enhanced easy-axis anisotropy along the z-direction. Surprisingly, for the skyrmion state case

it was found that the velocity is universal and independent of the non-adiabatic parameter and the impurities. Furthermore, the dependence of the velocity was found to be linear and all these characteristics are shown in the relation:

$$v_{||} = \frac{p\alpha^3}{2em} j. \tag{5.6}$$

Thus, the above relation also implies that skyrmions are ideal structures for moving them by spin polarised current and achieve high velocities with small current densities.

In opposition to the skyrmion state, the velocity of the helical state is dependent of both the non-adiabatic parameter and the impurity concentration. When only adiabatic effects ($\beta = 0$) are present in the system of helical state, the set of Bloch walls do not move for both systems (clean and dirty) due to the intrinsic pinning effect. Another observation is the difference in velocity between the clean and the dirty system for finite β and only without impurities follows the relation:

$$v_{||} \propto (\beta/\alpha_G)\, j. \tag{5.7}$$

In the presence of impurities, it seems that the motion is suppressed in low current density and the threshold density is larger.

5.6.2 Impurities and influence of the trajectory

It has now been established that skyrmions have a particle-like behaviour which explains their flexibility to avoid pinning centers in the sense of magnetic impurities [11, 104, 105]. A presence of magnetic impurity influence the trajectory of the skyrmions while they are moving and they show their preference to move around the impurity either if their size is small [11] or big [104]. The previous behaviour holds when there is nothing to constrain the motion of the skyrmions and they are moving "free" in the system (e.g. one individual skyrmion). On the other hand, when a whole skyrmion lattice is in motion, each skyrmion is pushed from the surroundings skyrmions, and as a result they are restricted and cannot move around the impurity but they are however able to move through it [11]. In the latter case, the skyrmion survives when the size of the impurity is smaller than the size of the skyrmion. For the skyrmions is not energetically very costly to travel through the impurity since the easy-axis magnetic anisotropy of the impurity is along $z-$direction which is in accordance with the direction of the skyrmion center.

In addition to the findings reported above that concerned magnetic impurities with large anisotropies, also non-magnetic impurities can affect the trajectories of current driven skyrmions as it shown from our simulations. In other words, when the impurities are in the form of empty sites (voids) and we can consider them as "holes" in the system. Around the void there is a repulsive

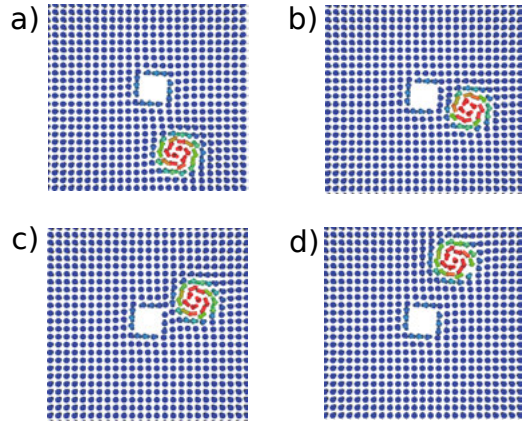

Figure 5.8. Motion of the skyrmion under the influence of spin polarised current in a system with non-magnetic impurity. The trajectory of the skyrmion structure is influenced and is moving around the impurity due to the repulsive potential.

potential which forces the skyrmion to move around, as it is shown in Fig. 5.8. The presence of the repulsive potential results from the lack of one neighbour of the magnetic moments in the neighbourhood of the "hole". This effect is explained in more detail in the following section of skyrmion annihilation where the edges of the system have identical behaviour with the voids since the also lack one neighbour.

5.6.3 Creation, annihilation and motion in finite system

It is well-known that the information carriers in the magnetic storage devices need to have three main characteristics: they should be easily transported in nanostructures, it should be possible to create and annihilate them at will. In the previous section was presented the ability of skyrmions to move in infinite systems with very low current densities compared to the domain walls, and their ability to avoid pinning centers. At the beginning of this section, we will see how skyrmions behave in finite systems, for example in a finite width channel, and their difference with the previous case of infinite systems. The presented results are from numerical calculations using the Hamiltonian of equation (5.2) and based on the LLG equation of motion (5.3).

In the presence of boundaries, skyrmions behave differently because of their interaction with the boundaries where they feel a potential. The origin of this potential is the lack of one neighbour from the magnetic moments at the end of the system and due to the presence of the Dzyaloshinskii-Moriya interaction those moments are not aligned with the ferromagnetic background of the rest of the system. In other words, there is a finite angle between the moments at the boundaries and the inner moments.

Previous studies have been shown that the skyrmion velocity depends on value of the non-adiabatic parameter β in a system with finite width [106]. Unlike the infinite systems, the skyrmion velocity is more influenced by the presence of the magnetic impurities in case of finite system and their effect is no longer negligible. By using the Thiele's equation, a relation for the component of the velocity which is parallel to the direction of conduction electrons of the current can be found:

$$\mathbf{v}_{||} = \frac{\beta}{\alpha_G}\mathbf{v}_s, \tag{5.8}$$

where $\mathbf{v}_{||}$ is the parallel component of velocity to $\mathbf{v}_s$, which is the velocity of the conduction electrons.

We will continue now with the interaction between skyrmions and the edges of the sample to see what happens when the annihilation process is taking place. In Fig. 5.9 we see two different behaviours of skyrmion at the edge of the sample. When the current density is big enough, the skyrmion is able to overcome the edge barrier, it reaches the boundary and the annihilation process starts (Fig. 5.9a-d). On the other hand, when the current density is lower, then the skyrmion is moving towards the edge but its energy is not enough to overcome the potential barrier. This results in a motion parallel to the edge (Fig. 5.9e-h). Our results are consistent with the micromagnetic simulations in the work of Iwasaki *et. al.* [106].

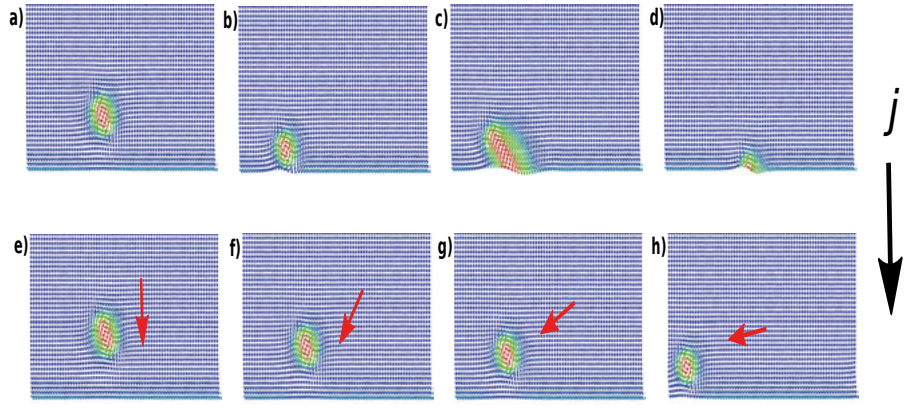

Figure 5.9. Snapshots of skyrmion dynamics when is driven to the edge of the sample under the influence of low current density (a-d) and under the influence of higher current density, where the skyrmion is annihilated at the edge of the sample (e-h). The red arrow is showing the direction of the skyrmion motion. The black arrow shows the direction of the current.

Lastly, an equally important procedure for information carriers along with the previous two (dynamics in finite system and annihilation at the edges) is the generation of the information itself, which in our case is the skyrmion.

Edges can be used as nucleation centers by applying a spin-polarised current into the system which is ferromagnetic, provided that the value of the perpendicular external magnetic field is in the range of the A-phase of the certain system [106]. As discussed above, the moments at the edges of the sample are slightly rotated compare to the inner moments which are totally aligned with the external field and they have a quite large in-plane component because of the DM interaction. As the spin-polarised current flows into the system, inner moments very close to the boundary starts rotating due to their interaction with the electrons of the current, which means that they gain an in-plane component as well. After some time, the region with in-plane components is growing and at some point due to the DM interaction a flipping of moments is taking place and their direction is opposite to the external field. This is the nucleation of the skyrmion core, and as the current keeps flowing a complete skyrmion pops out. The whole procedure as described above is shown in Fig. 5.10.

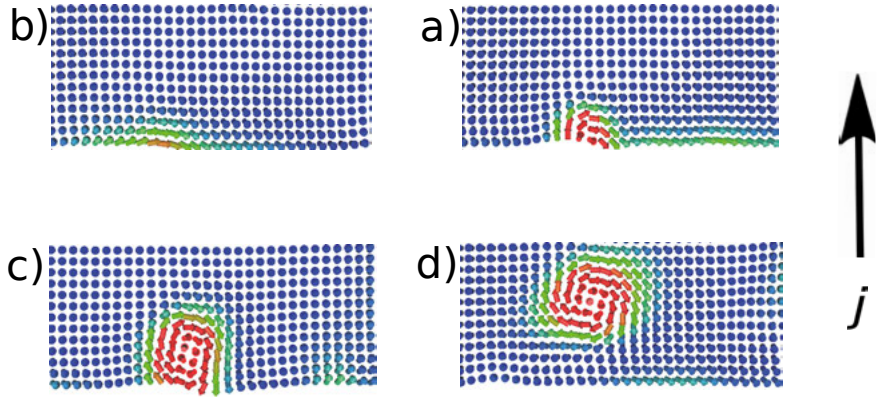

Figure 5.10. Snapshots of skyrmion nucleation at the edge of the system by applying spin polarised current. The direction of the current is shown by the black arrow.

6. Magnetic defects and helical spin-spiral state

6.1 Introduction

The examination of the helical magnetic texture is of great interest since the formation of skyrmions is promoted from the presence of defects [107], which are topological and in the form of edge dislocations [108, 88]. FeGe is a B20 structure which means that it has finite DM interactions and as a result FeGe exhibits a helical spin-spiral ground state. In **paper II** is studied, from the experimental and theoretical point of view, for the dynamics and emergent topological defects in the helical spin-spiral state of FeGe. The experimental study of the system is done by using magnetic force microscopy (MFM) [109] and Nitrogen-vacancy (NV) center-based magnetometry [110, 111]. The NV technique gives the opportunity to study the sample in atomic scale and the advantage over the MFM is that secures the absence of extrinsic effects (e.g. tip-induced effects). For the theoretical study, ab-initio calculations were used to extract the parameters of the system following by spin dynamics simulations of the topological defects.

6.2 Experimental techniques

6.2.1 Magnetic force microscopy

Magnetic force microscopy (MFM) is a technique which is used to scan magnetic samples. The tip of the microscope is coated with a ferromagnetic film and it interacts with a magnetic sample through the magnetostatic forces. Depending on the polarisation of each region, the tip feels an attractive or repulsive force which makes it possible to characterise the magnetic domains of the sample. The magnetostatic interaction is very strong and it does not depend much on the surface purity (if it is clean or not) which gives the advantage of using it under any environmental conditions.

MFM gives the ability to measure the variation of the stray field near the surface, even individual interdomain boundaries [112] and sometimes even magnetic structures that are not only on the surface [113]. The previous achievements make MFM a very important tool when the variation of magnetisation is of main interest. MFM technique keeps evolving through the years with breakthrough methods since magnetic thin films are widely studied for the development of magnetic devices for industrial applications.

6.2.2 Nitrogen vacancy (NV) center based magnetometry

Since understanding the magnetic phenomena taking place on the nanometer scale is very important and there is a strong drive to improve the detection, as well as the imaging, of the weak magnetic fields in this scale. In order to improve the sensitivity and the resolution of the scanning, single spins were proposed [114, 115] as nanoscale magnetic field sensors. When the tip is close to the surface of the scanned sample, the local magnetic field coming from it is evaluated by the Zeeman shift of the electron spin resonance frequency [116, 117] which provides a high spatial resolution. For implementing this idea it proved that the nitrogen vacancy (NV) center in a diamond is a very good choice [118, 119]. The main advantage of this technique is the reliability since the information is coming only from the sample's stray field by excluding any contribution from the tip which makes it very successful on studying more complex structures like domain walls [120, 121], vortices [122] and spin-spirals [123]. In the **paper II**, is the first reported application of NV magnetometry on spin-spiral materials.

6.3 Results of magnetic defects in FeGe

By the usage of both experimental techniques described above, a helical spin-spiral ground state have been observed with a spiral wavelength of $\lambda = 70 \pm 5$ nm. The important exchange interactions J and DM were extracted from ab-initio calculations with the use of LKAG formalism which was described in Chapter 3. Afterwards, the calculated interactions were coarse grained, with the method described in Chapter 4, which makes it possible to study the magnetization of the system, including the movement and annihilation of topological defects in the micromagnetic regime. The spiral wavelength from theoretical studies was found $\lambda \approx 100$ nm by using the Monte Carlo method for the stabilisation of the ground state. With the same method, the critical temperature of FeGe was examined and found $T_N = 240$ K, which is in good agreement with the experimental value $T_N = 276$ K [124].

The MFM data from the experiment that can be seen in Fig. 6.1 a, b, and e, showed that over time, a jump in the period of helical spin-spiral state would occur during the MFM scans which can clearly be seen in Fig. 6.1e. In Fig. 6.1a is the MFM scan at the temperature of $T = 255$ K, where the black and white regions indicate the different orientation of the magnetic moments. In the same figure (a), green arrows are showing defects in the magnetic structure of the sample which according to our simulations are characterised by non-trivial topology [76, 88, 108] and they are responsible for the jumps of the period during the measurements. The change in the period can be explained easier by looking at the schematic representation of Fig. 6.1c, in which is shown the helical spin-spiral state and how the defect influences the period.

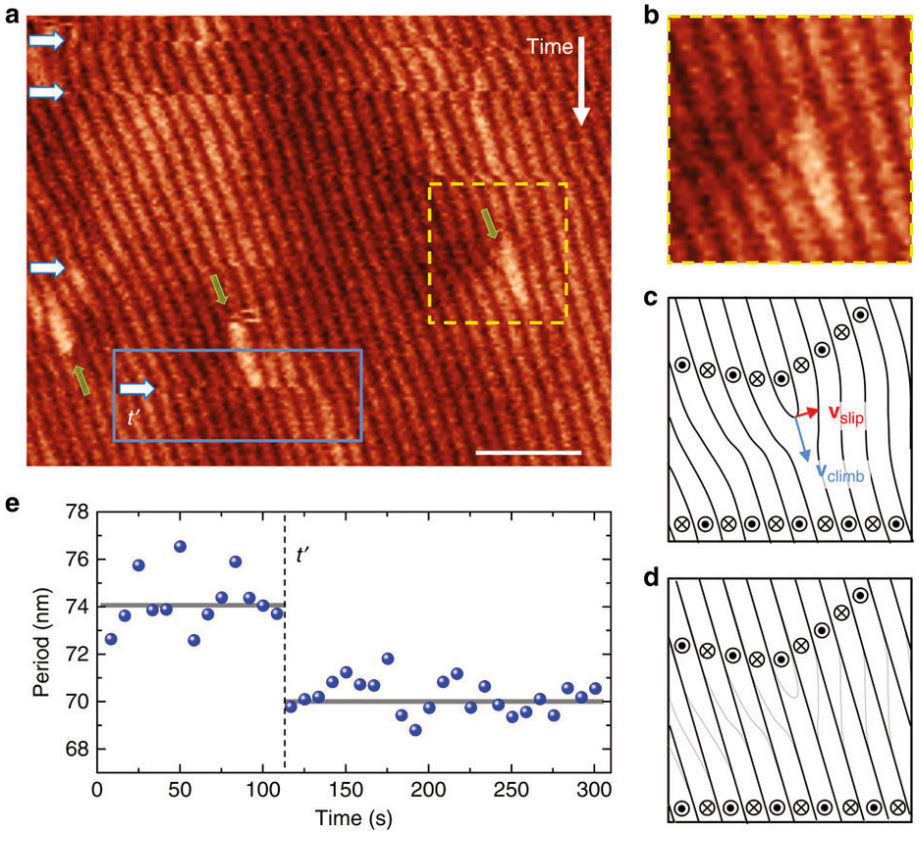

Figure 6.1. **(a)** Results of the helical spin-spiral state by MFM measurements in temperature $T = 255$ K. The black and white regions indicate the orientation of the magnetic moments and the white arrows are pointing the jumps in period during the measurement. **(b)** Zoomed-in figure of the non-trivial defect of the yellow box in (a). **(c)** Schematic representation of the defect in (b) and of its two possible motions shown by the blue and the red arrow. **(d)** Schematic representation of the helical spin-spiral after the removal of the defect. **(e)** The evolution of the period in time as captured in the blue box of (a).

For further studies of the spin-spiral period change captured from the experiment, we performed micromagnetic calculations of the system based on our ab-initio calculations. In the presence of finite temperature ($T > 0$ K), the thermal fluctuations of the magnetic atoms influence the structure of the helimagnet and when temperature near but below T_N is reached, the helimagnetic order is broken at some regions of the lattice. These kind of dislocations are present in the structure even at low temperature, which are quasi-stable because of their topological properties (non-zero topological number).

The defects are active in finite temperature due to the thermal fluctuations as it is presented in Fig. 6.2. In this figure, three different mechanisms of defect

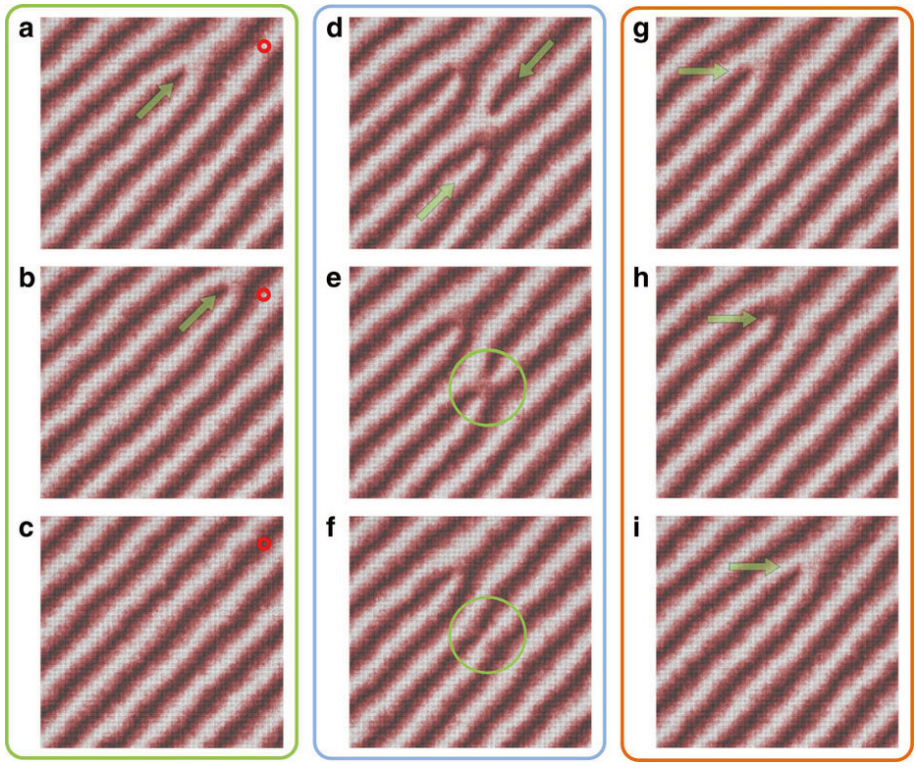

Figure 6.2. Spin dynamic simulations of three different defect motions at temperature $T = 0.5 \cdot T_N$. **(a-c)** The topological defect is climbing through the helimagnetic structure. **(d-f)** Annihilation of two opposite topologically charged defects when they come close to each other. **(g-i)** Slip motion of the defect.

annihilation are shown, which are called climbing (a-c), pair annihilation (d-f) and slipping (g-h). In the first case, the defect is moving perpendicular to the wave-vector **q** and it causes a phase shift (opposite orientation of the magnetic moments in a red circle between (a) and (c)). In the second case (d-f), when positive and negative defects meet, they annihilate each other and in the last case (g-i), the edge is moving parallel to the wave-vector. The defect dynamics shown by using the LLG simulations are in fact similar with topological defects in crystals and nematics.

In summary, from the detailed examination of topological magnetic defects in FeGe by combining two experimental techniques and micromagnetic LLG simulations it was demonstrated that mobile magnetic edge dislocations are very important for the development of spin-spiral ground state. These motions which are described above, reduce the free energy of the system and it is necessary to be controlled for device applications. Despite the fact that with our coarse graining methodology we might not get the correct time scale of the events, overall the simulations seem to agree very well with the experiments.

7. One dimensional magnetic structures within ASD

7.1 Introduction to 1D solitons

Studying low-dimensional magnetic structures remains extremely challenging and represents an exciting part of modern condensed matter physics. As discussed earlier in this thesis, in crystalline structures with lack of inversion symmetry, Dzyaloshinskii-Moriya (DM) interactions can emerge and they can cause the formation of two-dimensional chiral modulations like helical spin-spirals and skyrmions. In fact, the competition between Heisenberg exchange and DM allows for nontrivial topological texture to exist as a spin-spiral ground state configuration. Theoretically, such modulations were predicted by Bogdanov [72] and were originally identified as nonlinear configurations of a magnetic order parameter, or as solitons.

By applying a small perpendicular external magnetic field to a one dimensional helimagnetic structure with easy-plane anisotropy, it turns into a chiral magnetic soliton lattice [125, 126]. An isolated soliton structure along $z-$axis is represented in the left Fig. 7.2, where the $xy-$plane is the easy-plane according to the anisotropy in the model. The soliton is characterized by the soliton winding number, which is related to, yet different from the skyrmion winding number (N_{sk}) mentioned in chapter 5, and is given by:

$$w_{sol} = \frac{1}{2\pi}\int_{-\infty}^{\infty} \partial_z \Phi dz, \tag{7.1}$$

where $\Phi = \Phi(z,t)$, is the polar angle (Fig. 7.2) while z is the axis of the chain. The soliton winding number w_{sol} counts the number of twists of the magnetization along the chain. The result is an integer number and if it is equal to one, then it corresponds to one topological soliton.

Progress in the fabrication of quasi-one-dimensional metal-organic compounds and development of spintronics has opened new horizons for applications. In general, the class of quasi-one-dimensional magnetics includes a vast amount of systems and particularly the compound $Cr_{1/3}NbS_2$ [127] is for the purpose of this study of main interest since a chiral soliton lattice has been proposed for its magnetic structure [128]. Its hexagonal crystal structure is built up from NbS_2 layers intercalated by Cr ions. There are three basic magnetic interactions which constitute the spin structure: (i) the ferromagnetic exchange within the Cr layers $J_\perp$, (ii) another ferromagnetic coupling $J_\parallel$

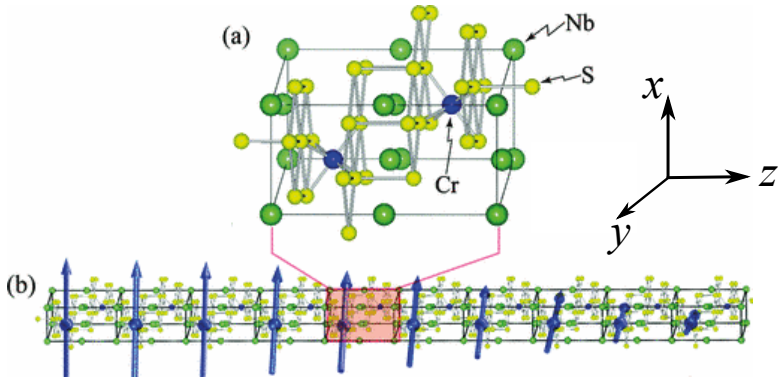

Figure 7.1. **(a)** A unit cell of the crystalline structure of $Cr_{1/3}NbS_2$. **(b)** Schematic representation of 10 unit cells along the $z-$axis, where the moments rotate in the $xy-$plane. This figure is taken from [128].

and (iii) the DM between Cr ions, the latter two interactions belong to the two intercalating layers separated by NbS_2 [129]. The competition between the latter two interactions forms a helicoidal structure in the absence of external magnetic field.

7.2 Analytical model

The behaviour of a quasi-one-dimensional helical structure can be studied analytically by using the micromagnetic Hamiltonian:

$$\tilde{h} = h_{\text{ex}} + h_{\text{DM}} + h_{\text{an}} + h_{\text{Z}}, \tag{7.2}$$

where the structure is located along the $z-$axis and the external field H along the $x-$axis. The first term of the Hamiltonian is the exchange interaction $h_{\text{ex}} = A\left(\partial_z \mathbf{M}\right)^2/2$, the second is the DM interaction $h_{\text{DM}} = D\mathbf{M}\cdot(\nabla\times\mathbf{M})$, the third is the anisotropy term with $xy-$plane being the easy plane $h_{\text{an}} = BM_z^2/2$ and the last term is the Zeeman term $h_{\text{Z}} = -\mathbf{M}\cdot\mathbf{H}$. The magnetization $\mathbf{M}(z,t)$ is a vector field with constant magnitude while the parameters A, D, and B provide the strength of the exchange interaction, DM interaction and the magnetic anisotropy respectively.

The magnetisation can be expressed in polar coordinates:

$$\mathbf{M}(z,t) = M_0\left(\sin\Theta\cos\Phi, \sin\Theta\sin\Phi, \cos\Theta\right), \tag{7.3}$$

where $\Phi \equiv \Phi(z,t)$ and $\Theta \equiv \Theta(z,t)$ are the polar and azimuthal angles. In the case of very strong anisotropy [130] the magnetization is almost confined to the $xy-$plane and for such systems we can use $\Theta = \pi/2 + \theta$, where $\theta \ll 1$. By using this expression of magnetism in the Landau-Lifshitz equation of motion, one arrives at the sine-Gordon model [131, 132]:

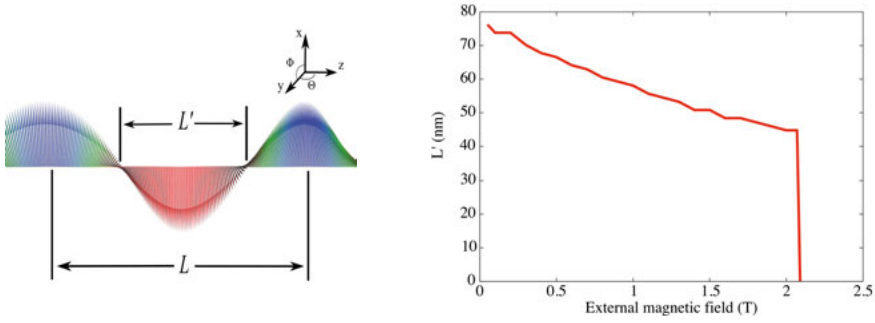

Figure 7.2. **Left:** Visualisation of the soliton where the direction of the external magnetic field is on $x-$axis. L stands for the period of the soliton and L' is the centre of the period. All the atomic magnetic moments are in $x-y$ plane. **Right:** Size of the centre of a soliton as a function of the external magnetic field.

$$\Phi_{\tilde{t}\tilde{t}} - \Phi_{\tilde{z}\tilde{z}} + \sin\Phi = 0. \tag{7.4}$$

The sine-Gordon equation has soliton solutions and this is very interesting because is giving us the analytical tool for the one-dimensional helical structures.

7.3 Calculations within ASD

In Fig. 7.2 a one-dimensional soliton structure is presented and, as described above, the rotation of the magnetic moments is taking place in the $xy-$plane whereas an external magnetic field is applied along the $x-$axis. For studying the behaviour and the dynamics of one-dimensional solitons we perform calculations by means of atomistic spin dynamics method [43], as implemented in the UppASD package [47]. For the calculations, the magnetic Hamiltonian described in Chapter 3 is used, where the strength of the ferromagnetic exchange interaction is chosen to be $J = 1.88$ mRy and the strength of the DM interaction is $D = 0.08$ mRy. The magnetic moments are treated as classical vectors with fixed length and the magnitude 1 μ_B. When applying an external field of 0.1 T at zero temperature, a soliton is stabilised, where the size of its center L' depends on the D/J ratio and the strength of the external field. By increasing the external magnetic field, the size of the soliton decreases (Fig. 7.2) and at some point, the soliton collapses when the Zeeman term becomes dominant.

Since the solitons have a continuously varying magnetic texture, they can be manipulated by spin-polarised current where an exchange of angular momentum takes place between the electrons of the current and the magnetic moments of the soliton structure. This exchange of angular momentum gives motion to the structure and the interaction between solitons can be investigated.

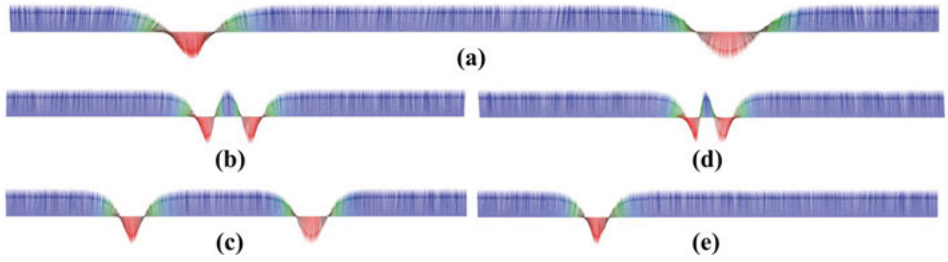

Figure 7.3. **Collision (b and c) and annihilation (d and e) of two solitons when they are moving in the opposite direction. (a)** The initial positions of the stabilised solitons. **(b)** Snapshot of the position of the solitons at the moment of their collision when spin-polarised current is applied with $j = 0.19 \times 10^{12}$ A/m^2 and $\beta = 0.2$. **(c)** Relaxed position of the solitons after the removal of the spin current. **(d)** Snapshot during the annihilation of solitons after applying spin current with $j = 0.38 \times 10^{12}$ A/m^2 and $\beta = 0.2$ and **(e)** creation of one soliton after the annihilation and turn off the spin current.

In order to investigate soliton-soliton interactions we stabilize by applying local field two solitons at the edges of the system (Fig. 7.3a) and by using the SLLG equation of motion (Eq. 4.14), two opposite spin polarised currents with direction from the edges to the center of the system drive the solitons towards each other and eventually make them collide. For the particular choice of exchange and anisotropy in our model, it is found that when the value of the current density is $j = 0.19 \times 10^{12}$ A/m^2 the solitons start moving and when the are close enough the current is removed. This value of the current density is not enough to overcome the repulsive potential between the solitons and as a result the solitons are moving back and relax as soon as the distance between them is big enough in order not to feel the potential (Fig. 7.3b and c). This is in agreement with the obtained 2-soliton solutions of the sine-Gordon equation which shows that solitons with the same chirality interact and push each other away. With an increase of the current density ($j = 0.38 \times 10^{12}$ A/m^2) the solitons overcome the repulsive potential which results on the "merging" in one soliton (Fig. 7.3d and e). The two opposite currents are turned off when the two solitons are almost annihilated and due to the emission of spin-waves which small fluctuations of the magnetization are caused which results in the emergence of new soliton. The final position of the emerged soliton (Fig. 7.3e) is not controllable because of the stochastic fluctuations which are present in the system. For more details see **paper I**.

7.4 Application of solitons in logic gates

A logic gate is a building block of any digital system which has one or more inputs and only one output. The connection between the inputs and the output

is based on a specific logic depending on the type of the gate. Two of the most famous types of gate is the AND and OR gate which consist of two input signals and one output signal. In the first case the output logic state is "1" only if both of the inputs are in logic state "1", otherwise the output signal is "0". On the other hand, the OR gate gives output signal "1" if one or more of the input signals are also "1". Another type of logic gate which is studied in this chapter is the majority gate which has three or more, odd number, inputs and one output which is defined by the majority logic state of inputs in the binary code ("0" or "1").

Nowadays, micro- and nanoelectronics are based on the complementary metal-oxide- semiconductor (CMOS) transistors, but for better functionality a fair amount of attention has been put into alternative approaches where CMOS can be replaced by other technologies [133, 134]. The major attributes of the new devices should be lower power dissipation and nonvolatility. This can be achieved by exploiting spin electron degree of freedom and the use of currents for transferring the information [9]. Non-collinear magnetic configurations such as solitons obey the forenamed requirements and are candidates for these new devices.

In **paper III** we build on our previous work on soliton-soliton interactions and use these results to study a three input majority gate based on 1D-solitons. The majority gate can perform AND and OR operations if one of the inputs considered as a regulator (input 1 in Table 7.1). In the solitonic majority gate that we propose here, the information is encoded in the chirality of the soliton as indicated in Fig. 7.4 where the helicity is determined by DMI exclusively. The strength and the sign of the DM interaction is possible to be controlled by circularly polarised laser which provides an ability to choose the input state.

Table 7.1. *Table of the logic operations for the solitonic majority gate. When the input signal 1 is controlled, the device performs an AND- operation when the input signal 1 is "0" an OR- operation when it is "1".*

Input 1	Input 2	Input 3	Output	Input 1	Input 2	Input 3	Output
AND-				OR-			
0	0	0	0	1	1	0	1
0	0	1	0	1	0	1	1
0	1	0	0	1	0	0	0
0	1	1	1	1	1	1	1

Similar to the previous section, for our study we use the atomistic spin dynamics approach and the solitons are driven by applying spin-polarised current. The parameters of the input part of our toy model (the three input arms on the left of Fig. 7.4) are $J = 1$ mRy, $D = 0.2$ mRy and the anisotropic constant is $K = 0.3$ mRy with the easy plane being the xz. It should also be mentioned here that the three left edges of the system have easy axis anisotropy along the

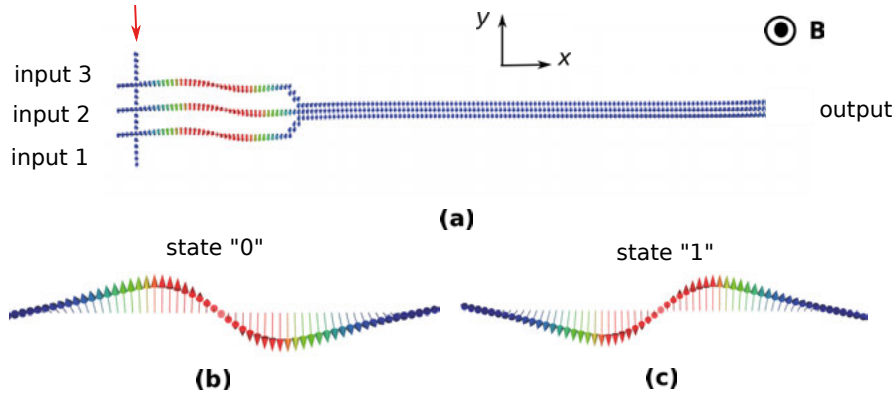

Figure 7.4. **(a)** The solitonic majority gate device, where on the left there are three input signals and on the right one single output signal. One soliton is stabilised in each branch with input states: "0" for input 1, "0" for input 2 and "0" for input 3. **(b, c)** Zoomed-in snapshots of the two different logic states "0" (left figure) and "1" (right figure).

$z-$axis with constant $K = 0.9$ mRy in order to supress the undesirable case of generating solitons at the edge of the system when the spin-polarised current is applied. In the output single arm, there is no DM interaction but anisotropy and exchange interaction are still present with a strength of $J' = 0.3$ mRy. The direction of the external field is perpendicular to the plane of the device (shown as **B** in Fig. 7.4), the coloured blue magnetic moments are parallel to it, whereas the red ones at the center of the soliton are antiparallel.

By applying a spin-polarised current along the $x-$direction, the solitons start moving towards the output arm. When they reach the thicker arm, they start interaction with each other and due to the lack of DM coupling in this part of the device, the magnetic moments prefer to be aligned in accordance with Heisenberg exchange interaction J'. This leads to a change in the direction of the edge moments of the minority soliton (edge moments of the soliton at input 2 of Fig. 7.5) and the resulted soliton of the output branch has the same chirality with the majority solitons as it is presented in Fig. 7.5. Since the output soliton is not well defined (there is no DM coupling between the moments) our interest is focused on the right edge of the solitons and when the rotation of this edge is along the $-y$ direction the output signal is "0" otherwise is "1".

The bottleneck of the suggested device is its sensitivity to the chosen parameters of the system and especially the strength of J' which if it is bigger than the threshold value of 0.3 mRy then the device looses its functionality and there is no output signal at all. Furthermore, the value of the current density has to be much bigger (4 orders of magnitude) than the depinning current in order to receive the output signal.

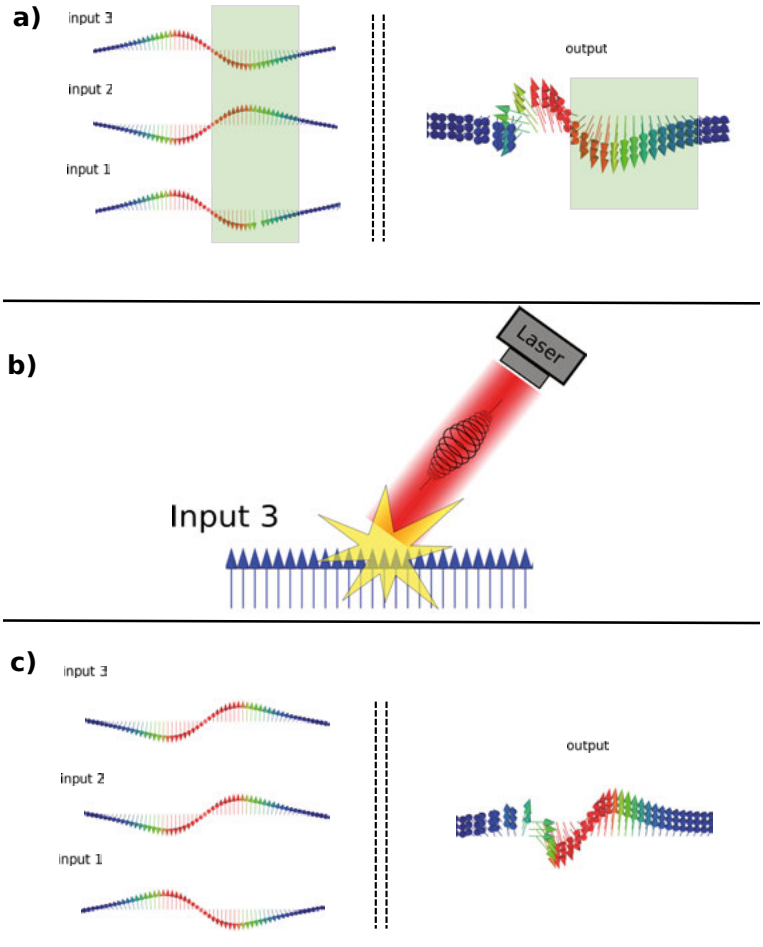

Figure 7.5. Snapshots from atomistic spin dynamics simulations which show the input and output signals before (a) and after (c) applying an external circularly polarised electromagnetic field at input 3 in order to inverse the DM vector and create a soliton afterwards with opposite chirality (b).

8. Magnetic heterostructures on heavy metal substrates

8.1 Introduction

Magnetic heterostructures on heavy metal substrate is currently attracting a lot of interest due to their unexpected behaviour of domain wall dynamics [55, 135], which is not compatible with the volume spin transfer torque (STT). These observations have triggered the interest of investigating the properties of such materials by ab-initio calculations and an extended study of different types of materials is done in **paper IV**. The majority of the systems under investigation perform perpendicular magnetic anisotropy (PMA) which is very important for the devices using domain walls since that allows for higher information density. Furthermore, it has been proposed [135] that relativistic effects are responsible for the unusual behaviour of the domain walls in these materials and more specific, the DM interaction and the spin-Hall effect. Based on the previously experimentally characterized materials, Co monolayers, Co trilayers and heterostructures of Co/Ni/Co deposited on different types of heavy metals are studied here. Our interest is focused on the Dzyaloshinskii-Moriya vectors and the magnetocrystalline anisotropy (MAE) which are crucial for a proper description of the magnetization dynamics of these systems.

In addition to the effect on the domain wall dynamics, the existence of strong DMI in this type of heterostructures is also very interesting because it favors the existence of skyrmions. In addition to the ab-initio characterization of the Co based PMA structures presented in **paper VI**, we have also studied the resulting dynamics in these kinds of system. In **paper VI** the domain wall and skyrmion dynamics are studied, under the influence of STT and the torque which arises from spin-Hall effect (SHE). The simulations have been done on model systems where the chosen parameters are based on the ab-initio studies of **paper IV**.

8.2 Computational methods and systems

The ab-initio calculations for the electronic and magnetic properties of the system are done by using the Korringa-Kohn-Rostoker approach, as implemented in the SPR-KKR package [40] and fully relativistic effects are taken

into account. Structural relaxation has also been considered for all the systems where the atoms are allowed to relax only along the $z-$axis. In order to determine the pairwise exchange interactions between the magnetic atoms (J_{ij} and $\mathbf{D}_{ij}$), LKAG formalism is used with the Ebert and Mankovsky approach [42] for the DM vectors. The distance of each calculated interaction set to 8 lattice spacings in order to take into account any possible RKKY interactions in the system [136, 137, 138]. The dynamics of the model systems is studied in terms of atomistic spin dynamics as implemented in UppASD package [47] and the torque resulting from SHE is given by equation (4.17) in Chapter 4.

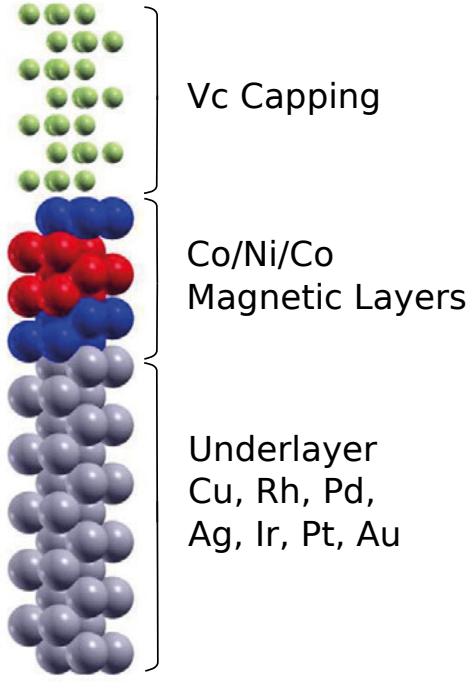

Figure 8.1. Visualization of the studied systems in the [111] direction in the interest region, the same kind of ordering is considered for the stacking in the [001] direction. The number of layers in each of the zones is kept constant.

In Fig. 8.1, the Co/Ni/Co superlattice on top of the heavy metal substrate is presented. As a substrate, they are used Cu, Rh, Pd, Ag, Ir, Pt and Au, while the systems are capped with Cu. For all the above systems, [001] and [111] stackings are studied with and without relaxation.

8.3 Results

For the atomistic spin dynamics study of the model system, the unit cell is given by a fcc (001) monolayer and the strength of the Heisenberg exchange

is fixed to $J = 1$ mRy for both cases of DWs and skyrmions. The strength of the DM interaction is $D = 0.025$ mRy for DWs and $D = 0.1$ mRy for the skyrmions. The direction of the DM vector stabilizes Néel DWs and Néel skyrmions. The value of the magnetocrystalline anisotropy is taken to be $K = 0.01$ mRy and the easy axis anisotropy is out-of-plane. The magnitude of the magnetic moments is $m = 1\mu_B$. Lastly, the damping parameter is considered to be $a = 0.01$, for simplicity, the non-adibacity parameter is maintained constant at $\beta = a$ and the spin-Hall angle Θ_{SHE} varies from 0.01 to 0.1.

8.3.1 Monolayers and trilayers of Co

The effect of the substrate on the magnetic properties of the simple case of monolayers and trilayers of Co studied and our interest is focused on the MAE and the pairwise exchange interactions. All the structures are relaxed along the $z-$direction as mentioned before and are examined in fcc [001], fcc [111] and the hcp [0001] when the Co is deposited on Tc and Re. For both monolayers and trilayers of Co, the easy axis of magnetisation depends on the crystallographic direction which is in-plane for the fcc [001], while in the case of fcc[111] and hcp [0001] stackings is out-of-plane. The magnitude of the anisotropy depends on the material of the underlayer and the change of the Fermi energy.

Similar to the MAE, the exchange stiffness of both monolayers and trilayers of Co are strongly dependent on the material of the underlayer. For the Co monolayers, the exchange stiffness of fcc [001] crystallographic direction is much larger than the case of bulk Co for all the underlayer materials. On the other hand, in the case of fcc [111] stacking there is however a larger variation where the exchange stiffness is larger than the bulk Co for monolayers on x, y, z while for when the substrate consists of q, w, r the stiffness is smaller than the bulk value. In the hcp [0001] stackings, the nearest neighbour interactions are much weaker and their values are smaller than the fcc stackings and the bulk case. For the Co trilayers, in the hcp [0001] stacking the value of the exchange stiffness is increased significantly in comparison with the Co monolayers and it becomes larger than the bulk Co.

The magnitude and the chirality of the DMI for both monolayers and trilayers of Co depend on the underlayer as well as the crystallographic direction. From our calculations, it is shown that in general, the DMI in the Co monolayers is larger than the trilayers and this results from the fact that the DMI is stronger at the interface where the spin-orbit coupling is larger due to the broken inversion symmetry. This means that in the layers far away from the interface the DMI is decreasing. More details can be found in the Tables I and II of **paper IV**.

8.3.2 Multilayers with heavy metal substrate

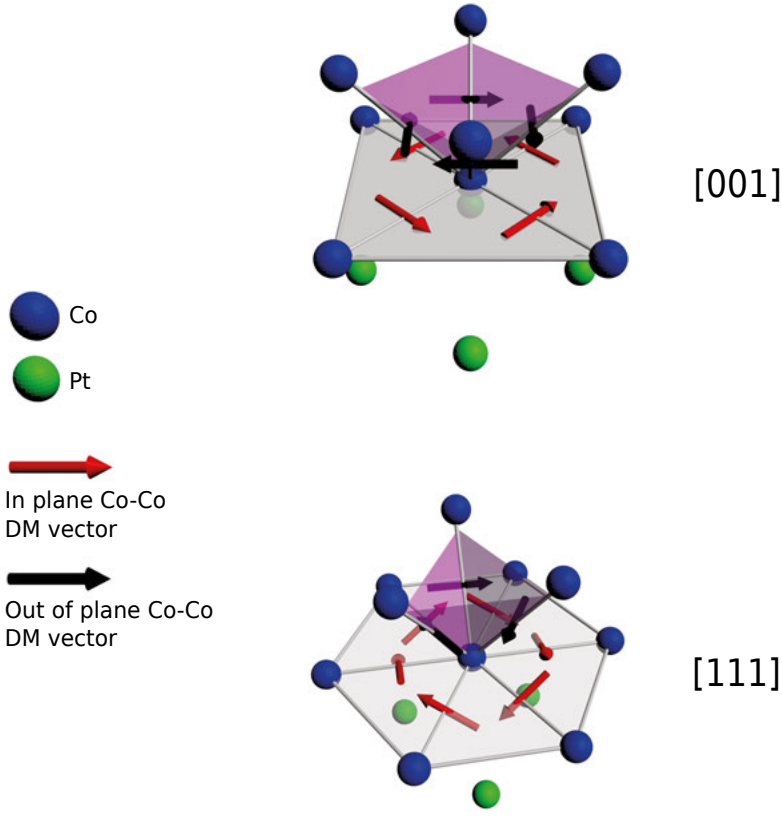

Figure 8.2. Diagrams for DM vectors for the central atom of the Co layer over the Pt substrate. **Top:** Unrelaxed structure for the [001] crystallographic direction. **Bottom:** Unrelaxed structure for the [111] crystallographic direction.

In this section, the electronic and magnetic properties of Co/Ni/Co multilayers on top of a heavy metal substrate (Cu, Rh, Pd, Ag, Ir, Pt and Au) will be presented. For the same crystallographic directions as in the previous section ([001] and [111]) and both relaxed and unrelaxed structures are considered. Again the relaxation is allowed to take place only along the $z-$direction. For the case of [001] growth without considering relaxation, changing the substrate the properties of the structure have a variation which is not dramatic for most of the substrates, except in the case of Ir substrate. By performing a structural relaxation, the exchange stiffness for each substrate increasing. Concerning the magnetocrystalline anisotropy, it does change significantly upon the relaxation for Cu and Ir substrates. Comparing our results between the two different crystalographic directions, most of the properties do not exhibit any

severe change, apart from E_{MAE} which is smaller for the [111] direction. For more details see Table III and IV of **paper IV**.

The ab-initio calculations, for both crystallographic directions, give DM interactions in the interface of the multilayers with the heavy metal substrate. In the case of [001] direction, the DM vectors between two neighbouring Co atoms are perpendicular to the bond and in-plane, and their directions are not changing with the structural relaxation. The magnitude of the DM vector depends on the material of the substrate. When the growth is taking place along the [111] direction, the DM vectors are still perpendicular to the distance vector between the two Co atoms, but compared to the situation for the unrelaxed structures they have also an out-of-plane component as presented at the bottom of Fig. 8.2. The relaxation, in this case, does thus not only change the magnitude but also the direction of the DM vectors which makes the relaxation very important. The strong relaxation dependence of the DM vectors could open up a possibility of tuning the DMI of a material by straining it, which could be achieved by alloying the substrate.

8.3.3 Domain wall and skyrmion motion

As mentioned in the introduction of this chapter, magnetic heterostructures on top of heavy metal exhibit an unexpected dynamical behaviour of domain walls [55, 135, 56]. This behaviour is observed in the case of Néel DWs and its origin is the torque coming from the spin-Hall effect (SHE) [135]. In our studies, in order to investigate the effect of the SHE on the dynamics of magnetic textures, a Néel domain wall is stabilised by choosing the direction of the DM interaction in our toy model. Furthermore, since DMI is usually strong in this kind of interfaces, skyrmions can be stabilised by introducing an external magnetic field. By applying spin polarised current to move the DW, a dependence of domain wall speed on the chirality of the DMI is observed as it can be seen in Fig. 2 of **paper VI**. This is consistent with the experimental results of reference [55].

When a magnetic layer is in contact with a non-magnetic one with a large spin-orbit coupling, then while the electronic current flows through the non-magnetic layer a transverse spin current is created and this is called spin-Hall effect. The SHE affects the dynamics of the spin textures [135, 60, 139, 140, 141] as shown on the left of Fig. 8.3. The magnitude of the spin-Hall angle influences the speed of the DW and a larger value of it results in higher speed.

The SHE torque has also impact to the total skyrmion velocity (on the right of Fig. 8.3) and in the direction of the motion. By using only the STT ($\Theta_{SHE} = 0$) to move the skyrmion and when the damping and the non-adiabatic parameter are $a = \beta = 0.01$, then the skyrmion is travelling almost parallel to the current, while the u_y contribution is almost negligible. This can be seen from the diagram on the right of Fig. 8.3, where for zero spin-Hall angle the

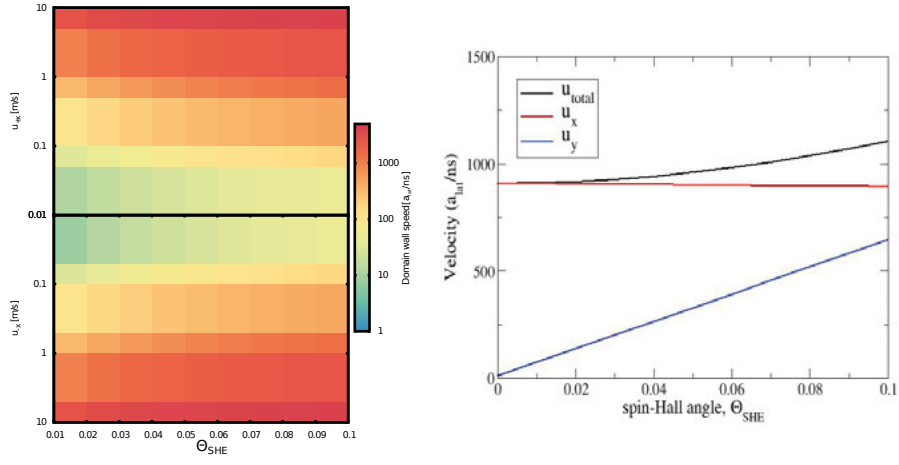

Figure 8.3. **Left:** Domain wall speed as a function of u factor and spin-Hall angle Θ_{SHE}. The subscript of the u parameter indicates the direction of the flow of the electronic current. **Right:** Total and the components of skyrmion velocity under the influence of SHE.

u_y is extremely small compare to the u_x. On the other hand, the SHE forces the skyrmion to move perpendicular to the direction of the current (along the $y-$axis) [142] and as the spin-Hall angle is increased the u_y contribution becomes larger. This behaviour of the perpendicular motion due to the SHE can be explained by the torque given in equation (4.17) of Chapter 4. As the current flows along the $x-$axis, the SHE torque is acting on the magnetic moments which have $y-$component (0,m_y,0) and it starts rotating them in the opposite direction (from -y direction to +y direction). Thus, when both STT and SHE torque are present in the system results in a skyrmion motion by a finite angle and not in a straight line.

8.4 Conclusions

At the interfaces of the studied systems there is a strong spin-orbit coupling but the magnetic properties which are derived from this coupling are also very sensitive to the local symmetry of the system and thus the crystallographic direction and possible relaxations can have a dramatic influence on the MAE and DMI. On the other hand, exchange stiffness is not influenced by the change of the growth direction. Furthermore, in the case of Co/Ni/Co multilayers, the value of MAE is affected by the underlayer material.

It is observed that the DM vectors depend on both the substrate and the crystallographic direction. The highlighted difference of DM vectors is the influence of their direction by the stack ([001] or [111]). Thus, in [001] direction the vectors have only in-plane components while in [111] an out-of-plane com-

ponent appears which is determined by the substrate. An impact of the DMI is the stabilization of the SHE which exerts a torque to the magnetic textures which results in higher speed for the DW and in higher value of skyrmion's velocity u_{total}.

9. Importance of edge interactions on creation and annihilation of skyrmions

As referred in detail in Chapter 5, there is a response of skyrmions to the spin polarised electronic current through spin transfer torques (STT) [97, 87, 100] and in this way it is possible to manipulate such spin textures efficiently. As was mentioned in Chapter 5, skyrmions have some advantages such as small depinning current and their ability to avoid defects, which make them promising candidates as information carriers for the next generation spintronic devices. However, in order to utilize skyrmions for this purpose, controlling their motion is not enough but of crucial importance is also the possibility of nucleating and annihilating skyrmions at will. Moreover, the information should be stable and protected during the transfer from the input to the output parts of the digital device. This means that the skyrmions should not be easily annihilated at the edges of a finite system. In the following chapter, we will demonstrate the impact of different edges to the annihilation and generation of skyrmions.

In order to study the interaction between skyrmion and edges, we evaluate the LLG equation of motion for a magnetic Hamiltonian with model parameters that resemble a generic skyrmion material. The simulations follows the methodology described in Chapter 4. The considered system is a two-dimensional model with 5,184 atoms (72×72) in the $xy-$plane with open boundaries conditions. The exchange interactions are taking place between nearest neighbours only with values of $J = 1$ mRy and $D = 0.32$ mRy. The atomistic magnetic moments are treated as classical vectors with fixed length and magnitude 1 μ_B, while the dimensionless damping parameter is $a = 0.1$. The mechanisms described below has also been simulated for other sets of exchange and damping parameters in order to conclude that the observed effects are not particularly sensitive to the choice of these parameters. The involved energies will however change with the choice of interaction strengths used in the Hamiltonian.

9.1 Generation of skyrmions

In order to examine which mechanisms and parameters that are important for current-induced skyrmion creation, we have simulated the effect of varying the exchange interactions present at the edges of the considered system.

As a starting point for the simulations, a ferromagnetic state is first stabilized by applying an external magnetic field along the $z-$direction. A spin polarised current is then injected into the system along the $y-$direction where we here have neglected non-adiabatic effects of the current by using a value of the $\beta = 0$ and we measure the threshold current density for nucleation of skyrmions at the edge. This procedure is also described in Chapter 4. The different edges are created by adding two rows at the bottom edge of the system and both the strength and the sign of the Heisenberg exchange has been varied. The values which are used for the edges are $J' = -J, J/2$ and $2J$ which represent the antiferromagnetic, the magnetically soft and stiff edge respectively. In Fig. 9.1 is illustrated the model system with the antiferromagnetic edge. The calculations show, as expected, that the magnetically soft edge has the lower current density threshold (2.9×10^{12} A/m^2) for generating skyrmion and the highest value is for the stiff edge (1.3×10^{13} A/m^2). While the threshold current for generating skyrmions in the normal system is 7.2×10^{12} A/m^2 and in the case of the anti-ferromagnetic edge is slightly smaller (5.1×10^{12} A/m^2). In the case of the magnetically soft edge, the strength of the exchange interaction is $J' = 0.5$ mRy $< J$ and since all the other parameters are the same as the rest of the system, the effective field B_i^{eff} of the magnetic Hamiltonian is smaller and is easier to rotate the magnetic moment at the edge by applying spin polarised current.

For more details see Table I in **paper VII**.

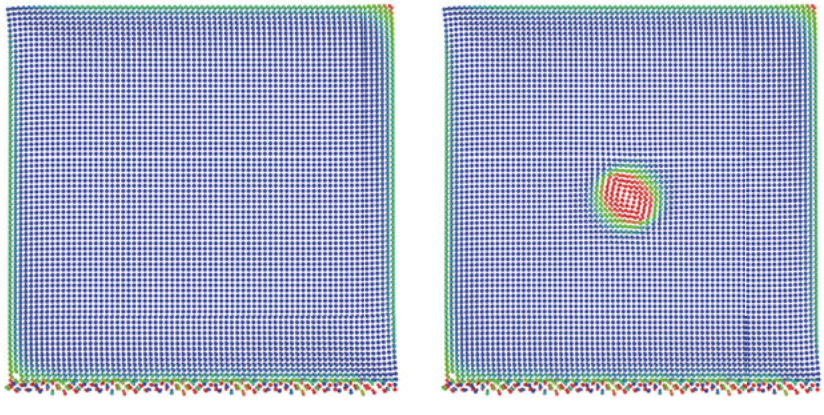

Figure 9.1. Vizualisation of the sytem with the antiferromagnetic edge with the stabilized ferromagnetic state for skyrmion nucleation (left figure) and stabilized skyrmion for the annihilation procedure (right figure).

9.2 Annihilation of skyrmions

For using skyrmions as information carriers, the annihilation process is equally important as for the creation process. When the skyrmion is close to the edge, there is a repulsion between the outer boundary of skyrmion and the edge of the system. The repulsive nature of the potential comes from the opposite orientation of the magnetic moments at the edge and at the outer boundary of the skyrmion. Responsible for this opposite orientation is the direction of the DMI in the system which means that it would cost energy to the system if a rotation of these magnetic moments takes place. Thus, in order to annihilate the skyrmion at the edge, it has to overcome this energy barrier. By applying a spin polarised current into the system, the skyrmion can be driven to the edge but the energy barrier infers that in order to annihilate the skyrmion by driving it out of the sample, the spin current density must be larger than a given threshold value. On the other hand, if the strength of the current is smaller than the threshold value, then the skyrmion is not able to overcome the energy barrier but instead it moves parallel to the edge of the system. In this section, we investigate the effect of the energy barriers for different kind of edges similar to what was done in the previous section for the nucleation process.

Table 9.1. *Energy barrier for different kind of edges. The applied current density for moving the skyrmion is* $j = 8.45 \times 10^{11}$ *A/m*^{2}.

Type of edge	Energy barrier (mRy)
Normal edge	0.0011
AF edge	0.0012
Soft edge	0.0007
Stiff edge	0.0014

First, a single skyrmion is stabilised at the center of the system (Fig. 9.1) and then is driven to the bottom edge by injecting current. The current density is $j = 8.45 \times 10^{11}$ A/m^2. The highest and the lowest energy barrier are reported for the case of the magnetically stiff and soft edge respectively as it is shown in Table 9.1. As previously mentioned, the strength of the exchange interaction of the soft edge J' is smaller than the J of the rest of the system. This means that it favours a slower rotation of the magnetic moments since DMI is not changed at the edge. In other words, the angle between the magnetic moments at the soft edge and the direction of the external field is smaller compare to the case of the normal edge. This smaller angle explains the lower repulsive potential and therefore the smaller energy barrier.

A particularly interesting observation that was obtained from the simulations is that there are actually two different annihilation processes observed, depending on the choice of interaction strengths. For all the different edges,

except for the stiff edge, the skyrmion is approaching the edge and a rotation of the magnetic moments at the edge is taking place. The rotation results in the reduction of the repulsive potential and as the skyrmion is getting closer, the repulsive potential keeps decreasing. At some point, the skyrmion will be attached to the edge and the annihilation process starts (Fig. 9.2a-c). A different procedure is on the other hand found for the annihilation process against the magnetically stiff edge. In this case, there is no rotation of the moments at the edge of the system but instead it is the moments at the perimeter of the skyrmion who start to rotate. This has an impact on the size of the skyrmion which is getting smaller and smaller as the current keeps pushing it at the edge. At the end, the skyrmion collapses as is shown in Fig. 9.2d-f. Therefore, the energy barrier n Table 9.1 for the magnetically stiff edge (0.0014 mRy) it does not come from the edge but it is actually the intrinsic energy of the skyrmion. The interpretation of the two observed scenarios is that the energy barrier, or associated current density threshold, can be lowered by softening the magnetic interactions at the edges of a skyrmion-carrying material. On the other hand, it is not possible to increase the barrier by a magnetically hard edge because the maximum strength of the annihilation barrier is in fact determined by the intrinsic exchange interactions in the material where the skyrmion exists.

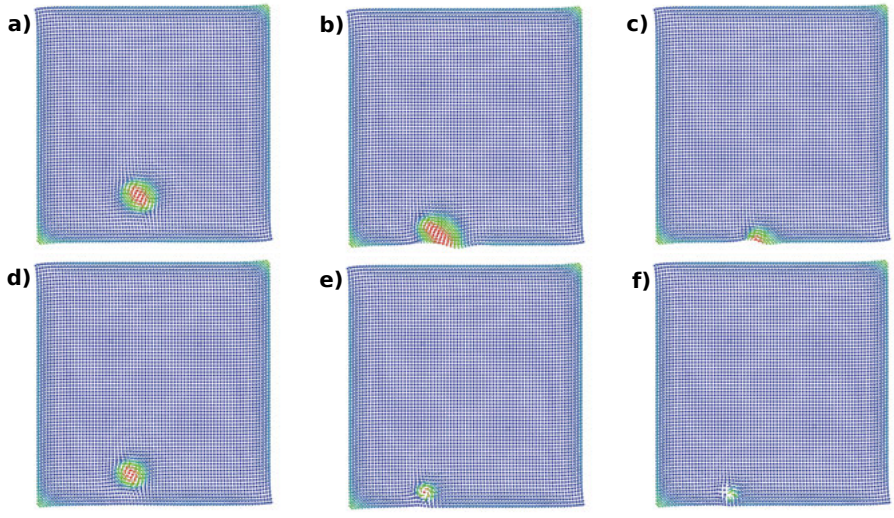

Figure 9.2. Vizualisation of the two different procedures of annihilation. (**a-c**) Skyrmion forces the edge moments to rotate and eventually is attached to the edge and is getting out of the system. (**d-f**) In the case of magnetically stiffer edge, the skyrmion does not penetrate into that region which results in the shrinking of the skyrmion which is followed by collapsing.

10. Skyrmion phase in $MnPt_{0.99}Ir_{0.01}Sn$ half-Heusler alloy

It is already mentioned throughout this thesis that the most important interaction for the stabilization of skyrmions is the DM interaction and its competition with the Heisenberg exchange. Materials with large spin-orbit coupling and lack of inversion symmetry exhibit strong DM interaction. The most famous and studied class of materials for stabilising skyrmions are the ones with non-centrosymmetric B20 structure (e.g MnSi [10] and FeGe [77, 76]). Skyrmions have also been observed in low dimensional structures as Fe monolayer on top of Ir(111) [61] or in a ferromagnet/heavy metal bilayer [92]. Another promising class of materials for skyrmion observation are some Heuslers alloys, such as Mn_2RhSn [143], which show a non-collinear ground state.

From energy considerations, it is evident that the skyrmion size can be altered by varying the D/J ratio. Changing this ration can be achieved by alloying, as has been demonstrated for $Mn_{1-x}Fe_xGe$ B20 structure [81]. In **paper V**, MnZSn half-Heusler systems have been studied from first-principles with Z being Tc, Ru, Rh, Os, Ir and Pt in order to explore which of them perform a non-collinear ground state. The ground state of MnPtSn is a spin-spiral, thus the alloy $MnPt_{1-x}Ir_xSn$ has also studied from first-principles in order to examine how its spin-spiral wavelength λ_{spiral} changes. Afterwards, the phase diagram of lowest Ir concentration ($x = 0.01$) investigated in terms of atomistic spin dynamics calculations.

10.1 Magnetic interactions and spin-spiral wavelength

The magnetic interactions of all half-Heusler compounds which are referred in the introduction are calculated in order to investigate if they exhibit non-collinear magnetic order. The Mn-Mn Heisenberg exchange interactions for the studied systems show strong anti-ferromagnetic interactions, except for the case Z=Pt as presented in Fig. 10.1. It is further found from the calculations that the strength and the direction of the DM interaction depend on the Z material. From all the studied compounds only MnPtSn was found to have ferromagnetic exchange interaction and its ground state is a spin-spiral with short wavelength due to the small Heisenberg exchange and the large DMI. More details of the electronic structure for the Heusler compounds can be found in **paper V**.

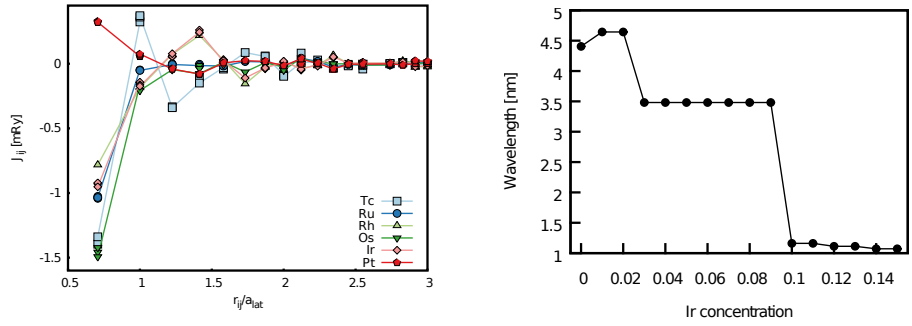

Figure 10.1. **Left:** Pairwise exchange interactions as a function of distance for MnZSn. **Right:** Spin-spiral wavelength as a functon of Ir concentration in $MnPt_{1-x}Ir_xSn$.

The electronic structure of MnPtSn is affected by partial alloying, in our case by substituting Pt with Ir. As the Ir concentration increases in the compound, the pairwise Heisenberg exchange interaction between the Mn-Mn nearest neighbours decreases and this behaviour can be understood by looking the left panel of Fig. 10.1, where it is shown that the MnIrSn has antiferromagnetic Mn-Mn interaction. In contrast to the Heisenberg exchange interaction, the x and y component of the DM vector are increased while there is no significant change of the z component as it can be seen in Fig. 10.2. Since the D/J ratio is tuned as a function of Ir concentration, the spin-spiral wavelength is also tuned as is illustrated in the right plot of Fig. 10.1. From our results, we observe that the wavelength is much shorter compare to the B20 structures.

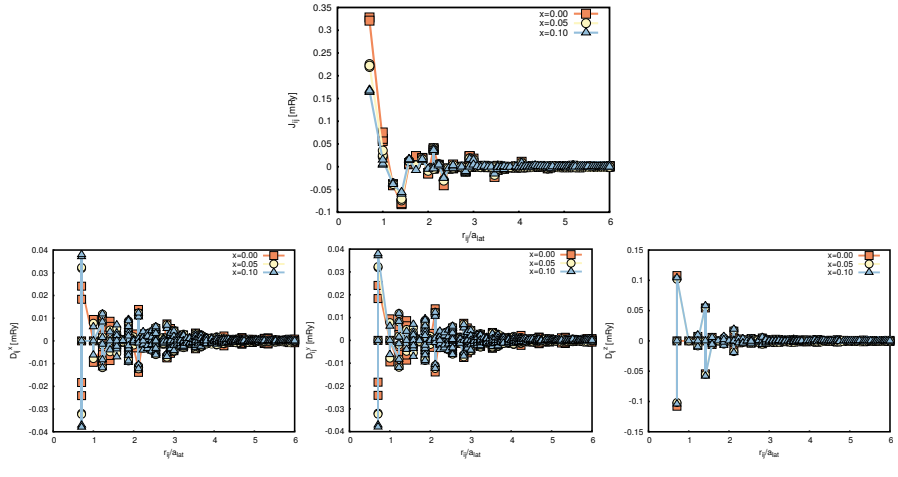

Figure 10.2. In the upper panel are shown the exchange interactions as a function of distance for $MnPt_{1-x}Ir_xSn$ for three different concentration of Ir (0.0, 0.05 and 0.10). In the three bottom panels are shown the components of the Dzyaloshinskii-Moriya interactions (D^x_{ij}, D^y_{ij} and D^z_{ij}) for the same concentrations of Ir.

10.2 Phase diagram of $MnPt_{1-x}Ir_xSn$ thin film

Guided by the results for the fully ordered Heusler compounds studied in the previous section, the existence of skyrmions has also been investigated in the thin film $MnPt_{0.99}Ir_{0.01}Sn$ alloy by performing atomistic spin dynamics simulations. A thin film is used in our calculations because of the fact that several experimental results [76, 88, 144, 145] agree on the wider region of SkX-phase in the $T - B_{ext}$ (T is the temperature and B_{ext} is the external magnetic field) phase space, when the thickness of the sample is smaller or slightly bigger than the spin-spiral wavelength.

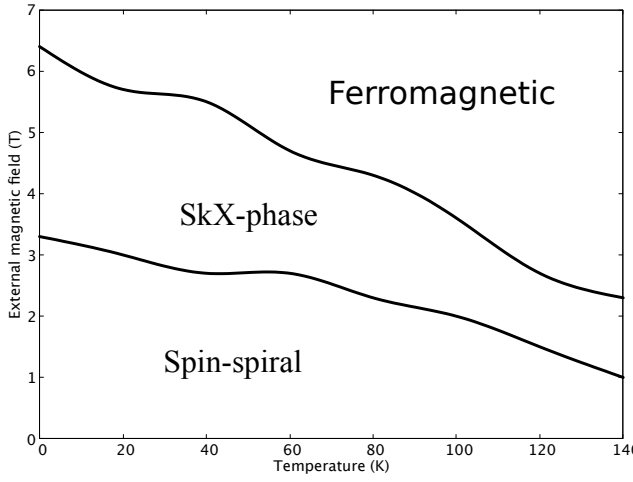

Figure 10.3. Calculated phase diagram of thin film $MnPt_{1-x}Ir_xSn$ alloy.

The results show a skyrmion phase for the certain half-Heusler compound as it is presented in Fig. 10.3, where the SkX-phase is the skyrmion phase. As seen in Fig. 10.3, skyrmions are stable when an external magnetic field is applied even when the temperature is zero. The spiral wavelength in the ground state is $\lambda_{spiral} = 4.6$ nm and the thickness is chosen $t = 3.7$ nm. The critical temperature of the system is $T_C = 140$ K and above this temperature, the system exhibits a paramagnetic behaviour. At $T = 0$ K and in low external field the spin-spiral configuration is stabilised and the transition to skyrmion phase takes place at $B_{ext} = 3.3$ T. When the external field is increased further, then the Zeeman term of the magnetic Hamiltonian is the dominant one and the ferromagnetic state is stabilised. Those three states exist in the whole temperature range up to the T_C and it is observed that in higher T lower external field is needed for the stabilisation of skyrmions and for the ferromagnetic state as well. It is worth mentioning here, that the range of the magnetic field in which the skyrmion phase exists in the thin film $MnPt_{0.99}Ir_{0.01}Sn$ alloy is quite large ($\sim$3 T at zero temperature) compare to the one of B20 structure thin films. For

instance, the experimental observation of FeGe thin film [77] gives a range of $\sim$0.3 T at zero temperature where skyrmion phase is present.

By applying a spin-polarised current through the thin film we are able to move the stabilised skyrmions and discover the depinning current density. For the $MnPt_{0.99}Ir_{0.01}Sn$ thin film under the influence of $B_{ext} = 4.7$ T and at $T = 0$ K the depinning current density is $j = 8.3 \times 10^9 A/m^2$.

Because of the observed spin-spiral ground state, the half-Heusler MnPtSn compound and the $MnPt_{1-x}Ir_xSn$ alloy are suggested to be promising candidates for realising the skyrmion state in the Heusler family. The advantage of the $MnPt_{1-x}Ir_xSn$ alloy is that the magnetic properties can be tuned, by changing the Ir concentration in order to achieve small size skyrmions. In the case of the small Ir concentration ($x = 0.01$), the skyrmionic state is stable in a wide range of external magnetic field even at zero temperature in the case of thin film.

11. Conclusions and outlook

Devices used in technology nowadays are getting smaller in size, which means that the characterization of magnetic properties and the investigation of magnetization dynamics on the atomic level becomes more and more important. This characterization can be done by combining first-principles calculations and the atomistic spin dynamics method. We have demonstrated that first-principles calculations, by the use of density functional theory, can describe the magnetic ground state properties, while the LKAG formalism can describe the pairwise exchange interactions, J and DM, of the studied materials quite well. In addition, the magnetic ground state and the evolution of magnetization in time can be studied with atomistic spin dynamics by using the Landau-Lifshitz-Gilbert equation of motion. Combining these two methods provides a valuable and powerful tool for studying the static and dynamic magnetic properties on an atomistic level.

Both methods described above, have been used in this thesis with the overall goal of studying the mechanisms behind skyrmion manipulation and also characterizing materials suitable for future skyrmion-based applications.

Regarding the investigation of suitable skyrmion materials we have studied the MnZSn half-Heuslers compounds. First, first-principles studies are used in order to discover the magnetic properties of these half-Heuslers compounds and the results show that the alloy $MnPt_{1-x}Ir_xSn$ has a ferromagnetic coupling ($J > 0$) and a strong DM interaction. Then, atomistic spin dynamics simulations show that the competition between these two exchange interactions results in a spin-spiral ground state. The wavelength of the helimagnetic ground state is influenced by the Ir concentration and as the concentration is increasing, the wavelength is decreasing. By applying an external magnetic field to the thin film of $MnPt_{0.99}Ir_{0.01}$, the skyrmion phase is observed even at zero temperature.

The same methods have been also used for the investigation of the dynamics of topological magnetic defects in FeGe which are combined with experiments (MFM and single-spin magnetometry with NV centers). From this study it was found how thermally induced defects, especially in the shape of magnetic edge dislocations, move. The understanding of the defect dynamics in helimagnets is important for explaining the development of the helimagnetic ground state. The defect motion takes over micromagnetic distances and it explains the magnetic instabilities in helical magnets.

Furthermore, the LKAG formalism has also been used to study the exchange interactions of low-dimensional Co heterostructures on top of a non-magnetic heavy metal substrate. From this study it is found that the choice

of substrate determines the magnitude and the direction of DM interactions. Also, the crystallographic direction of the stacks plays a major role to the DM vector. Based on the results of the previous heterostructures, toy models are used in order to investigate the motion of domain wall and skyrmion by the use of SLLG equation of motion. It is found that the speed of the domain wall and both the speed and the direction of skyrmion are influenced by the presence of SHE.

Concerning the dynamics of topological magnetic structures and individual solitons several studies on how such systems can be manipulated has been performed. Magnetization dynamics studies show that it is possible to annihilate and create one-dimensional solitons by means of a spin-polarised currents. Furthermore, these nanostructures are able to perform logic operations by encoding the logic state ("0" or "1") in the chirality of the structure. A three-input majority gate been proposed which requires the absence of DMI in the output arm. The choice of the encoded input has been proposed to be achieved by the use of a laser which gives the opportunity to change the sign of the DMI and tune the strength if necessary.

Regarding skyrmion dynamics, the interaction between skyrmions and the edges of the system on which they are confined have been investigated by means of atomistic spin dynamics simulations. In particular, the annihilation and nucleation processes that can be obtained at the edge of a sample, by injecting spin polarised current has been studied. It is demonstrated that the current density threshold strongly depends on the strength and type of the magnetic interactions present at the edge. Being able to modify the current thresholds needed for annihilating and creating skyrmions has an an obvious impact on the energy consumption associated with these processes. This is important since skyrmions are candidates as information carriers in the future magnetic storage devices.

The presented methods offer the tool for designing magnetic materials for new technological applications which can improve the performance and the energy consumption of the computer technologies. The atomistic discrete description gives also the opportunity for the examination of more complex magnetic structures which attract a lot of interest lately, such as antiferromagnetic skyrmions. By further development of the atomistic spin dynamics method, it will be possible to study the magnetization dynamics of such structures by applying spin-polarised currents.

One of the challenges for magnetic skyrmions is the ordering temperature which in B20 structures is below room temperature and for that reason different classes of materials with strong DMI have to be investigated for magnetic skyrmions. In this thesis, we found out that skyrmion state exists in a thin film of half-Heusler alloy ($MnPt_{0.99}Ir_{0.01}$) in which the ordering temperature is again below the room temperature but it shows that the huge class of Heusler alloys are also candidates for investigating the skyrmion phase. Another challenge is the size of magnetic skyrmions where a small size is

desirable since a higher bit density can be achieved. Interfaces between thin magnetic layers and non-magnetic heavy metal substrates are promising candidates because some of them exhibit strong DM interaction and perpendicular magnetic anisotropy as it is shown from our first-principles studies. Moreover, it has been shown in the thesis that the exchange interactions (both J and DM) can be tuned by alloying half-Heusler compounds which could result in a small size magnetic skyrmions.

The physical and topological stability of magnetic skyrmions are of particular interest for spintronic applications. These properties make skyrmions robust against defects and each skyrmion could be used to store 1 bit of information. This type of structure is possible to be created with a magnetic field, electric field or low-density current which it can be also used for manipulating them. However, until recently, skyrmions did exist at very low temperatures but it is predicted that they also exist at room temperature by stacking magnetic and non-magnetic thin layers. In other words, there is an opportunity of creating next generation very high density information storage devices due to the nanometer size of each skyrmion. Moreover, the properties of the magnetic skyrmions as previously mentioned, improve the stability of the bits as well as the speed and the efficiency of writing and reading the information due to their fast motion through the material. In addition, compare to the HDD or SDD storage devices, skyrmion-based devices do not require mechanical moving parts but only low-density current which makes it possible to reduce the energy consumption. Furthermore, these proposed devices are compatible with conventional integrated circuit technology but of course, there are still challenges that have to overcome in order to use skyrmions as information carriers. Some of these challenges are the difficulties of fully controlling their motion and their nucleation as well as the issue of protecting them from the boundaries of the device in order to avoid undesirable annihilations. There is still a long way to go until the first memory applications based on magnetic skyrmions are produced.

12. Summary in Swedish

Magnetisk datalagring är ett forskningsområde som har varit aktivt långt mer än bara senaste årtiondena, vilket många kanske tror. Grundidén är dock fortfarande densamma: skriv- och läshuvuden används för att spara och hämta data. Under de senaste 30-35 åren har den här sortens magnetisk lagring utvecklats enormt, kapaciteten har ökat från kilobytes till terabytes och överföringshastigheten har ökat från enstaka bytes per sekund till 100+ megabytes per sekund. Dessa framsteg har till stor del möjliggjorts genom upptäckandet av nya elektroniska komponenter, som utför snabbare logiska beräkningar genom att använda sig av elektriska strömmar. Det verkar dock som att taket snart är nått för prestandan hos de elektroniska komponenterna på grund av problem från oönskad Joulevärme som uppkommer av elektronernas rörelse. Ett alternativ för att fortsätta att öka prestandan kan vara att använda komponenter som utnyttjar elektronernas spinn (spinntropik) eller förändringar av materialets magnetiska struktur såsom spinnvågor (magnonik), istället för konventionella elektroniska komponenter. Utvecklandet av spinntropik kan sägas ha startat på bred front med upptäckandet av Giant Magneto-Resistance-effekten (GMR) [2, 3] av Peter Grünberg och Albert Fert som fick Nobelpriset i fysik 2007 för det arbetet om magnetisk manipulation av elektriska strömmar. Användandet av spinn för att transportera information har sedan dess lett till en ny generation av snabbare och energisnålare komponenter med ökad datalagringsförmåga.

Ett fenomen som kan ses som en invers av GMR är möjligheten att påverka magnetismen i ett material med hjälp av spinnpolariserade elektriska strömmar. Den effekten kallas på engelska spin transfer torque (STT) eftersom den orsakas av att det sker en överföring av rörelsemängdsmoment mellan elektronerna i strömmen och elektronerna i det magnetiska materialet. Baserat på det här fenomenet har Stuart Parkin föreslagit en datalagringslösning, där STT-effekten används för att flytta domänväggar i ett ferromagnetiskt material. Deras höga hastighet är en egenskap, som gör domänväggar till en lockande metod för att skapa logiska komponenter, t.ex. Magnetic Random Access Memories (MRAMs). Dock måste man, för att nå de här höga hastigheterna, använda en väldigt hög strömtäthet i storleksordningen $j \sim 10^{12}$ A/m^2.

2009 upptäcktes en icketrivial magnetisk struktur som sedan dess har fått ett väldigt stort intresse inom området av kondenserad materialteori. Strukturen kallas skyrmion och dess beskrivning härstammar ursprungligen från en högenergimodell inom partikelfysiken. Magnetiska skyrmioner är topologiskt stabila och kirala spinnstrukturer som kan beskrivas av en virvel av

de magnetiska momenten och där den magnetiska strukturen har en väldigt mjuk övergång i materialet. Den sistnämnda egenskapen får skyrmionerna att koppla väldigt effektivt till spinnpolariserade elektriska strömmar, vilket resulterar i ett extremt låg tröskelvärde för den kritiska strömtätheten, i storleksordningen $j \sim 10^6$ A/m^2. Men skyrmioner är lovande kandidater för framtida datalagringskomponenter inte bara på grund av det lilla strömtröskelvärde som behövs för att förflytta dem, utan även för att deras rörelser inte påverkas mycket av eventuella defekter i materialet.

För att fullkomligt förstå fenomenen på nanonivå hos de nya föreslagna spinnbaserade komponenterna, oavsett om de är uppbygda av domänväggar eller skyrmioner, behövs en karaktärisering av dess magnetiska egenskaper samt deras magnetiseringsdynamik på atomär nivå. Enkla modeller används ofta för att beskriva magnetismen i material. En väldigt populär och vanlig modell är Heisenbergmodellen [12], vilken beskriver kopplingen mellan lokaliserade magnetiska moment. Heisenberghamiltonianen kan expanderas så att den förutom kopplingskonstanten J, också innehåller termer som beskriver ett materials magnetiska anisotropi (MAE), samt ett tredje magnetiskt bidrag som kallas Dzyaloshinskii-Moriyaväxelverkan (DMI). Det sistnämnda bidraget är en antisymmetrisk utbytesinteraktion mellan de magnetiska momenten och den spelar en avgörande roll för stabiliseringen av skyrmioner och liknande magnetiska strukturer. Alla parametrar i den utökade Heisenbergmodellen kan beräknas med hjälp av metoder baserade på täthetsfunktionalteori (DFT). För att studera magnetiseringsdynamiken för atomära magnetiska moment kan Landau-Lifshitzekvationen (LL) eller Landau-Lifshitz- Gilbertekvationen (LLG) [13, 14] användas. Kombinationen av LLG simuleringar på atomär nivå, som också kallas atomistisk spinndynamik (ASD), med DFT beräkningar av de viktigaste parameterarna i den magnetiska Hamiltonianen ger en metod som är väldigt användbar för att undersöka tidsutvecklingen av magnetism på små längdskalor och i komplexa magnetiska strukturer.

Denna avhandling rymmer ett antal studier där DFT beräkningar och ASD simuleringar har använts för att undersöka hur skyrmioner, domänväggar och andra magnetiska strukturer kan manipuleras genom spinnpolariserade strömmar. En familj av lovande system för framtida skyrmiontillämpningar är tunnfilmsbaserade material där övergångsmetallen Co kombineras med tyngre metaller som Pt, Ir och Au. Dessa system har undersökts med hjälp av DFT beräkningar som visat att såväl materialens MAE och DMI uppvisar ett starkt beroende på vilken metall som kombinerats med Co. Beroendet är så kraftigt att till och med tecknet på växelverkan kan ändras mellan de olika systemen. DFT beräkningar har också använts för att undersöka magnetiska egenskaper hos Mn-baserade metalliska legeringar med Heuslerstruktur. För lämpligt valda legeringsammansättningar såsom $MnPt_{0.99}Ir_{0.01}Sn$ indikerar beräkningarna att legeringens DMI är sådan att det går att stabilisera skyrmioner i materialet.

Genom att kombinera DFT beräkningar och ASD simuleringar har magnetiseringsdynamiken i det heliska spinnspiralmaterialet FeGe studerats, framför

allt med avseende på hur magnetiska defekter uppkommer och rör sig vid höga temperaturer. Den teoretiska undersökningen har här kombinerats med experimentella studier och tillsammans har det visat att de magnetiska defekterna i den helimagnetiska strukturen kan vara av topologisk karaktär och att de även beter sig på ett liknande sätt som defekter i helt andra system så som ordnade kristaller.

Dynamiken hos isolerade skyrmioner i tunna filmer har också studerats med ASD. Studierna har visat att det går att påverka hur lätt det är att skapa och förstöra individuella skyrmioner genom att ändra de magnetiska egenskaperna, framförallt Heisenberg och Dzyaloshinskii-Moriya inneraktionerna vid systemens kanter. Starkare Heisenbergkoppling bidrar till att en högre strömtäthet krävs för att skapa skyrmioner, medan den kritiska strömtäthet som behövs för att förstöra en skyrmion är begränsad av utbyteskopplingarna inne i materialet och inte främst vid kanterna.

Dessutom har magnetiseringsdynamiken för magnetiska solitoner i kvasiendimensionella material studerats med ASD simulerings och där har det visats att för enkla fall kan dynamiken beskrivas med analytiska uttryck som ges av sina-Gordonekvationen. Vidare har simuleringarna visat, givet att DMI i materialet kan påverkas genom yttre stimulans, att dessa magnetiska solitoner kan kombineras för att utföra fundamentala logiska operationer. Solitonerna skulle därmed kunna användas som byggklossar för framtida spinnbaserade tillämpningar för informationsbehandling.

13. Acknowledgements

First of all, I would like to thank my supervisors Anders, Olle, Corina and Manuel for all their help, for being available to discuss everything and at any time. Without their encouragement and guidance, this thesis would be impossible to complete. Furthermore, I would like to thank Jonathan, Lars and Dmitry for their ideas and valuable help with many projects as well as Danny and Attila for their detailed discussions on methods. It was my pleasure to be a part of spin dynamics group from which I gain a lot of my knowledge during our meetings, presentations and following discussions.

I would also like to thank my teaching partner Ritwik, for having a great time during our courses/schools and for his big smile and happy moments. Sotiris, my friend and flatmate who made my time at home (and not only) very very nice and enjoyable, Henry and Eya for the great Friday nights, Marco for his tips and support on bouldering and John for being a part of the lunch gang and his valuable help with the Swedish text of the thesis. A special thanks to Alex and Attila for their very interesting gatherings we had from time to time, the fruitful discussions and the very funny moments taking place in Sweden and abroad. To Pablo for always making noise and for transferring his happiness to everyone.

I was extremely lucky for having the best office mates ever who became also two of my best friends, Jonathan and Robert. Thank you guys for creating a perfect working environment, for the very nice lunch-breaks with the horrible jokes and movies discussions. Furthermore, I also thank you for the amazing movie nights with pizzas and masterpieces of the seventh art.

I want to express my appreciation to the weekends' fika members, Vasilis, Katerina, Alekos and Vicky who all of them have established tolerance to my very bad jokes and my meaningless sentences. Thank you for treating me like a normal person. I cannot forget of course the two new members of the company, the two beautiful, smiley and crazy babies, Elias/Sebastian and Dimitra.

To my parents for their huge effort to make it possible for me and my brother to study, for their patience and their guidance without putting any pressure for our choices. To my brother who is always there for me no matter how much he suffered in the past from me (I am just the older).

Last but not least, to Fotini who is always supporting me and helping me on taking hard decisions. Thank you for making my life happier, funnier and helping me to escape during hard times. You are the best.

References

[1] O. Smith, *Some possible forms of Phonograph*. The Electrical World, 1888.

[2] M. N. Baibich, J. M. Broto, A. Fert, F. N. Van Dau, F. Petroff, P. Etienne, G. Creuzet, A. Friederich, and J. Chazelas, "Giant magnetoresistance of (001) Fe/(001) Cr magnetic superlattices," *Physical review letters*, vol. 61, no. 21, p. 2472, 1988.

[3] G. Binasch, P. Grünberg, F. Saurenbach, and W. Zinn, "Enhanced magnetoresistance in layered magnetic structures with antiferromagnetic interlayer exchange," *Physical review B*, vol. 39, no. 7, p. 4828, 1989.

[4] S. Borlenghi, W. Wang, H. Fangohr, L. Bergqvist, and A. Delin, "Designing a spin-Seebeck diode," *Physical review letters*, vol. 112, no. 4, p. 047203, 2014.

[5] S. Borlenghi, S. Lepri, L. Bergqvist, and A. Delin, "Thermomagnonic diode: Rectification of energy and magnetization currents," *Physical Review B*, vol. 89, no. 5, p. 054428, 2014.

[6] A. V. Chumak, A. A. Serga, and B. Hillebrands, "Magnon transistor for all-magnon data processing," *Nature communications*, vol. 5, 2014.

[7] J. C. Slonczewski, "Current-driven excitation of magnetic multilayers," *Journal of Magnetism and Magnetic Materials*, vol. 159, no. 1, pp. L1–L7, 1996.

[8] L. Berger, "Emission of spin waves by a magnetic multilayer traversed by a current," *Physical Review B*, vol. 54, no. 13, p. 9353, 1996.

[9] S. S. Parkin, M. Hayashi, and L. Thomas, "Magnetic domain-wall racetrack memory," *Science*, vol. 320, no. 5873, pp. 190–194, 2008.

[10] S. Mühlbauer, B. Binz, F. Jonietz, C. Pfleiderer, A. Rosch, A. Neubauer, R. Georgii, and P. Böni, "Skyrmion lattice in a chiral magnet," *Science*, vol. 323, no. 5916, pp. 915–919, 2009.

[11] J. Iwasaki, M. Mochizuki, and N. Nagaosa, "Universal current-velocity relation of skyrmion motion in chiral magnets," *Nature communications*, vol. 4, p. 1463, 2013.

[12] W. Heisenberg, "Zur theorie des ferromagnetismus," *Zeitschrift für Physik*, vol. 49, no. 9-10, pp. 619–636, 1928.

[13] L. D. Landau and E. Lifshitz, "On the theory of the dispersion of magnetic permeability in ferromagnetic bodies," *Phys. Z. Sowjetunion*, vol. 8, no. 153, pp. 101–114, 1935.

[14] T. L. Gilbert, "A phenomenological theory of damping in ferromagnetic materials," *IEEE Transactions on Magnetics*, vol. 40, no. 6, pp. 3443–3449, 2004.

[15] J. Korringa, "On the calculation of the energy of a bloch wave in a metal," *Physica*, vol. 13, no. 6-7, pp. 392–400, 1947.

[16] W. Kohn and N. Rostoker, "Solution of the Schrödinger equation in periodic lattices with an application to metallic lithium," *Physical Review*, vol. 94, no. 5, p. 1111, 1954.

[17] A. Liechtenstein, M. Katsnelson, and V. Gubanov, "Exchange interactions and spin-wave stiffness in ferromagnetic metals," *Journal of Physics F: Metal Physics*, vol. 14, no. 7, p. L125, 1984.
[18] A. I. Liechtenstein, M. Katsnelson, V. Antropov, and V. Gubanov, "Local spin density functional approach to the theory of exchange interactions in ferromagnetic metals and alloys," *Journal of Magnetism and Magnetic Materials*, vol. 67, no. 1, pp. 65–74, 1987.
[19] L. Berger, "Exchange interaction between ferromagnetic domain wall and electric current in very thin metallic films," *Journal of Applied Physics*, vol. 55, no. 6, pp. 1954–1956, 1984.
[20] L. Berger, "Possible existence of a Josephson effect in ferromagnets," *Physical Review B*, vol. 33, no. 3, p. 1572, 1986.
[21] I. Dzyaloshinsky, "A thermodynamic theory of "weak" ferromagnetism of antiferromagnetics," *Journal of Physics and Chemistry of Solids*, vol. 4, no. 4, pp. 241–255, 1958.
[22] T. Moriya, "Anisotropic superexchange interaction and weak ferromagnetism," *Physical Review*, vol. 120, no. 1, p. 91, 1960.
[23] F. Keffer, *Encyclopedia of physics*, vol. 18. by HPJ Wijn, Springer-Verlag, New York, 1966.
[24] J. Coey, "Noncollinear spin structures," *Canadian journal of physics*, vol. 65, no. 10, pp. 1210–1232, 1987.
[25] L. Sandratskii, "Noncollinear magnetism in itinerant-electron systems: theory and applications," *Advances in Physics*, vol. 47, no. 1, pp. 91–160, 1998.
[26] M. Born and R. Oppenheimer, "Zur quantentheorie der molekeln," *Annalen der Physik*, vol. 389, no. 20, pp. 457–484, 1927.
[27] P. Hohenberg and W. Kohn, "Inhomogeneous electron gas," *Physical review*, vol. 136, no. 3B, p. B864, 1964.
[28] W. Kohn and L. J. Sham, "Self-consistent equations including exchange and correlation effects," *Physical review*, vol. 140, no. 4A, p. A1133, 1965.
[29] J. P. Perdew and A. Zunger, "Self-interaction correction to density-functional approximations for many-electron systems," *Physical Review B*, vol. 23, no. 10, p. 5048, 1981.
[30] J. P. Perdew and Y. Wang, "Accurate and simple analytic representation of the electron-gas correlation energy," *Physical Review B*, vol. 45, no. 23, p. 13244, 1992.
[31] J. P. Perdew, K. Burke, and M. Ernzerhof, "Generalized gradient approximation made simple," *Physical review letters*, vol. 77, no. 18, p. 3865, 1996.
[32] H. Eschrig, *The fundamentals of density functional theory*, vol. 32. Springer, 1996.
[33] J. M. Wills, M. Alouani, P. Andersson, A. Delin, O. Eriksson, and O. Grechnyev, *Full-potential electronic structure method: energy and force calculations with density functional and dynamical mean field theory*, vol. 167. Springer Science & Business Media, 2010.
[34] G. Kotliar, S. Savrasov, K. Haule, V. Oudovenko, O. Parcollet, and C. Marianetti, "Electronic structure calculations with dynamical mean-field theory," *Reviews of Modern Physics*, vol. 78, no. 3, p. 865, 2006.

[35] J. P. Perdew, "Density functional theory and the band gap problem," *International Journal of Quantum Chemistry*, vol. 30, no. 3, pp. 451–451, 1986.
[36] U. von Barth and L. Hedin, "A local exchange-correlation potential for the spin polarized case. i," *Journal of Physics C: Solid State Physics*, vol. 5, no. 13, p. 1629, 1972.
[37] P. A. Dirac, "The quantum theory of the electron," in *Proceedings of the Royal Society of London A: Mathematical, Physical and Engineering Sciences*, vol. 117, pp. 610–624, The Royal Society, 1928.
[38] S. Halilov, H. Eschrig, A. Y. Perlov, and P. Oppeneer, "Adiabatic spin dynamics from spin-density-functional theory: Application to Fe, Co, and Ni," *Physical Review B*, vol. 58, no. 1, p. 293, 1998.
[39] N. Rosengaard and B. Johansson, "Finite-temperature study of itinerant ferromagnetism in Fe, Co, and Ni," *Physical Review B*, vol. 55, no. 22, p. 14975, 1997.
[40] H. Ebert, D. Koedderitzsch, and J. Minar, "Calculating condensed matter properties using the KKR-Green's function method recent developments and applications," *Reports on Progress in Physics*, vol. 74, no. 9, p. 096501, 2011.
[41] L. Udvardi, L. Szunyogh, K. Palotás, and P. Weinberger, "First-principles relativistic study of spin waves in thin magnetic films," *Physical Review B*, vol. 68, no. 10, p. 104436, 2003.
[42] H. Ebert and S. Mankovsky, "Anisotropic exchange coupling in diluted magnetic semiconductors: Ab initio spin-density functional theory," *Physical Review B*, vol. 79, no. 4, p. 045209, 2009.
[43] V. Antropov, M. Katsnelson, B. Harmon, M. Van Schilfgaarde, and D. Kusnezov, "Spin dynamics in magnets: Equation of motion and finite temperature effects," *Physical Review B*, vol. 54, no. 2, p. 1019, 1996.
[44] B. Skubic, "Spin dynamics and magnetic multilayers," 2007.
[45] D. C. Ralph and M. D. Stiles, "Spin transfer torques," *Journal of Magnetism and Magnetic Materials*, vol. 320, no. 7, pp. 1190–1216, 2008.
[46] J. L. García-Palacios and F. J. Lázaro, "Langevin-dynamics study of the dynamical properties of small magnetic particles," *Physical Review B*, vol. 58, no. 22, p. 14937, 1998.
[47] B. Skubic, J. Hellsvik, L. Nordström, and O. Eriksson, "A method for atomistic spin dynamics simulations: implementation and examples," *Journal of physics: condensed matter*, vol. 20, no. 31, p. 315203, 2008.
[48] H. Nyquist, "Thermal agitation of electric charge in conductors," *Physical review*, vol. 32, no. 1, p. 110, 1928.
[49] D. Chandler, *Introduction to modern statistical mechanics*, vol. 1. Oxford University Press, 1987.
[50] C. Schieback, M. Kläui, U. Nowak, U. Rüdiger, and P. Nielaba, "Numerical investigation of spin-torque using the Heisenberg model," *The European Physical Journal B*, vol. 59, no. 4, pp. 429–433, 2007.
[51] S. Zhang and Z. Li, "Roles of nonequilibrium conduction electrons on the magnetization dynamics of ferromagnets," *Physical Review Letters*, vol. 93, no. 12, p. 127204, 2004.
[52] H. Kohno, G. Tatara, and J. Shibata, "Microscopic calculation of spin torques

in disordered ferromagnets," *Journal of the Physical Society of Japan*, vol. 75, no. 11, p. 113706, 2006.
[53] M. Dyakonov and V. Perel, "Current-induced spin orientation of electrons in semiconductors," *Physics Letters A*, vol. 35, no. 6, pp. 459–460, 1971.
[54] A. Manchon and S. Zhang, "Theory of spin torque due to spin-orbit coupling," *Physical Review B*, vol. 79, no. 9, p. 094422, 2009.
[55] K.-S. Ryu, L. Thomas, S.-H. Yang, and S. Parkin, "Chiral spin torque at magnetic domain walls," *Nature nanotechnology*, vol. 8, no. 7, pp. 527–533, 2013.
[56] J. Torrejon, J. Kim, J. Sinha, S. Mitani, M. Hayashi, M. Yamanouchi, and H. Ohno, "Interface control of the magnetic chirality in CoFeB/MgO heterostructures with heavy-metal underlayers," *Nature communications*, vol. 5, 2014.
[57] L. Liu, C.-F. Pai, Y. Li, H. Tseng, D. Ralph, and R. Buhrman, "Spin-torque switching with the giant spin Hall effect of tantalum," *Science*, vol. 336, no. 6081, pp. 555–558, 2012.
[58] Y. Niimi, Y. Kawanishi, D. Wei, C. Deranlot, H. Yang, M. Chshiev, T. Valet, A. Fert, and Y. Otani, "Giant spin Hall effect induced by skew scattering from bismuth impurities inside thin film CuBi alloys," *Physical review letters*, vol. 109, no. 15, p. 156602, 2012.
[59] C.-F. Pai, L. Liu, Y. Li, H. Tseng, D. Ralph, and R. Buhrman, "Spin transfer torque devices utilizing the giant spin Hall effect of tungsten," *Applied Physics Letters*, vol. 101, no. 12, p. 122404, 2012.
[60] S. Emori, E. Martinez, K.-J. Lee, H.-W. Lee, U. Bauer, S.-M. Ahn, P. Agrawal, D. C. Bono, and G. S. Beach, "Spin Hall torque magnetometry of Dzyaloshinskii domain walls," *Physical Review B*, vol. 90, no. 18, p. 184427, 2014.
[61] S. Heinze, K. Von Bergmann, M. Menzel, J. Brede, A. Kubetzka, R. Wiesendanger, G. Bihlmayer, and S. Blügel, "Spontaneous atomic-scale magnetic skyrmion lattice in two dimensions," *Nature Physics*, vol. 7, no. 9, pp. 713–718, 2011.
[62] M. Pajda, J. Kudrnovskỳ, I. Turek, V. Drchal, and P. Bruno, "Ab initio calculations of exchange interactions, spin-wave stiffness constants, and Curie temperatures of Fe, Co, and Ni," *Physical Review B*, vol. 64, no. 17, p. 174402, 2001.
[63] A. S. Schwartz, "Topology for physicists," 1994.
[64] R. Rajaraman, "Solitons and instantons," 1982.
[65] H.-B. Braun, "Topological effects in nanomagnetism: from superparamagnetism to chiral quantum solitons," *Advances in Physics*, vol. 61, no. 1, pp. 1–116, 2012.
[66] T. H. R. Skyrme, "A non-linear field theory," in *Proceedings of the Royal Society of London A: Mathematical, Physical and Engineering Sciences*, vol. 260, pp. 127–138, The Royal Society, 1961.
[67] T.-L. Ho, "Spinor Bose condensates in optical traps," *Physical review letters*, vol. 81, no. 4, p. 742, 1998.
[68] U. Al Khawaja and H. Stoof, "Skyrmions in a ferromagnetic Bose–Einstein condensate," *Nature*, vol. 411, no. 6840, pp. 918–920, 2001.

[69] J.-i. Fukuda and S. Žumer, "Quasi-two-dimensional skyrmion lattices in a chiral nematic liquid crystal," *Nature communications*, vol. 2, p. 246, 2011.
[70] C. Pfleiderer, "Magnetic order: Surfaces get hairy," *Nature Physics*, vol. 7, pp. 673–674, 2011.
[71] N. Nagaosa and Y. Tokura, "Topological properties and dynamics of magnetic skyrmions," *Nature nanotechnology*, vol. 8, no. 12, pp. 899–911, 2013.
[72] A. Bogdanov and D. Yablonskii, "Thermodynamically stable vortices in magnetically ordered crystals. the mixed state of magnets," *Zh. Eksp. Teor. Fiz*, vol. 95, pp. 178–182, 1989.
[73] A. Bogdanov and A. Hubert, "Thermodynamically stable magnetic vortex states in magnetic crystals," *Journal of magnetism and magnetic materials*, vol. 138, no. 3, pp. 255–269, 1994.
[74] U. Rößler, A. Bogdanov, and C. Pfleiderer, "Spontaneous skyrmion ground states in magnetic metals," *Nature*, vol. 442, no. 7104, pp. 797–801, 2006.
[75] B. Lebech, J. Bernhard, and T. Freltoft, "Magnetic structures of cubic FeGe studied by small-angle neutron scattering," *Journal of Physics: Condensed Matter*, vol. 1, no. 35, p. 6105, 1989.
[76] M. Uchida, N. Nagaosa, J. He, Y. Kaneko, S. Iguchi, Y. Matsui, and Y. Tokura, "Topological spin textures in the helimagnet FeGe," *Physical Review B*, vol. 77, no. 18, p. 184402, 2008.
[77] X. Yu, N. Kanazawa, Y. Onose, K. Kimoto, W. Zhang, S. Ishiwata, Y. Matsui, and Y. Tokura, "Near room-temperature formation of a skyrmion crystal in thin-films of the helimagnet FeGe," *Nature materials*, vol. 10, no. 2, pp. 106–109, 2011.
[78] H. Wilhelm, M. Baenitz, M. Schmidt, U. Rößler, A. Leonov, and A. Bogdanov, "Precursor phenomena at the magnetic ordering of the cubic helimagnet FeGe," *Physical review letters*, vol. 107, no. 12, p. 127203, 2011.
[79] J. Beille, J. Voiron, and M. Roth, "Long period helimagnetism in the cubic B20 Fe_x Co_{1-x} Si and Co_x Mn_{1-x} Si alloys," *Solid state communications*, vol. 47, no. 5, pp. 399–402, 1983.
[80] K. Ishimoto, Y. Yamaguchi, J. Suzuki, M. Arai, M. Furusaka, and Y. Endoh, "Small-angle neutron diffraction from the helical magnet $Fe_{0.8}Co_{0.2}Si$," *Physica B: Condensed Matter*, vol. 213, pp. 381–383, 1995.
[81] K. Shibata, X. Yu, T. Hara, D. Morikawa, N. Kanazawa, K. Kimoto, S. Ishiwata, Y. Matsui, and Y. Tokura, "Towards control of the size and helicity of skyrmions in helimagnetic alloys by spin-orbit coupling," *Nature nanotechnology*, vol. 8, no. 10, pp. 723–728, 2013.
[82] Y. Ishikawa, K. Tajima, D. Bloch, and M. Roth, "Helical spin structure in manganese silicide MnSi," *Solid State Communications*, vol. 19, no. 6, pp. 525–528, 1976.
[83] K. Motoya, H. Yasuoka, Y. Nakamura, and J. Wernick, "Helical spin structure in MnSi-NMR studies," *Solid State Communications*, vol. 19, no. 6, pp. 529–531, 1976.
[84] G. Shirane, R. Cowley, C. Majkrzak, J. Sokoloff, B. Pagonis, C. Perry, and Y. Ishikawa, "Spiral magnetic correlation in cubic MnSi," *Physical Review B*, vol. 28, no. 11, p. 6251, 1983.
[85] M. Ishida, Y. Endoh, S. Mitsuda, Y. Ishikawa, and M. Tanaka, "Crystal

chirality and helicity of the helical spin density wave in MnSi. II. Polarized neutron diffraction," *Journal of the Physical Society of Japan*, vol. 54, no. 8, pp. 2975–2982, 1985.
[86] K. Kadowaki, K. Okuda, and M. Date, "Magnetization and magnetoresistance of MnSi. I," *Journal of the Physical Society of Japan*, vol. 51, no. 8, pp. 2433–2438, 1982.
[87] A. Neubauer, C. Pfleiderer, B. Binz, A. Rosch, R. Ritz, P. Niklowitz, and P. Böni, "Topological Hall effect in the A phase of MnSi," *Physical review letters*, vol. 102, no. 18, p. 186602, 2009.
[88] X. Yu, Y. Onose, N. Kanazawa, J. Park, J. Han, Y. Matsui, N. Nagaosa, and Y. Tokura, "Real-space observation of a two-dimensional skyrmion crystal," *Nature*, vol. 465, no. 7300, pp. 901–904, 2010.
[89] X. Yu, N. Kanazawa, W. Zhang, T. Nagai, T. Hara, K. Kimoto, Y. Matsui, Y. Onose, and Y. Tokura, "Skyrmion flow near room temperature in an ultralow current density," *Nature communications*, vol. 3, p. 988, 2012.
[90] Y. Tokunaga, X. Yu, J. White, H. M. Rønnow, D. Morikawa, Y. Taguchi, and Y. Tokura, "A new class of chiral materials hosting magnetic skyrmions beyond room temperature," *Nature communications*, vol. 6, 2015.
[91] N. Romming, C. Hanneken, M. Menzel, J. E. Bickel, B. Wolter, K. von Bergmann, A. Kubetzka, and R. Wiesendanger, "Writing and deleting single magnetic skyrmions," *Science*, vol. 341, no. 6146, pp. 636–639, 2013.
[92] W. Jiang, P. Upadhyaya, W. Zhang, G. Yu, M. B. Jungfleisch, F. Y. Fradin, J. E. Pearson, Y. Tserkovnyak, K. L. Wang, O. Heinonen, *et al.*, "Blowing magnetic skyrmion bubbles," *Science*, vol. 349, no. 6245, pp. 283–286, 2015.
[93] A. Fert, "Magnetic and transport properties of metallic multilayers," in *Materials Science Forum*, vol. 59, pp. 439–480, Trans Tech Publ, 1990.
[94] A. Crépieux and C. Lacroix, "Dzyaloshinsky–Moriya interactions induced by symmetry breaking at a surface," *Journal of magnetism and magnetic materials*, vol. 182, no. 3, pp. 341–349, 1998.
[95] C. Moreau-Luchaire, C. Moutafis, N. Reyren, J. Sampaio, C. Vaz, N. Van Horne, K. Bouzehouane, K. Garcia, C. Deranlot, P. Warnicke, *et al.*, "Additive interfacial chiral interaction in multilayers for stabilization of small individual skyrmions at room temperature," *Nature nanotechnology*, vol. 11, no. 5, pp. 444–448, 2016.
[96] S. Woo, K. Litzius, B. Krüger, M.-Y. Im, L. Caretta, K. Richter, M. Mann, A. Krone, R. M. Reeve, M. Weigand, *et al.*, "Observation of room-temperature magnetic skyrmions and their current-driven dynamics in ultrathin metallic ferromagnets," *Nature materials*, 2016.
[97] F. Jonietz, S. Mühlbauer, C. Pfleiderer, A. Neubauer, W. Münzer, A. Bauer, T. Adams, R. Georgii, P. Böni, R. Duine, *et al.*, "Spin transfer torques in MnSi at ultralow current densities," *Science*, vol. 330, no. 6011, pp. 1648–1651, 2010.
[98] K. Everschor, M. Garst, R. Duine, and A. Rosch, "Current-induced rotational torques in the skyrmion lattice phase of chiral magnets," *Physical Review B*, vol. 84, no. 6, p. 064401, 2011.
[99] K. Everschor, M. Garst, B. Binz, F. Jonietz, S. Mühlbauer, C. Pfleiderer, and A. Rosch, "Rotating skyrmion lattices by spin torques and field or temperature

gradients," *Physical Review B*, vol. 86, no. 5, p. 054432, 2012.
[100] T. Schulz, R. Ritz, A. Bauer, M. Halder, M. Wagner, C. Franz, C. Pfleiderer, K. Everschor, M. Garst, and A. Rosch, "Emergent electrodynamics of skyrmions in a chiral magnet," *Nature Physics*, vol. 8, no. 4, pp. 301–304, 2012.
[101] J. Zang, M. Mostovoy, J. H. Han, and N. Nagaosa, "Dynamics of skyrmion crystals in metallic thin films," *Physical review letters*, vol. 107, no. 13, p. 136804, 2011.
[102] A. Aharoni, "Introduction to the theory of ferromagnetism, vol. 93 of international series of monographs on physics," 1996.
[103] A. Thiele, "Steady-state motion of magnetic domains," *Physical Review Letters*, vol. 30, no. 6, p. 230, 1973.
[104] A. Fert, V. Cros, and J. Sampaio, "Skyrmions on the track," *Nature nanotechnology*, vol. 8, no. 3, pp. 152–156, 2013.
[105] A. Rosch, "Skyrmions: moving with the current," *Nature nanotechnology*, vol. 8, no. 3, pp. 160–161, 2013.
[106] J. Iwasaki, M. Mochizuki, and N. Nagaosa, "Current-induced skyrmion dynamics in constricted geometries," *Nature nanotechnology*, vol. 8, no. 10, pp. 742–747, 2013.
[107] X. Yu, M. Mostovoy, Y. Tokunaga, W. Zhang, K. Kimoto, Y. Matsui, Y. Kaneko, N. Nagaosa, and Y. Tokura, "Magnetic stripes and skyrmions with helicity reversals," *Proceedings of the National Academy of Sciences*, vol. 109, no. 23, pp. 8856–8860, 2012.
[108] M. Uchida, Y. Onose, Y. Matsui, and Y. Tokura, "Real-space observation of helical spin order," *Science*, vol. 311, no. 5759, pp. 359–361, 2006.
[109] U. Hartmann, "Magnetic force microscopy," *Annual review of materials science*, vol. 29, no. 1, pp. 53–87, 1999.
[110] C. Degen, "Scanning magnetic field microscope with a diamond single-spin sensor," *Applied Physics Letters*, vol. 92, no. 24, p. 243111, 2008.
[111] L. Rondin, J. Tetienne, T. Hingant, J. Roch, P. Maletinsky, and V. Jacques, "Magnetometry with nitrogen-vacancy defects in diamond," *Reports on Progress in Physics*, vol. 77, no. 5, p. 056503, 2014.
[112] T. Göddenhenrich, U. Hartmann, M. Anders, and C. Heiden, "Investigation of bloch wall fine structures by magnetic force microscopy," *The Monthly Microscopical Journal*, vol. 3, no. 3, pp. 527–536, 1987.
[113] T. Göddenhenrich, H. Lemke, U. Hartmann, and C. Heiden, "Magnetic force microscopy of domain wall stray fields on single-crystal iron whiskers," *Applied physics letters*, vol. 56, no. 25, pp. 2578–2580, 1990.
[114] B. M. Chernobrod and G. P. Berman, "Spin microscope based on optically detected magnetic resonance," *Journal of applied physics*, vol. 97, no. 1, p. 014903, 2005.
[115] S. Sekatskii and V. Letokhov, "Nanometer-resolution scanning optical microscope with resonance excitation of the fluorescence of the samples from a single-atom excited center," *Journal of Experimental and Theoretical Physics Letters*, vol. 63, no. 5, pp. 319–323, 1996.
[116] J. Wrachtrup, C. Von Borczyskowski, J. Bernard, M. Orritt, and R. Brown, "Optical detection of magnetic resonance in a single molecule," 1993.

[117] J. Köhler, J. Disselhorst, M. Donckers, E. Groenen, J. Schmidt, and W. Moerner, "Magnetic resonance of a single molecular spin," 1993.
[118] G. Balasubramanian, I. Chan, R. Kolesov, M. Al-Hmoud, J. Tisler, C. Shin, C. Kim, A. Wojcik, P. R. Hemmer, A. Krueger, *et al.*, "Nanoscale imaging magnetometry with diamond spins under ambient conditions," *Nature*, vol. 455, no. 7213, pp. 648–651, 2008.
[119] J. Maze, P. Stanwix, J. Hodges, S. Hong, J. Taylor, P. Cappellaro, L. Jiang, M. G. Dutt, E. Togan, A. Zibrov, *et al.*, "Nanoscale magnetic sensing with an individual electronic spin in diamond," *Nature*, vol. 455, no. 7213, pp. 644–647, 2008.
[120] J.-P. Tetienne, T. Hingant, J.-V. Kim, L. H. Diez, J.-P. Adam, K. Garcia, J.-F. Roch, S. Rohart, A. Thiaville, D. Ravelosona, *et al.*, "Nanoscale imaging and control of domain-wall hopping with a nitrogen-vacancy center microscope," *Science*, vol. 344, no. 6190, pp. 1366–1369, 2014.
[121] J.-P. Tetienne, T. Hingant, L. Martinez, S. Rohart, A. Thiaville, L. H. Diez, K. Garcia, J.-P. Adam, J.-V. Kim, J.-F. Roch, *et al.*, "The nature of domain walls in ultrathin ferromagnets revealed by scanning nanomagnetometry," *Nature communications*, vol. 6, 2015.
[122] L. Rondin, J.-P. Tetienne, S. Rohart, A. Thiaville, T. Hingant, P. Spinicelli, J.-F. Roch, and V. Jacques, "Stray-field imaging of magnetic vortices with a single diamond spin," *Nature communications*, vol. 4, 2013.
[123] A. Dussaux, P. Schoenherr, K. Koumpouras, J. Chico, K. Chang, L. Lorenzelli, N. Kanazawa, Y. Tokura, M. Garst, A. Bergman, *et al.*, "Local dynamics of topological magnetic defects in the itinerant helimagnet FeGe," *Nature Communications*, vol. 7, p. 12430, 2016.
[124] N. Porter, J. C. Gartside, and C. Marrows, "Scattering mechanisms in textured FeGe thin films: Magnetoresistance and the anomalous Hall effect," *Physical Review B*, vol. 90, no. 2, p. 024403, 2014.
[125] Y. A. Izyumov, "Modulated, or long-periodic, magnetic structures of crystals," *Physics-Uspekhi*, vol. 27, no. 11, pp. 845–867, 1984.
[126] J.-i. Kishine, K. Inoue, and Y. Yoshida, "Synthesis, structure and magnetic properties of chiral molecule-based magnets," *Progress of Theoretical Physics Supplement*, vol. 159, pp. 82–95, 2005.
[127] T. Moriya and T. Miyadai, "Evidence for the helical spin structure due to antisymmetric exchange interaction in $CrNbS_2$," *Solid State Communications*, vol. 42, no. 3, pp. 209–212, 1982.
[128] Y. Togawa, T. Koyama, K. Takayanagi, S. Mori, Y. Kousaka, J. Akimitsu, S. Nishihara, K. Inoue, A. Ovchinnikov, and J. Kishine, "Chiral magnetic soliton lattice on a chiral helimagnet," *Physical review letters*, vol. 108, no. 10, p. 107202, 2012.
[129] T. Miyadai, K. Kikuchi, H. Kondo, S. Sakka, M. Arai, and Y. Ishikawa, "Magnetic properties of $Cr_{1/3}NbS_2$," *Journal of the Physical Society of Japan*, vol. 52, no. 4, pp. 1394–1401, 1983.
[130] A. Borisov, J.-i. Kishine, I. Bostrem, and A. Ovchinnikov, "Magnetic soliton transport over topological spin texture in chiral helimagnet with strong easy-plane anisotropy," *Physical Review B*, vol. 79, no. 13, p. 134436, 2009.
[131] A. Borisov and V. Kiseliev, "Topological defects in incommensurate magnetic

and crystal structures and quasi-periodic solutions of the elliptic sine-gordon equation," *Physica D: Nonlinear Phenomena*, vol. 31, no. 1, pp. 49–64, 1988.
[132] A. Borisov and V. Kiselev, "Quasi-one-dimensional magnetic solitons," *Fizmatlit, Moscow*, 2014.
[133] K. Bernstein, R. K. Cavin, W. Porod, A. Seabaugh, and J. Welser, "Device and architecture outlook for beyond CMOS switches," *Proceedings of the IEEE*, vol. 98, no. 12, pp. 2169–2184, 2010.
[134] D. E. Nikonov and I. A. Young, "Overview of beyond-CMOS devices and a uniform methodology for their benchmarking," *Proceedings of the IEEE*, vol. 101, no. 12, pp. 2498–2533, 2013.
[135] K.-S. Ryu, S.-H. Yang, L. Thomas, and S. S. Parkin, "Chiral spin torque arising from proximity-induced magnetization," *Nature communications*, vol. 5, 2014.
[136] M. A. Ruderman and C. Kittel, "Indirect exchange coupling of nuclear magnetic moments by conduction electrons," *Physical Review*, vol. 96, no. 1, p. 99, 1954.
[137] T. Kasuya, "A theory of metallic ferro-and antiferromagnetism on Zener's model," *Progress of theoretical physics*, vol. 16, no. 1, pp. 45–57, 1956.
[138] K. Yosida, "Magnetic properties of Cu-Mn alloys," *Physical Review*, vol. 106, no. 5, p. 893, 1957.
[139] A. Manchon and K.-J. Lee, "Spin Hall effect-driven spin torque in magnetic textures," *Applied physics letters*, vol. 99, no. 2, p. 022504, 2011.
[140] S.-H. Yang, K.-S. Ryu, and S. Parkin, "Domain-wall velocities of up to 750 m/s driven by exchange-coupling torque in synthetic antiferromagnets," *Nature nanotechnology*, vol. 10, no. 3, pp. 221–226, 2015.
[141] A. Khvalkovskiy, V. Cros, D. Apalkov, V. Nikitin, M. Krounbi, K. Zvezdin, A. Anane, J. Grollier, and A. Fert, "Matching domain-wall configuration and spin-orbit torques for efficient domain-wall motion," *Physical Review B*, vol. 87, no. 2, p. 020402, 2013.
[142] R. Tomasello, E. Martinez, R. Zivieri, L. Torres, M. Carpentieri, and G. Finocchio, "A strategy for the design of skyrmion racetrack memories.," *Scientific reports*, vol. 4, p. 6784, 2014.
[143] O. Meshcheriakova, S. Chadov, A. Nayak, U. Rößler, J. Kübler, G. André, A. Tsirlin, J. Kiss, S. Hausdorf, A. Kalache, *et al.*, "Large noncollinearity and spin reorientation in the novel Mn_2RhSn Heusler magnet," *Physical review letters*, vol. 113, no. 8, p. 087203, 2014.
[144] A. Tonomura, X. Yu, K. Yanagisawa, T. Matsuda, Y. Onose, N. Kanazawa, H. S. Park, and Y. Tokura, "Real-space observation of skyrmion lattice in helimagnet MnSi thin samples," *Nano letters*, vol. 12, no. 3, pp. 1673–1677, 2012.
[145] S. Huang and C. Chien, "Extended skyrmion phase in epitaxial FeGe (111) thin films," *Physical review letters*, vol. 108, no. 26, p. 267201, 2012.

Acta Universitatis Upsaliensis

Digital Comprehensive Summaries of Uppsala Dissertations from the Faculty of Science and Technology 1467

Editor: The Dean of the Faculty of Science and Technology

A doctoral dissertation from the Faculty of Science and Technology, Uppsala University, is usually a summary of a number of papers. A few copies of the complete dissertation are kept at major Swedish research libraries, while the summary alone is distributed internationally through the series Digital Comprehensive Summaries of Uppsala Dissertations from the Faculty of Science and Technology. (Prior to January, 2005, the series was published under the title "Comprehensive Summaries of Uppsala Dissertations from the Faculty of Science and Technology".)

Distribution: publications.uu.se
urn:nbn:se:uu:diva-312462

ACTA
UNIVERSITATIS
UPSALIENSIS
UPPSALA
2017